Development of scalable processes for the manufacture of nanocarriers

Development Of

SCALABLE PROCESSES

for the manufacture of

NANOCARRIERS

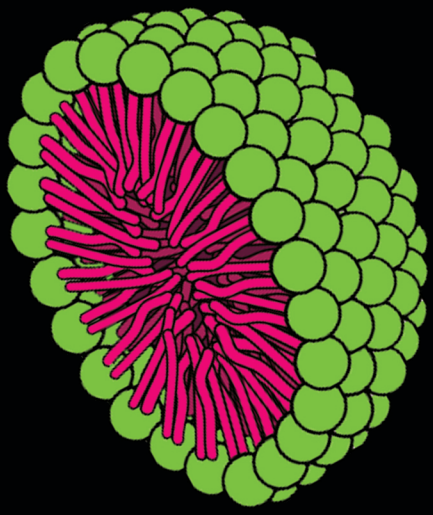

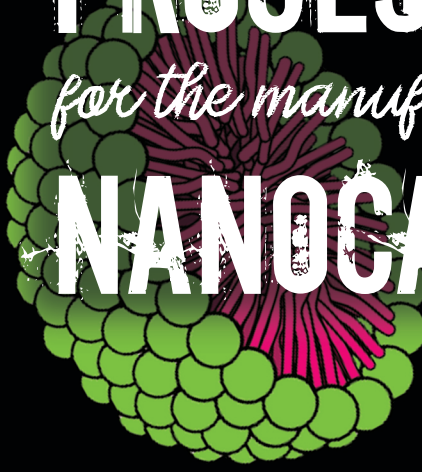

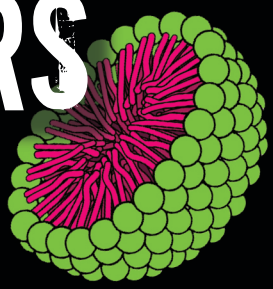

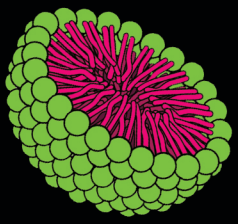

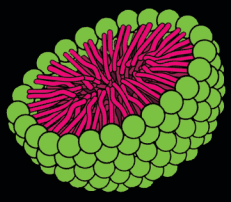

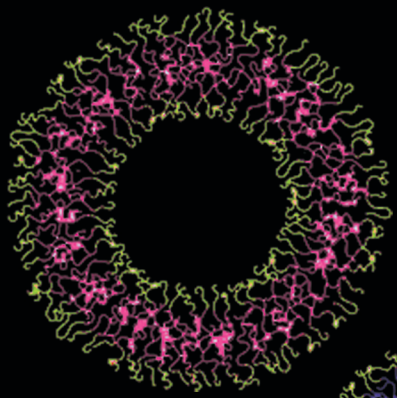

Jaleesa Bresseleers

Development of Scalable Processes for the Manufacture of Nanocarriers

PROEFSCHRIFT

ter verkrijging van de graad van doctor aan de Technische Universiteit Eindhoven, op gezag van de rector magnificus prof.dr.ir. F.P.T. Baaijens, voor een commissie aangewezen door het College voor Promoties, in het openbaar te verdedigen op woensdag 18 november 2020 om 16:00 uur

door

Jaleesa Bresseleers

geboren te Merksem (Antwerpen), België

Dit proefschrift is goedgekeurd door de promotoren en de samenstelling van de promotiecommissie is als volgt:

voorzitter:	prof.dr. M. Merkx
1e promotor:	prof.dr.ir. J.C.M. van Hest
2e promotor:	prof.dr. W.E. Hennink (Universiteit Utrecht)
copromotor:	dr. S.A. Meeuwissen (ChemConnection – Ardena BV)
leden:	prof.dr. K. Raemdonck (Universiteit Gent)
	prof.dr. R.P. Sijbesma
	prof.dr. I. Voets
	dr. T Noël
adviseur:	dr. L.K.E.A. Abdelmohsen

Het onderzoek of ontwerp dat in dit proefschrift wordt beschreven is uitgevoerd in overeenstemming met de TU/e Gedragscode Wetenschapsbeoefening.

Development of Scalable Processes for the Manufacture of Nanocarriers

DOCTORAL DISSERTATION

to obtain the degree of doctor from Eindhoven University of Technology, on the authority of the rector magnificus prof.dr.ir. F.P.T. Baaijens, before a committee asigned by the Doctorate Board, to be defended in public on Wednesday 18 November 2020 at 16:00

by

Jaleesa Bresseleers

born in Merksem (Antwerpen), België

This doctoral dissertation has been approved by the promotors and the doctorate committee consists of:

chairman:	prof.dr. M. Merkx
1st promotor:	prof.dr.ir. J.C.M. van Hest
2nd promotor:	prof.dr. W.E. Hennink (Universiteit Utrecht)
copromotor:	dr. S.A. Meeuwissen (ChemConnection – Ardena BV)
members:	prof.dr. K. Raemdonck (Universiteit Gent)
	prof.dr. R.P. Sijbesma
	prof.dr. I. Voets
	dr. T Noël
advisor:	dr. L.K.E.A. Abdelmohsen

The research described in this dissertation was financially supported by the European Union's Horizon 2020 research and innovation program Marie Sklodowska-Curie Innovative Training Networks (ITN) under grant No. 676137 and has been carried out in accordance with the TU/e Code of Scientific conduct.

Paranymphs: Kelly Klingenberg
Sjoerd Rutgers

Cover design: Harry Schipper

Printed by: ADC Dereumaux, Netherlands

A catalogue record is available from the Eindhoven University of Technology Library.

ISBN: 978-90-386-5150-7

Table of contents

Chapter 1

Introduction

NANOMEDICINES

The field of nanotechnology has experienced a tremendous development over the years. One of the areas in which it has been regarded as a potential break-through technology is the biomedical field, where its application is commonly referred to as nanomedicine. The term nanomedicine is applied for very specific medical interventions at the nano-scale for screening, diagnosis, control and treatment purposes of biological systems.[1,2] In a description of the application of nanotechnology offered by the Food and Drug Administration (FDA), it is stated that nanomaterials feature structures between 1 and 100 nm in any of the 3 spatial dimensions. However, in drug delivery, a broader definition is often used in which particles with dimensions up to 1 μm are still considered nanomedicines.[3]

The term nanotechnology was first used in 1959 at the annual meeting of the American Physical Society by the later Nobel Prize winner Richard Feynman who presented his vision of manipulating and controlling matter on the nanoscale.[4] The first nanomedical formulations followed shortly after in the 60's and 70's of the 20th century. For example, in those years the concept of lysosomotropic delivery using carriers was discussed by de Duve et al..[5] Simultaneously, the rational design of polymer-based drug conjugates for delivery was also introduced.[6] Furthermore, lipid-based formulations were developed and many intravenous liposome formulations have been extensively studied ever since.[7,8]

Attractive features of nanomedicines are their capability of transporting and delivering multiple components, like for example therapeutic agents and imaging contrast enhancers. Due to their small size, nanomedicines can overcome various biological barriers and localize into target tissue.[9] Therefore, nanomedicines allow for the development of more selective and efficient therapies and it is envisioned that the area of nanomedicines will further revolutionize medical treatment with more potent, less toxic, smart, targeted and personalized therapeutics.[10,11]

Three generations of nanomedicines

The development of nanomedicines can be classified into three generations (**Figure 1.1**).[12,13] The first generation is characterized by 'simple' nanomedicine formulations that were engineered as delivery systems for indirect targeting to overcome physicochemical barriers such as poor solubility of drug molecules e.g. in oral or transdermal delivery. Intravenously administered liposomal formulations were also developed that showed higher efficacy and less toxicity compared to non-encapsulated drugs.[12]

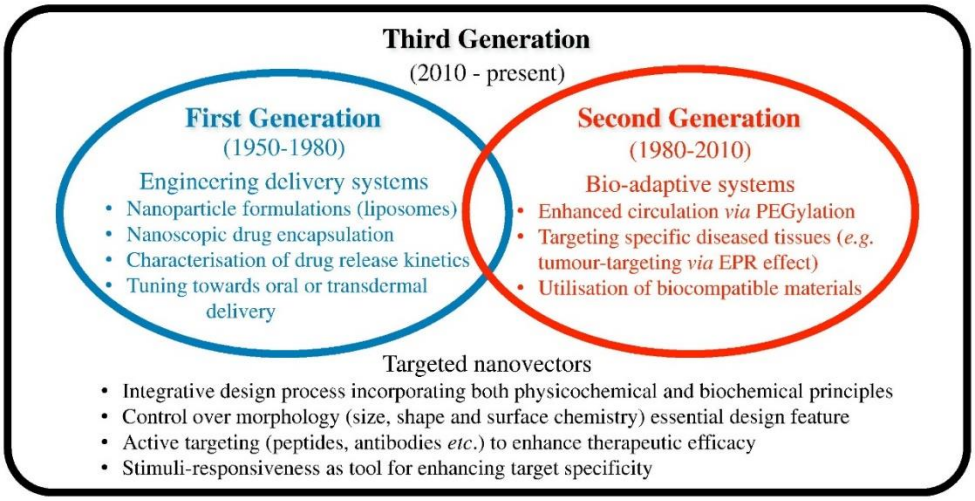

Figure 1.1. The three different generations of NPs in drug delivery. Adapted with permission from Williams et al.[12]

The introduction of a "stealth" layer like poly(ethylene glycol) (PEG) on the surface of nanoparticles (NPs) and the recognition of the enhanced permeation and retention (EPR) effect, led to the development of the second generation of nanomedicines. The EPR effect is based on the fact that fast growing tumors have a leaky vasculature, because of fenestrated blood capillaries, and a lack of lymphatic drainage. Therefore, nanoparticles tend to accumulate into tumor tissue, a phenomenon known as passive targeting.[14–16] Nanomedicines from this second generation, exploiting the EPR effect, reduce systemic side effects while improving therapeutic effects.[17,18] What makes these nanomedicine systems even more effective, is their decoration with a stealth-layer, usually PEG, which helps to prolong their circulation time and which results in higher tumor accumulation.[19,20] The efficacy of the EPR effect in patients, however,

is still under debate and will be discussed more extensively in the "biological challenges" section of this chapter. The first FDA-approved nanomedicine product, Doxil, is an example of a nanomedicine with a PEG stealth-layer that exploits the EPR effect and passively delivers doxorubicin to tumors.[21]

The third generation of NPs is characterized by active targeting and stimuli responsiveness. NPs decorated by active targeting moieties can increase efficacy in terms of target cell internalization and retention.[22,23] Most active targeting moieties are antibodies which bind specific biomarkers on cellular surfaces.[24] Stimuli responsive NPs are activated by either physical or chemical triggers.[25] An example of physical-responsive NPs are thermo-responsive systems which release their content after local heat treatment using e.g. high intensity focused ultrasound.[26,27] pH responsive NPs are activated by the acidic microenvironment of tumor tissue or in endo/lysosomes after cellular internalization.[28] More recently, nanomedicines have been designed that are multifunctional and possess a combination of more than one of the above-mentioned strategies. They can consist of a targeting moiety and are stimulus responsive, even toward multiple stimuli.[25,29] Another development, referred to theranostics or nanotheranostics, involves particles which provide both therapeutic and imaging properties and are often combined with triggered release.[10]

TYPES OF NANOMEDICINES

When considering the composition of specific particulate nanomedicine formulations, a variety of structures can be considered. In the following part a number of important NP structures are highlighted.

Liposomes

Liposomes are the best clinically established NPs for drug delivery. They are small, artificial, spherical vesicles consisting of an aqueous core surrounded by at least one lipid bilayer that is often composed of phospholipids.[30] These features make liposomes very attractive as they allow for the unique combination of being able to encapsulate both hydrophilic compounds in their aqueous core and hydrophobic and amphiphilic molecules in the membrane. Liposomes are often decorated by the previously mentioned stealth PEG layer, to substantially prolong circulation times.

One of the most famous and already mentioned examples of liposomal products, the first FDA-approved nanomedicine Doxil®, relies on pegylated, doxorubicin-loaded liposomes.[21] Doxorubicin is an anti-cancer drug, widely used for different types of cancer such as ovarian and breast cancer. Unfortunately, its application in free form is limited due to its high toxicity, affecting healthy tissues like the heart.[31] Liposomal formulations of doxorubicin resulted in the reduction of this toxicity and in some patients an increased accumulation in tumor tissue, due to the EPR effect, was also observed.[32,33]

Despite their high potential as nanomedicines, which is demonstrated by the fact that a range of liposome products has already reached the market, many limitations have emerged since their first application. This has led to the search towards other types of nanomedicine formulations. Especially polymer-based nanomedicines are very interesting and have attracted much attention, as they display often an improved robustness and chemical versatility compared to the lipid-based analogues. An important class of polymer-based nanomedicines are self-assembled from amphiphilic block copolymers.

Effect of polymer composition on the morphology of NPs

The self-assembly of amphiphilic molecules can result in various NP morphologies. This depends on the ratio between the hydrophobic and hydrophilic part of the molecule and the repulsive interaction strength of the hydrophobic part with water. For small amphiphilic molecules these factors influence the geometry of the amphiphile, its packing parameter, leading to different molecule conformations varying between conical and cylindrical (**Figure 1.2**).[34] As a result, they can form a wide range of nanostructures like vesicles, cylindrical micelles and spherical micelles. These different structures and morphologies can be predicted using the following equation:

$$P = \frac{V}{a_0 L_c}$$

Where P is the packing parameter, V the volume of the hydrophobic chain, a_0 is the area occupied by the hydrophilic head group and L_c is the length of the hydrophobic tail. This dimensionless packing parameter can predict which morphology will be formed (**Figure 1.2**). Spherical micelles are expected to be formed when $P \leq 1/3$, whereas cylindrical micelles are more likely to form when $1/3 \leq P \leq 1/2$ and vesicles are most likely obtained when $1/2 \leq P \leq 1$.

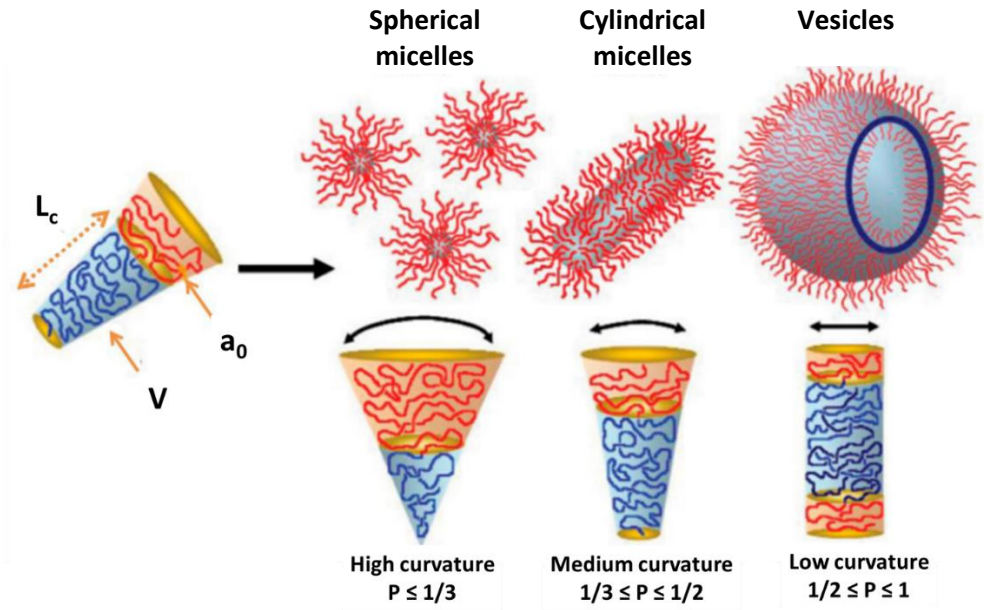

Figure 1.2. Schematic representation of assemblies formed by amphiphilic molecules. Depending on the inherent curvature, estimated by calculating the packing parameter, other types of nanostructures are formed. Adapted with permission of Ryan et al.[34]

For larger amphiphilic molecules like block copolymers, the hydrophilic weight fraction (*f*) is used more often to predict the formed aggregate morphology. In general, spherical micelles are expected to be formed when *f* is > 50 %, whereas cylindrical or wormlike micelles are more likely to form when *f* is between 40 and 50 % and vesicles are most likely formed when *f* is between 25 and 40 %.[35] For polymersomes (also named polymeric vesicles) the total molecular weight of the block copolymer has a direct influence on membrane thickness, which logically increases with increasing molecular weight.[34,35] Though the self-assembly into NPs is predominately determined by the characteristics of the block copolymer, the actual formed morphology and size of the NP are also dependent on the process parameters that are applied during assembly.[36,37]

Polymeric micelles

Morphologies like spherical micelles have attracted a lot of attention as nanomedicine due to their simplicity. They are composed of amphiphilic block polymers in a core-shell structure. In most cases, the core of the micelles comprises the hydrophobic tails and can accommodate poorly water-soluble drugs.[38,39] The hydrophilic shell provides often similar stealth-like properties as also displayed by liposomes. Micelles are easy to handle in terms of encapsulating hydrophobic drugs and offer relatively easy surface manipulation options. Their main advantage is that drug-loaded micelle formulations mostly improve the pharmacokinetics as compared to the free drugs. Though several polymeric micelle formulations are being investigated in clinical studies, for now only one of them has been FDA approved (Genexol^{TM}-PM).[39–41]

Polymersomes

Besides micelles, polymeric vesicles have also become a topic of growing interest. Polymeric vesicles, or polymersomes, are spherical vesicles of nano- to micrometer size. They consist of a bilayer structure, comprised of amphiphilic block copolymers, enclosing an aqueous lumen. Regarding the overall structure, it should be apparent that polymersomes resemble liposomes in many aspects (**Figure 1.3**).[42] Like liposomes, polymersomes have the capability to encapsulate both hydrophilic compounds in the aqueous lumen and hydrophobic compounds in the bilayer membrane. There are, however, some differences between liposomes and polymersomes. Polymersomes are formed through the self-assembly of amphiphilic block copolymers instead of the low molecular weight lipids that liposomes are self-assembled of.[43] Varying the molecular weight of the block copolymers has a direct influence on the thickness of the assembled bilayer and can be tuned from 5 to 50 nm, compared to 3 to 5 nm for liposomes.[42,44] The flexibility and permeability of these membranes can be tuned by the glass-transition temperature (T_g) of the hydrophobic block.[45] In terms of size, both small vesicles of the nanometer range and giant vesicles in the micrometer range can be formed depending on the molecular weight and chemical constitution of the used polymer and the preparation method.[46] Therefore, by synthesizing a library of block polymers, vesicles with different properties can be prepared and tuned for the aimed application.

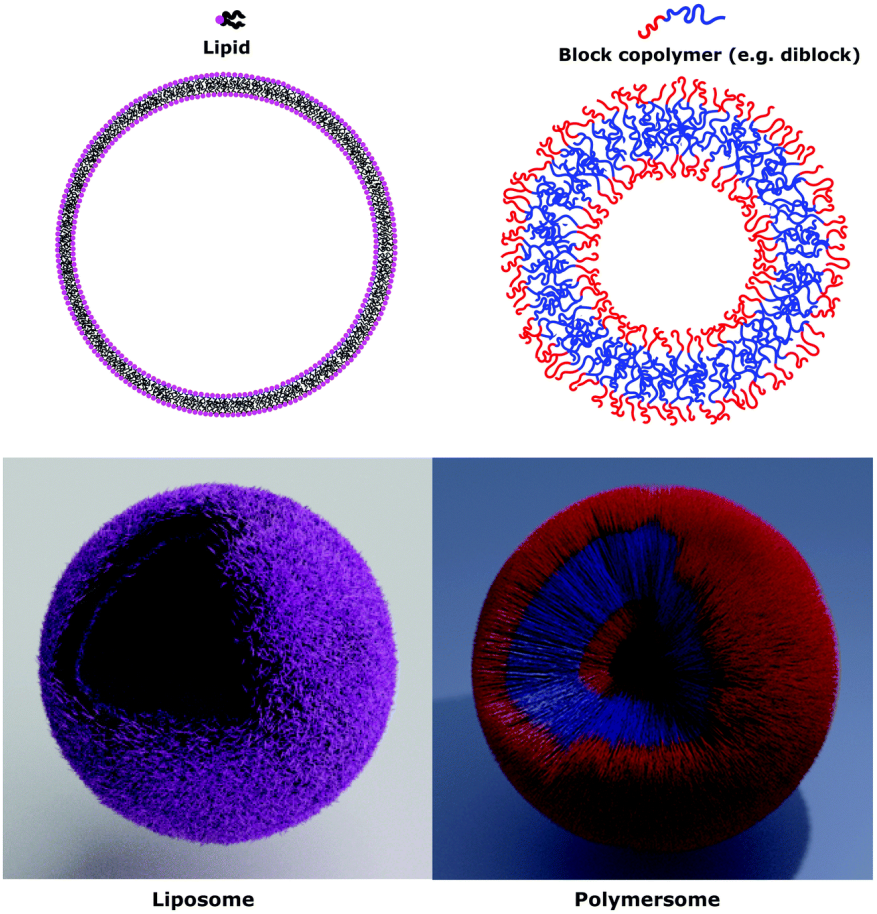

Figure 1.3. 2D and 3D schematic representation of a liposome (left) and a polymersome (right). Reprinted with permission from Rideau et al.[42]

Polymersomes have received widespread scientific attention, and significant progress has been made regarding the use of these polymersomes as drug delivery systems (DDSs).[47–49] Although they have been considered to be promising, so far, no polymersome formulations are FDA approved and on the market.

Non-spherical NPs

Even though polymersomes consist of a relatively robust membrane, their morphology can be transformed. This shape transformation can occur in response to external stimuli such as for example osmotic pressure [50–52], pH [53]

or chemical modification via membrane crosslinking[54]. Non-spherical NPs can be obtained with either oblate (discoid) or prolate (tubular) morphology. Non-spherical NPs are also observed for micellar topologies, such as the wormlike micelles.[55]

Recently the shape of NPs (besides their size) has emerged as an important aspect of nanomedicine efficacy. The shape of NPs can be essential regarding their function *in vivo* and can enable new biomedical opportunities. It has for example been shown that high aspect ratio particles coated with ICAM-mAb circulate longer, provide reduced nonspecific adhesion and increase the specificity of endothelial targeting to the lungs compared to spherical particles.[56] It has for example been demonstrated that although elongated particles adhered more effectively to macrophages compared to spheres, their internalization process was slower.[57] This can be explained by the more complex actin network that is necessary to initiate phagocytosis for rods compared to spheres, which affects the phagocytotic capability of the macrophages.[58]

CHALLENGES

As mentioned before, nanomedicines offer several advantages such as reduction in systemic toxicity of active pharmaceutical ingredients and improvement of pharmacokinetics. This is also reflected in the increasing number of publications and patents regarding promising nanomedicines. But, despite these perceived advantages and the vast amount of work performed in the field of nanomedicine, the translation to the clinic and market is still limited. This is mainly due to the many challenges that need proper consideration, as discussed in the following sections.

Biological and physical challenges

One of the challenges is the complexity of the interaction of NPs with biological systems. In research regarding nanomedicines against cancer, for example, for many years exploiting the enhanced permeability and retention (EPR) effect was the holy grail. It is only within the last couple of years that scientists started realizing that the EPR effect is not a general concept, with high variability in occurrence between patients, tumors, and even within the same patient. The effect even changes in the various stages of tumor development and on top of that is possibly even transient.[59–62] Therefore, the outcome of using passive targeting with nanomedicines for cancer treatment is

very difficult to predict. It should also be mentioned that the current knowledge regarding the EPR effect is mostly based on animal data. EPR effectiveness data in patients should be further gathered to gain a better understanding in humans and clinical use of nanomedicines that exploit the EPR should be performed in a more focused manner.

In the meantime, substantial attention has been directed towards the enhancement of the EPR effect in order to maximize the therapeutic efficacy of nanomedicines. The use of specific molecular markers for the tumor microenvironment (TME), the physical alteration of the TME by external sources and also the physiological remodeling of the TME are strategies that can be used (**Figure 1.4**).[59,63,64]

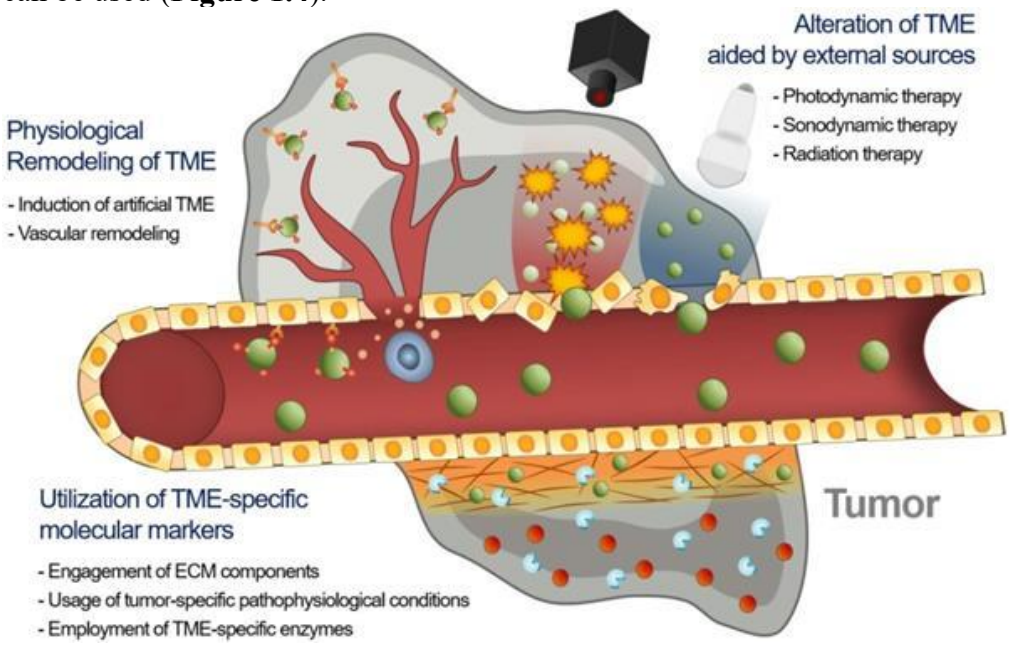

Figure 1.4. Schematic illustration of strategies for the alteration of tumor microenvironments. Adapted with permission of Park et al.[59]

Another important biological challenge is the interaction of blood proteins with nanomedicines, which is still not fully understood. Proteins can adsorb onto the surface of nanomedicines when the NPs are in biological fluids and therewith altering their size and shape. The formed coating that appears is called the protein corona, which can have a critical effect on the circulation kinetics and efficacy of the nanomedicines.[65] It was already mentioned above

that the shape of the NP can alter the therapeutic efficacy in the body, but the size of the NPs is also extremely important.[66–68] It was for example reported by Kataoka et al. that micelles smaller than 50 nm penetrated into poorly permeable tumors, whereas micelles with a size range up to100 nm only penetrated the highly permeable tumors.[67] Another study, by Shen et al., confirmed this and demonstrated that though micelles with a size of 100 nm accumulated in higher concentrations at the peripheral side of tumors compared to 30 nm micelles, this did not translate in improved therapeutic efficacy due to better penetration of the smaller micelles in less permeable areas of the tumors.[66] It should furthermore be noted that the protein corona is not static but rather changes in time. In some cases it actually provides the stealth-like effects that PEG coated NPs require to prevent non-specific cellular uptake.[69] In this way the protein corona can direct the fate of the nanomedicines into specific directions, depending on the proteins that are involved. For example, it was shown that the amount of β2 glycoprotein I associated with liposomes is correlated with the clearance rate from circulation.[70] A further level of complexity is that it has been shown that there are some proteins known that can promote internalization into cells whereas others will actually impede this process.[71]

In general, the surface composition and charge of NPs has a substantial impact on the type and composition of the protein corona. This eventually plays a major role in how the nanomedicines interact with cells and will give varying outcomes in terms of circulation kinetics, cytotoxicity, membrane adhesion, uptake and transport.[72]

A third distinct effect that definitely needs to be considered is shear stress. Upon iv injection NPs are exposed to the shear stress that comes with regular blood flow.[73] This shear stress can alter the shape of the NPs and influences the interactions between NPs and endothelial cells. It has been shown that under dynamic conditions cellular uptake of cationic polystyrene NPs by endothelial cells was higher compared to static conditions, whereas this effect was not observed for anionic polystyrene NPs.[74] Considering that most *in vitro* uptake studies of NPs by endothelial cells are performed under static conditions, NPs might not act in a similar fashion once administered to actual human bodies where they do experience shear stress.

Reproducibility and scalability during manufacturing of NPs

One of the other very important challenges in bringing nanomaterials to the market lies in the scalability and reproducibility of their synthesis. Nanomedicines are typically complex assemblies of multiple components that form three-dimensional constructs with preferred spatial arrangements of their functional moieties. This complexity requires a high level of control regarding the chemistry, manufacturing and quality controls involved. Subtle changes in the production process can already affect the eventual composition of the components. Therefore a thorough physicochemical understanding of the individual components and how they assemble is essential in order to get to a reproducible manufacturing process.[22,75]

First of all, the synthesis and purification methods of both the building blocks and the actual NPs can be very resource-intensive with limited yields. Second, subtle variations in NP preparation conditions can already critically affect physicochemical properties of the NPs such as size, drug-loading and surface charge, which all influence the eventual therapeutic outcome.[22,76–78] The building blocks are subsequently formulated into particles. The applied processes generally consist of multiple steps that can include homogenization, sonication, centrifugation, solvent evaporation, extrusion, size reduction, sterilization and lyophilization. Often the entire formulation and production process can be achieved in a relatively easy and reproducible manner on a small scale. It becomes however more challenging and complex when large-scale production is performed where robust manufacturing processes are required to minimize batch-to-batch variations.[22,77]

It is clear that on top of the physicochemical complexity of the formulations themselves, a forthcoming major challenge concerns the scalability and large-scale industrial production.[79] Even though preparations of nanomedicines on a laboratory scale are very well documented and reproducibility is quite achievable, the translation for industrial factorial design is considered less during development. This is reflected by the very limited number of experiments and publications regarding reproducibility and scalability of nanomedicine products. Most traditional pharmaceutical industries have very well-established infrastructures for the production of conventional drug formulations. However, nanomedicine production requires more complicated and expensive approaches, together with specially trained and experienced staff. Besides that, there is insufficient information available in general on

scale-up technologies for nanomedicines, which hinders the entrance of these medicines to the market.[78,80]

Another process limitation includes the stability of the produced nanomedicines. Since nanomedicines are complex systems, over time, changes may occur. This includes changes in size, morphology and surface charge, drug leakage and degradation of the particles. Research regarding relevant storage conditions is therefore also highly important.

Sterilization of NPs

After scaling up the process for the manufacturing of nanomedicines, sterilization of the product is required. Unfortunately, this gives rise to a range of other challenges depending on the size of the particles and their chemical composition. The main challenge lies in the fact that nanomedicines are built up from multiple components, of which each needs different sterilization procedures. Even though multiple options for sterilization are available for nanomedicines, each and every single one of them have the potential to negatively impact the physicochemical characteristics of the nanomedicines.[81,82]

One of the most commonly used methods for sterilization of nanomedicines is filtration. It is used for the physical removal of microorganisms by pressing the nanomedicines through 0.22 μm membrane filters. If the structure or flexibility of the NP allows for it, it does not appear to have any adverse effects and is therefore widely applicable.[82–85] Nonetheless, in some cases adjusting the size and rigidity of NPs to enable them to pass through the filter is not feasible. This can result in tremendous difficulties in filtration and may also result in substantial loss in amounts of the NPs and of the active ingredients during filtration.[82]

A second commonly used method is sterilization by autoclaving, also known as moist heat sterilization. It is a very effective method that uses high temperatures of usually 120 °C. Unfortunately, the high temperatures and the presence of steam can induce adverse side effects including chemical changes on both the NPs and the excipients that are heat sensitive. In liposomes it has been shown that due to the physical structure of the bilayer, which is not stabilized by covalent bonds, the bilayer is easily disrupted by the high temperatures necessary for autoclaving.[86] In other NP cases it has been shown that autoclaving can lead to changes in morphology of the NPs or in some cases

even lead to aggregation and degradation.[85,87] Additionally, it seems that these effects also depend on the methodology and reagents used during synthesis and not only on the type of NP that is made.

A third commonly used method for sterilization is gamma radiation (γ-radiation). It is a procedure that has been used for NPs that are not heat-tolerant and thus cannot be sterilized using autoclaving. The main challenge with γ-radiation comes from the formation of reactive free radicals in the presence of water and molecular oxygen. It can eventually lead to the unwanted formation of (hydro)peroxides in the NPs. These peroxides might alter the NPs, react with the incorporated drugs and also increase toxicity.[81,83,88,89] Importantly, gamma irradiation can also result in unwanted polymer chain scission and/or crosslinking, which can change the drug release kinetics from the particles and adversely affect the degradation profile of NPs.[81,90]

Other sterilization techniques include chemical agents among which ethylene oxide and formaldehyde. However, very little information is available regarding their effect. The very few studies that have been conducted though, indicate that both agents may not be recommended for NPs because of the introduction of chemical and structural changes in the NPs.[81,82]

Finally, analysis of the successful sterilization of NPs is also not straightforward. Traditional methods to study the endotoxin contamination levels in NP formulations include the well-known *in vitro* quantitative Litmus Amebocyte Lysate (LAL) assay and the *in vivo* qualitative rabbit pyrogen test. Unfortunately, most NPs interfere with both of the tests.[91,92] This interference actually decreases the confidence in the assay results.

There are many NP formulations that cannot be end product sterilized. Consequently, starting with sterile materials and working under aseptic conditions is the only option to produce sterile products making manufacturing even more laborious and thus expensive.

Characterization of NPs

Another aspect that makes NPs more complex than traditional drug formulations is their characterization and validation. This is due to the number of components and parameters that have to be analyzed. A systematic approach for particle analysis is of great importance as it will allow a better comparison between different particles with respect to their efficacy. A perspective has

been written that also stresses the need for standardized protocols of particle analysis.[93] The first challenge already lies in identifying the appropriate methods for the characterization. This challenge is both from a technical as well as regulatory point of view. Overall, preclinical characterization should include a comprehensive description of the manufacturing process, physicochemical characteristics, quality, efficacy, safety and stability.[94] In addition to only finished product tests, it is useful to constantly perform in-process tests during early development. The focus lies on understanding the physicochemical aspects including size, size-distribution, surface morphology, chemistry and charge, drug loading, release characteristics, etcetera. Such understanding is very valuable to establish acceptable ranges for the process and formulation parameters. This in turn can provide a better understanding of the effect of those parameters on the eventual properties of nanomedicines.[78,95] The most important physicochemical parameters of nanomaterials and available suitable characterization methods are listed in **Table 1.1**.[96–98]

Table 1.1. Physicochemical characterization of nanomedicines and their building blocks.[97,98]

Parameters	**Methods**
Particle Size (size range and number size distribution; indicating batch to batch variation) Important: at least two methods, one being electron microscopy, should be used	- Scattering techniques: dynamic light, Raman, X-ray diffraction, small-angle X-ray and field flow fractionation - Microscopy: near-field scanning optical, scanning-electron, transmission electron, scanning tunneling and atomic force - Spectroscopy: Fluorescence and UV visible - Miscellaneous: time of flight – mass spectrometry, analytical ultra-centrifugation, gel electrophoresis and capillary electrophoresis
Surface charge	- Miscellaneous: zeta potential (ELS) measurements, gel electrophoresis and capillary electrophoresis
Physical form and morphology	- Scattering techniques: X-ray diffraction and small-angle X-ray - Microscopy: near field scanning optical, scanning electron, transmission electron, scanning tunneling and atomic force - Miscellaneous: analytical ultracentrifugation

Continuation of Table 1.1. Physicochemical characterization of nanomedicines and their building blocks.[97,98]

Structure	- Scattering techniques: Raman, X-ray diffraction and small-angle X-ray - Microscopy: scanning electron and atomic force - Spectroscopy: tip-enhanced Raman, circular dichroism, infrared and fluorescence - Miscellaneous: mass spectrometry nuclear magnetic resonance, differential scanning calorimetry and analytical ultracentrifugation
Chemical composition/identity	- Miscellaneous: mass spectrometry, nuclear magnetic resonance, high performance liquid chromatography and hydrodynamic chromatography
Dispersion	- Microscopy: environmental scanning electron, transmission electron, scanning tunneling and atomic force
Surface properties (including chemical/biochemical modifications)	- Microscopy: modified atomic force - Spectroscopy: circular dichroism coupled to enzyme-linked immunosorbent assay, infrared and X-ray photoelectron - Miscellaneous: time-of-flight secondary ion mass spectrometry
Protein corona	- Scattering techniques: dynamic light - Microscopy: transmission electron - Spectroscopy: fluorescence correlation, circular dichroism - Miscellaneous: size exclusion chromatography, differential centrifugal sedimentation, polyacrylamide gel electrophoresis, Liquid chromatography-mass spectrometry/mass spectrometry, simulations, surface plasmon resonance and isothermal titration calorimetry
Physical Stability	- For physical stability all of the mentioned above characterization techniques can be used in (accelerated) aging studies over time

In short, compared to standard pharmaceutical products, the nature of nanomedicines is more complex and analytical characterization can therefore be more challenging. The advantage of this intensive testing, also in early development, is to gain a better understanding of the properties of nanomedicines. It is then more likely that a successful manufacturing process can be developed in a very reproducible manner.

GMP production and regulatory challenges

As mentioned above, one of the challenges in using nanomedicines lies in the complexity of chemistry, manufacturing and quality control during production and scaling up the process. Besides that, good manufacturing practice (GMP) is also a requirement once the nanomedicine transitions to clinical development. This is nothing new, since all drug products must be manufactured in accordance with GMP. Though to a high extent, the standards of GMP resemble standard chemistry, manufacturing and quality controls, achieving GMP standards is subject to more regulatory challenges.[99]

Even though this is a vital part of the production process, there is not much information readily available regarding GMP requirements to manufacture nanomedicines. It should be noted that the FDA does not formally use the term 'nanomedicines' and the European Medicines Agency (EMA) has only recently acknowledged it. On top of that, the scope of the FDA on nanomaterials is limited, since the FDA is not yet convinced that nanomedicines behave differently compared to other small drug products with regards to biodistribution, toxicity, pharmacokinetics and excretion profiles.[100] The guiding principle is therefore that the FDA regulates end products. It is for this reason that the FDA only governs case by case nanoproducts and not nanotechnology in general.[101] Accordingly, there is only a draft guidance available from the FDA regarding drug nanomaterials, which was published in 2017.[102] Even in this document the FDA states that "*A comprehensive body of knowledge of nanomaterial attributes and the effects of these attributes on the quality and manufacturing process of drug products does not currently exist.*" The complete nanomaterial package (building blocks, active pharmaceutical ingredient, drug product, etcetera) would therefore have to be evaluated individually regarding the nanomaterials and their physicochemical properties.

The EMA, on the other hand, does have a couple of guidelines for marketing authorization applications for human nanomedicines. The EMA website

provides guidelines only for specific types of nanomedicines including iron-based nano-colloidal products [103], liposomal products [104], block-copolymer-micelle products [105] and surface coatings [106]. The fact that no concrete guidelines exist for all types of nanomedicines, can make it difficult and costly for companies to produce nanomedicines. In the end, each new nanomedicine product will need to be evaluated case by case. To make it even more challenging, the pharmaceutical companies are required to fully test their end product for its ultimate application, just like bulk drug products. But, as opposed to bulk drug products, nanomaterials behave differently in various biological environments as discussed in the "biological challenges" section of this chapter, which makes it difficult to fully test the newly developed nanomedicines.

OUTLINE OF DISSERTATION

It should be apparent from this introduction that even though nanomedicines have a high potential for clinical translation and treatment of patients suffering from chronic and life-threatening diseases, there is still a long road ahead regarding the translation to clinical products. To contribute to this goal, this dissertation reports on novel insights regarding the development of robust and scalable manufacturing processes for nanocarriers and their polymeric building blocks.

Chapter 2 discusses an in-depth study that was performed to gain more knowledge on the correlation between the formulation and process parameters and the resulting physicochemical characteristics of polymeric micelles. Among the tested parameters were the degree of polymerization and the hydrophilic to hydrophobic ratio of the used block copolymers, homopolymer content, concentration, addition rates and solvent used during particle formulation. The outcome of the study was a robust protocol for the formation of polymeric micelles.

Chapter 3 continues with the research of ***Chapter 2*** where particle formulation was investigated more extensively by using microfluidics. The advantage of microfluidic systems is that these allow for control of minute fluidic volumes of polymer dissolved in organic solvent and water in the nanoliter range. Exploiting this advantage provided precise control in mixing rates into a micromixer chip, which led to control regarding the resulting morphologies (micelles, bigger micelles and polymersomes) and their sizes that are formed using the same block copolymers.

Chapter 4 continues with the research of ***Chapter 2 and 3*** and focusses on the set up of a scalable manufacturing process for the production of drug-loaded micelles. For this, both batch and flow processes were evaluated to ensure product quality and consistency of the manufacturing processes. Meanwhile, quality requirements of EMA and FDA were also taken into account for the entire process and end product. The resulting manufacturing processes can eventually be readily translated for GMP production of the corresponding clinical product.

Chapter 5 reports on the attempt for improvement of drug loading of spherical polymersomes and its manufacturing process that can be readily translated for large-scale production. Both batch and flow processes for production and

purification were evaluated. Meanwhile, quality and consistency of the manufacturing processes were ensured.

Chapter 6 summarizes the results reported in this dissertation and provides recommendations for future research and product development.

NANOMED ITN

The research as described in this dissertation was performed within the NANOMED Innovative Training Network (ITN), which was formed to train a new generation of a total of 15 multi-disciplinary nanotechnology experts. Within the network, we were all working together to develop a broad understanding of the entire process of nanomedicine development. This included everything from formulation, pharmacokinetics and dynamics and toxicological aspects to production and regulatory aspects. The main goal of the network was to train experts capable of supporting and managing the effective translation of molecular innovations into therapeutic solutions for clinical applications. Due to the unique cross-disciplinary exchange of knowledge and skills in chemistry, pharmacology and chemical engineering on a GMP level, we obtained first-hand insight on how to develop effective, safe and efficiently producible nanomedicines. It can therefore be concluded, that the NANOMED ITN was a very valuable network for the acquisition of personal, scientific and professional skills.

The executed research that led to this dissertation would not have been possible without the financial support by the European Union's Horizon 2020 research and innovation program Marie Sklodowska-Curie ITN under grant No. 676137 for which we would like to express our immense gratitude.

REFERENCES

(1) Riehemann, K.; Schneider, S. W.; Luger, T. A.; Godin, B.; Ferrari, M.; Fuchs, H. *Angew. Chemie - Int. Ed.* **2009**, *48* (5), 872–897.
(2) Moghimi, S. M.; Hunter, A. C.; Murray, J. C. *FASEB J.* **2005**, *19* (3), 311–330.
(3) Food and Drug Administration. Guidance for Industry Considering Whether an FDA-Regulated Product Involves the Application of Nanotechnology. **2011**.
(4) Feynman, R. In *American Physical Society meeting*; 1959.
(5) de Duve, C.; de Barsy, T.; Poole, B.; Trouet, A.; Tulkens, P.; van Hoof, F. *Biochem. Pharmacol.* **1974**, *23*, 2495–2531.
(6) Ringsdorf, H. *J Polym Sci Polym Symp* **1975**, *153* (51), 135–153.
(7) Fenske, D. B.; Cullis, P. R. *Expert Opin. Drug Deliv.* **2008**, *5* (1), 25–44.
(8) Crommelin, D. J. A.; van Hoogevest, P.; Storm, G. *J. Control. Release* **2020**, *318*, 256–263.
(9) Alonso, M. J.; Csaba, N. S. (Eds.). *Nanostructured Biomaterials for Overcoming Biological Barriers*; The Royal Society of Chemistry, 2012.
(10) Mura, S.; Couvreur, P. *Adv. Drug Deliv. Rev.* **2012**, *64* (13), 1394–1416.
(11) Fornaguera, C.; García-Celma, M. J. *J. Pers. Med.* **2017**, *7* (4), 14–21.
(12) Williams, D. S.; Pijpers, I. A. B.; Ridolfo, R.; van Hest, J. C. M. *J. Control. Release* **2017**, *259*, 29–39.
(13) Yun, Y. H.; Lee, B. K.; Park, K. *J. Control. Release* **2015**, *219*, 2–7.
(14) Maeda, H.; Wu, J.; Sawa, T.; Matsumura, Y.; Hori, K. *J. Control. Release* **2000**, *65* (1–2), 271–284.
(15) Fang, J.; Nakamura, H.; Maeda, H. *Adv. Drug Deliv. Rev.* **2011**, *63* (3), 136–151.
(16) Torchilin, V. *Adv. Drug Deliv. Rev.* **2011**, *63* (3), 131–135.
(17) Bharali, D. J.; Mousa, S. A. *Pharmacol. Ther.* **2010**, *128* (2), 324–335.
(18) Rizzo, L. Y.; Theek, B.; Storm, G.; Kiessling, F.; Lammers, T. *Curr. Opin. Biotechnol.* **2013**, *24* (6), 1159–1166.
(19) Milton Harris, J.; Chess, R. B. *Nat. Rev. Drug Discov.* **2003**, *2* (3), 214–221.
(20) Salmaso, S.; Caliceti, P. *J. Drug Deliv.* **2013**, *2013*, 1–19.
(21) Barenholz, Y. *J. Control. Release* **2012**, *160* (2), 117–134.
(22) Desai, N. *AAPS J.* **2012**, *14* (2), 282–295.
(23) van der Meel, R.; Vehmeijer, L. J. C.; Kok, R. J.; Storm, G.; van Gaal, E. V. B. *Adv. Drug Deliv. Rev.* **2013**, *65* (10), 1284–1298.
(24) Brannon-Peppas, L.; Blanchette, J. O. *Adv. Drug Deliv. Rev.* **2012**, *64*, 206–212.
(25) Liao, J.; Jia, Y.; Wu, Y.; Shi, K.; Yang, D.; Li, P.; Qian, Z. *Wiley Interdiscip. Rev. Nanomedicine Nanobiotechnology* **2020**, *12* (1), 1–19.
(26) Ta, T.; Porter, T. M. *J. Control. Release* **2013**, *169* (1–2), 112–125.
(27) Gray, M. D.; Lyon, P. C.; Mannaris, C.; Folkes, L. K.; Stratford, M.; Campo, L.; Chung, D. Y. F.; Scott, S.; Anderson, M.; Goldin, R.; Carlisle, R.; Wu, F.; Middleton, M. R.; Gleeson, F. V.; Coussios, C. C. *Radiology* **2019**, *291* (1), 232–238.
(28) Fattal, E.; Tsapis, N. *Clin. Transl. Imaging* **2014**, *2* (1), 77–87.
(29) Ferrari, M. *Nat. Rev. Cancer* **2005**, *5* (3), 161–171.
(30) Akbarzadeh, A.; Rezaei-Sadabady, R.; Davaran, S.; Joo, S. W.; Zarghami, N.; Hanifehpour, Y.; Samiei, M.; Kouhi, M.; Nejati-Koshki, K. *Nanoscale Res. Lett.* **2013**, *8* (1), 1–8.

(31) Thorn, C. F.; Oshiro, C.; Marsh, S.; Hernandez-Boussard, T.; McLeod, H.; Klein, T. E.; Altman, R. B. *Pharmacogenet. Genomics* **2011**, *21* (7), 440–446.
(32) Abraham, S. A.; Waterhouse, D. N.; Mayer, L. D.; Cullis, P. R.; Madden, T. D.; Bally, M. B. *Methods Enzymol.* **2005**, *391* (SPEC. ISS.), 71–97.
(33) Safra, T.; Jeffers, F. M. S.; Groshen, S.; Lyass, O.; Henderson, R.; Berry, G.; Gabizon, a. *Ann. Intern. Med.* **2000**, *11*, 1029–1033.
(34) Blanazs, A.; Armes, S. P.; Ryan, A. J. *Macromol. Rapid Commun.* **2009**, *30* (4–5), 267–277.
(35) Discher, D. E.; Ahmed, F. *Annu. Rev. Biomed. Eng.* **2006**, *8* (1), 323–341.
(36) Pagels, R. F.; Edelstein, J.; Tang, C.; Prud'homme, R. K. *Nano Lett.* **2018**, *18* (2), 1139–1144.
(37) Zhou, J.; Ni, R.; Chau, Y. *RSC Adv.* **2017**, *7* (29), 17997–18000.
(38) Cabral, H.; Miyata, K.; Osada, K.; Kataoka, K. *Chem. Rev.* **2018**, *118* (14), 6844–6892.
(39) Varela-Moreira, A.; Shi, Y.; Fens, M. H. A. M.; Lammers, T.; Hennink, W. E.; Schiffelers, R. M. *Mater. Chem. Front.* **2017**, *1* (8), 1485–1501.
(40) Anselmo, A. C.; Mitragotri, S. *Bioeng. Transl. Med.* **2019**, *4* (3), 1–16.
(41) Ali, I.; Alsehli, M.; Scotti, L.; Scotti, M. T.; Tsai, S. T.; Yu, R. S.; Fa Hsieh, M.; Chen, J. C. *Polymers (Basel).* **2020**, *12* (3).
(42) Rideau, E.; Dimova, R.; Schwille, P.; Wurm, F. R.; Landfester, K. *Chem. Soc. Rev.* **2018**, *47* (23), 8572–8610.
(43) Messager, L.; Gaitzsch, J.; Chierico, L.; Battaglia, G. *Curr. Opin. Pharmacol.* **2014**, *18* (1), 104–111.
(44) Bermudez, H.; Brannan, A. K.; Hammer, D. A.; Bates, F. S.; Discher, D. E. *Macromolecules* **2002**, *35* (21), 8203–8208.
(45) So, S.; Yao, L. J.; Lodge, T. P. *J. Phys. Chem. B* **2015**, *119* (48), 15054–15062.
(46) Kita-Tokarczyk, K.; Grumelard, J.; Haefele, T.; Meier, W. *Polymer* **2005**, *46* (11), 3540–3563.
(47) Lee, J. S.; Feijen, J. *J. Control. Release* **2012**, *161* (2), 473–483.
(48) Meerovich, I.; Dash, A. K. Elsevier Inc., 2019.
(49) Anajafi, T.; Mallik, S. *Ther. Deliv.* **2015**, *6* (4), 521–534.
(50) Rikken, R. S. M.; Engelkamp, H.; Nolte, R. J. M.; Maan, J. C.; Van Hest, J. C. M.; Wilson, D. A.; Christianen, P. C. M. *Nat. Commun.* **2016**, *7*, 1–7.
(51) Meeuwissen, S. A.; Kim, K. T.; Chen, Y.; Pochan, D. J.; Van Hest, J. C. M. *Angew. Chemie - Int. Ed.* **2011**, *50* (31), 7070–7073.
(52) Abdelmohsen, L. K. E. A.; Williams, D. S.; Pille, J.; Ozel, S. G.; Rikken, R. S. M.; Wilson, D. A.; Van Hest, J. C. M. *J. Am. Chem. Soc.* **2016**, *138* (30), 9353–9356.
(53) Robertson, J. D.; Yealland, G.; Avila-Olias, M.; Chierico, L.; Bandmann, O.; Renshaw, S. A.; Battaglia, G. *ACS Nano* **2014**, *8* (5), 4650–4661.
(54) Van Oers, M. C. M.; Rutjes, F. P. J. T.; Van Hest, J. C. M. *J. Am. Chem. Soc.* **2013**, *135* (44), 16308–16311.
(55) Wang, X.; Manners, I.; Winnik, M. a. *Science* **2007**, *644* (August), 644–648.
(56) Kolhar, P.; Anselmo, A. C.; Gupta, V.; Pant, K.; Prabhakarpandian, B.; Ruoslahti, E.; Mitragotri, S. *Proc. Natl. Acad. Sci. U. S. A.* **2013**, *110* (26), 10753–10758.
(57) Sharma, G.; Valenta, D. T.; Altman, Y.; Harvey, S.; Xie, H.; Mitragotri, S.; Smith, J. W. *J. Control. Release* **2010**, *147* (3), 408–412.

(58) Champion, J. A.; Mitragotri, S. *Proc. Natl. Acad. Sci. U. S. A.* **2006**, *103* (13), 4930–4934.
(59) Park, J.; Choi, Y.; Chang, H.; Um, W.; Ryu, J. H.; Kwon, I. C. *Theranostics* **2019**, *9* (26), 8073–8090.
(60) Nagy, J. A.; Chang, S. H.; Shih, S. C.; Dvorak, A. M.; Dvorak, H. F. *Semin. Thromb. Hemost.* **2010**, *36* (3), 321–331.
(61) Lammers, T.; Kiessling, F.; Hennink, W. E.; Storm, G. *J. Control. Release* **2012**, *161* (2), 175–187.
(62) van der Meel, R.; Lammers, T.; Hennink, W. E. *Expert Opin. Drug Deliv.* **2017**, *14* (1), 1–5.
(63) Ojha, T.; Pathak, V.; Shi, Y.; Hennink, W. E.; Moonen, C. T. W.; Storm, G.; Kiessling, F.; Lammers, T. *Adv. Drug Deliv. Rev.* **2017**, *119*, 44–60.
(64) Zhang, B.; Hu, Y.; Pang, Z. *Front. Pharmacol.* **2017**, *8* (DEC), 1–16.
(65) Hadjidemetriou, M.; Kostarelos, K. *Nat. Nanotechnol.* **2017**, *12* (4), 288–290.
(66) Wang, J.; Mao, W.; Lock, L. L.; Tang, J.; Sui, M.; Sun, W.; Cui, H.; Xu, D.; Shen, Y. *ACS Nano* **2015**, *9* (7), 7195–7206.
(67) Cabral, H.; Matsumoto, Y.; Mizuno, K.; Chen, Q.; Murakami, M.; Kimura, M.; Terada, Y.; Kano, M. R.; Miyazono, K.; Uesaka, M.; Nishiyama, N.; Kataoka, K. *Nat. Nanotechnol.* **2011**, *6* (12), 815–823.
(68) Sun, Q.; Ojha, T.; Kiessling, F.; Lammers, T.; Shi, Y. *Biomacromolecules* **2017**, *18* (5), 1449–1459.
(69) Schöttler, S.; Becker, G.; Winzen, S.; Steinbach, T.; Mohr, K.; Landfester, K.; Mailänder, V.; Wurm, F. R. *Nat. Nanotechnol.* **2016**, *11* (4), 372–377.
(70) Chonn, A.; Semple, S. C.; Cullis, P. R. *J. Biol. Chem.* **1995**, *270* (43), 25845–25849.
(71) Ritz, S.; Schöttler, S.; Kotman, N.; Baier, G.; Musyanovych, A.; Kuharev, J.; Landfester, K.; Schild, H.; Jahn, O.; Tenzer, S.; Mailänder, V. *Biomacromolecules* **2015**, *16* (4), 1311–1321.
(72) Abdelkhaliq, A.; Van Der Zande, M.; Punt, A.; Helsdingen, R.; Boeren, S.; Vervoort, J. J. M.; Rietjens, I. M. C. M.; Bouwmeester, H. *J. Nanobiotechnology* **2018**, *16* (1), 1–13.
(73) Gomez-Garcia, M. J.; Doiron, A. L.; Steele, R. R. M.; Labouta, H. I.; Vafadar, B.; Shepherd, R. D.; Gates, I. D.; Cramb, D. T.; Childs, S. J.; Rinker, K. D. *Nanoscale* **2018**, *10* (32), 15249–15261.
(74) Kang, T.; Park, C.; Choi, J. S.; Cui, J. H.; Lee, B. J. *J. Drug Deliv. Sci. Technol.* **2016**, *31*, 130–136.
(75) Hua, S.; de Matos, M. B. C.; Metselaar, J. M.; Storm, G. *Front. Pharmacol.* **2018**, *9*, 1–14.
(76) Kaur, I. P.; Kakkar, V.; Deol, P. K.; Yadav, M.; Singh, M.; Sharma, I. *J. Control. Release* **2014**, *193*, 51–62.
(77) Agrahari, V.; Hiremath, P. *Nanomedicine* **2017**, *12* (8), 819–823.
(78) Agrahari, V.; Agrahari, V. *Drug Discov. Today* **2018**, *23* (5), 974–991.
(79) Muthu, M. S.; Wilson, B. *Nanomedicine* **2012**, *7* (3), 307–309.
(80) Saraf, S. *Expert Opin. Drug Deliv.* **2009**, *6*, 187–196.
(81) Subbarao, N. *Handb. Immunol. Prop. Eng. Nanomater. Second Ed.* **2016**, *1*, 53–75.
(82) Vetten, M. A.; Yah, C. S.; Singh, T.; Gulumian, M. *Nanomedicine Nanotechnology, Biol. Med.* **2014**, *10* (7), 1391–1399.

(83) Masson, V.; Maurin, F.; Fessi, H.; Devissaguet, J. P. *Biomaterials* **1997**, *18* (4), 327–335.
(84) Özcan, I.; Bouchemal, K.; Freimar, S.-S.; Abacıa, Ö.; Özer, Ö.; Güneri, T.; Ponchel, G. *Acta Pharm. Sci.* **2009**, *51*, 211–218.
(85) Bos, G. W.; Trullas-Jimeno, A.; Jiskoot, W.; Crommelin, D. J. A.; Hennink, W. E. *Int. J. Pharm.* **2000**, *211* (1–2), 79–88.
(86) Zuidam, N. J.; Lee, S. S. L.; Crommelin, D. J. A. *Pharm. Res.* **1993**, *10* (11), 1591–1596.
(87) Sommerfeld, P.; Schroeder, U.; Sabel, B. A. *Int. J. Pharm.* **1998**, *164* (1–2), 113–118.
(88) Zheng, J. *J. Nanomed. Nanotechnol.* **2011**, *S5* (01), 1–15.
(89) Lin, J. J.; Hsu, P. Y. *Sensors* **2011**, *11* (9), 8769–8781.
(90) Athanasiou, K. A.; Niederauer, G. G.; Agrawal, C. M. *Biomaterials* **1996**, *17* (2), 93–102.
(91) Dobrovolskaia, M. a; Neun, B. W.; Clogston, J. D.; Ding, H.; Ljubimova, J.; Mcneil, S. E. *Nanomedicine* **2010**, *5* (4), 555–562.
(92) Mcneil, S. E. *Methods Mol. Biol.* **2011**, *697* (October), 9–15.
(93) Faria, M.; Björnmalm, M.; Thurecht, K. J.; Kent, S. J.; Parton, R. G.; Kavallaris, M.; Johnston, A. P. R.; Gooding, J. J.; Stevens, M.; Prestidge, C. A.; Porter, C. J. H.; Parak, W. J. **2018**, *13* (9), 777–785.
(94) Ragelle, H.; Danhier, F.; Préat, V.; Langer, R.; Anderson, D. G. *Expert Opin. Drug Deliv.* **2017**, *14* (7), 851–864.
(95) Grossman, J. H.; Crist, R. M.; Clogston, J. D. *AAPS J.* **2017**, *19* (1), 92–102.
(96) Marques, M. R. C.; Choo, Q.; Ashtikar, M.; Rocha, T. C.; Bremer-Hoffmann, S.; Wacker, M. G. *Adv. Drug Deliv. Rev.* **2019**, No. June 2017.
(97) SCENIHR. 2015.
(98) Lin, P. C.; Lin, S.; Wang, P. C.; Sridhar, R. *Biotechnol. Adv.* **2014**, *32* (4), 711–726.
(99) Shi, J.; Kantoff, P. W.; Wooster, R.; Farokhzad, O. C. *Nat. Rev. Cancer* **2016**, *17*, 20.
(100) Farjadian, F.; Ghasemi, A.; Gohari, O.; Roointan, A.; Karimi, M.; Hamblin, M. R. 2019; Vol. 14.
(101) Bawa, R. In *Regulatory Issues and Nanogovernance*; 2020.
(102) Food and Drug Administration. Guidance for Industry on Drug Products, Including Biological Products, That Contain Nanomaterials. *draft* **2017**, No. December.
(103) European Medicine Agency. *EMA/CHMP/SWP/620008/2012* **2015**, *44* (March), 1–1.
(104) European Medicine Agency. *EMA/CHMP/806058/2009/Rev. 02* **2013**, *44* (February), 1–13.
(105) Committee for Medicinal Products for Human Use; European Medicine Agency. *EMA/CHMP/13099/2013* **2013**, *44* (December 2013).
(106) European Medicine Agency. *EMA/325027/2013* **2013**, *44* (May).

Chapter 2

The Effect of Formulation and Processing Parameters on the Size of mPEG-b-p(HPMA-Bz) Polymeric Micelles

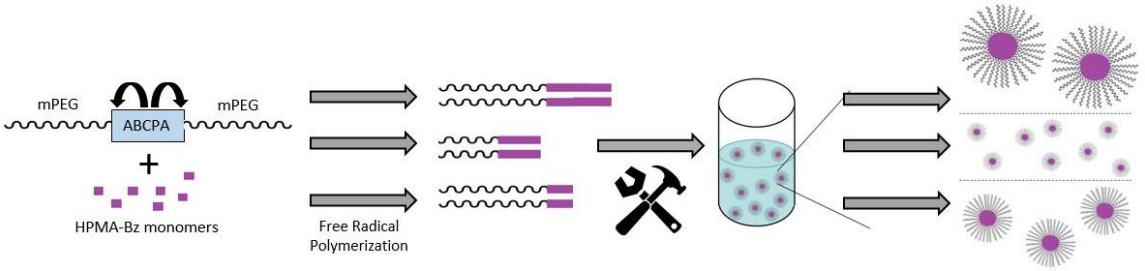

This work has been published as:

Bagheri, M. *; Bresseleers, J. *; Varela-Moreira, A.; Sandre, O.; Meeuwissen, S. A.; Schiffelers, R. M.; Metselaar, J. M.; Van Nostrum, C. F.; Van Hest, J. C. M.; & Hennink, W. E., *Langmuir* **2018**, *34* (50), 15495–15506.

* These authors contributed equally to this work.

ABSTRACT.

Micelles composed of block copolymers of poly(ethylene glycol)-*b*-poly(*N*-2-benzoyloxypropyl methacrylamide) (mPEG-*b*-p(HPMA-Bz)) have shown great promise as drug delivery carriers due to their excellent stability and high loading capacity. In this chapter, parameters influencing micelle size were investigated to tailor sizes in the range of 25 to 100 nm. Micelles were prepared by a nanoprecipitation method and their size was modulated by the block copolymer properties such as molecular weight, their hydrophilic to hydrophobic ratio, homopolymer content, as well as formulation and processing parameters. It was shown that the micelles have a core-shell structure using a combination of dynamic light scattering and transmission electron microscopy analysis. By varying the degree of polymerization of the hydrophobic block (N_B) between 68 and 10, at a fixed hydrophilic block $mPEG_{5K}$ (N_A=114), it was shown that the hydrophobic core of the micelles was collapsed following the power law of $(N_B \times N_{agg})^{1/3}$. Further, the calculated brush height was similar for all the micelles examined (10 nm), indicating that crew-cut micelles were made. Both addition of homopolymer and preparation of micelles at lower concentrations or lower rates of addition of the organic solvent to the aqueous phase increased the size of micelles due to partitioning of the hydrophobic homopolymer chains to the core of the micelles and lower nucleation rates, respectively. Furthermore, it was shown that by using different solvents, the size of the micelles substantially changed. The use of acetone, acetonitrile, ethanol, THF and dioxane, resulted in micelles in the size range from 45 to 60 nm after removal of the organic solvents. The use of DMF and DMSO led to markedly larger sizes of 75 and 180 nm respectively. In conclusion, the results show that by modulating polymer properties and processing conditions, micelles with tailorable sizes can be obtained.

INTRODUCTION

Over the last decades, a large variety of nanomedicines has been developed to improve drug disposition at the target site. [1–5] Particularly polymeric micelles, core-shell structures composed of amphiphilic polymers, with a diameter in the size range of 10-100 nm, have attracted much attention. The shell mainly consists of a hydrophilic block, usually poly(ethylene glycol) (PEG), which offers good colloidal stability as well as stealth properties by protecting the micelles from serum/protein interactions and fast uptake by the reticuloendothelial system after injection. The hydrophobic core can accommodate poorly water-soluble drugs like chemotherapeutics for cancer treatment. [6–12]

In order to have a clinically interesting tumor targeted nanomedicine, the formulation should provide sufficient stability and drug retention in the blood circulation. This stability can either be provided by physical interactions [13–15], or through chemical crosslinking. [16] Once circulating in the bloodstream, nanomedicines can penetrate the fenestrated blood capillaries of tumors. Due to the lack of lymphatic drainage, the nanoparticles tend to retain in the tumor region. This phenomenon is the so-called enhanced permeation and retention effect (EPR). [17–19] Nanomedicines that exploit the EPR effect have shown to both significantly improve therapeutic effects and reduce systemic side effects. [20,21]

It has been shown that the size of nanomedicines, like drug-loaded polymeric micelles, is an important factor for an improved therapeutic efficacy. [22–24] Therefore, in recent years, many studies have been devoted to understanding the effect of size of nanomedicines on their efficacy of cancer treatment. To highlight some of them, Huang et al. demonstrated that tiopronin coated gold nanoparticles of 2 and 6 nm have longer blood circulation times and better tumor penetration than 15 nm nanoparticles. [25] Kataoka et al. prepared micelles of different sizes by adding poly(glutamic acid) (p(Glu)) homopolymer to PEG–b-p(Glu) copolymer achieving micelle sizes ranging from 30 nm without homopolymer to around 100 nm at a 0.3 homopolymer/copolymer molar ratio. They reported that polymeric micelles in the range of 30 to 100 nm could penetrate highly permeable tumors while only the micelle formulations that were smaller than 50 nm penetrated into poorly permeable tumors and showed antitumor effect. [23] Chilkoti et al. showed that dextrans with a molecular weight of 40 to 70 kDa did accumulate in tumors after intravenous administration,

whereas dextrans of 3.3 and 10 kDa provided deeper and more homogeneous tumor penetration.[26] Shen et al. prepared micelles, based on PEG and a 10-OH methacrylate ester of 7-ethyl-10-hydroxylcamptothecin (PEG-p(HEMASN38)), of 20 to 300 nm by varying the process parameters. Although the 100 nm micelles reached a higher concentration at the peripheral side of the tumor compared to the 30 nm size micelles, due to higher liver accumulation of the 30 nm size micelles, this did not translate in an improved therapeutic effect since the latter micelles had better tumor penetration.[22] Smaller sized nanoparticles also showed better penetration in tumor stroma-containing 3D spheroids which are a suitable model to study penetration of nanoparticles. The results indicated deeper penetration of 30 nm silica nanoparticles compared to particles of 100 nm.[27] In conclusion, various studies have convincingly demonstrated that smaller drug-loaded particles resulted in better tumor penetration and thus better efficacy of the treatment.[24]

Recently Hennink et al. reported on a polymeric micelle formulation based on poly(ethylene glycol)-*block*-poly(*N*-2-benzoyloxypropyl methacrylamide) (mPEG-*b*-p(HPMA-Bz)). Micelles based on this polymer combine excellent particle stability, also in circulation, with improved drug retention as a result of π-π stacking interactions in the core of the micelles. When loaded with paclitaxel, these micelles have shown very promising results regarding pharmaceutical formulation characteristics (loading and stability) and therapeutic efficacy in animal studies demonstrating complete tumor regression.[28] In this chapter, a systematic evaluation is described to understand which parameters affect the size and stability of micelles prepared from mPEG-*b*-p(HPMA-Bz) block copolymers. The goal was to find a robust method to obtain micelles with tailorable sizes in the range of 25 to 100 nm. This was achieved by synthesizing block copolymers with a hydrophilic 5 kDa poly(ethylene glycol) methyl ether mPEG block, but also some studies were done with a 2 kDa mPEG block copolymer, and a varying molecular weight of poly(*N*-2-benzoyloxypropyl methacrylamide) (p(HPMA-Bz)). Furthermore, the effect of formulation variables among which the homopolymer p(HPMA-Bz) content, polymer concentration, type of solvent and the effect processing variables, particularly the addition rate of the solution of the block copolymer to the aqueous phase, on the size of polymeric micelles were investigated.

RESULTS AND DISCUSSION

mPEG-ABCPA-mPEG macro-initiator synthesis

The macro-initiator (MI) used for polymerization, mPEG-ABCPA-mPEG, was previously synthesized by the reaction of 2 equivalents mPEG with 1 equivalent 4,4-azobis(4-cyanopentanoic acid) (ABCPA). [29,30] According to this previous procedure, all the components except mPEG were dissolved simultaneously in a 1:1 mixture of DCM and dry DMF and put on ice. In this way, the COOH groups of ABCPA were first activated with DCC and subsequently mPEG was added. After addition of mPEG, the ice bath was removed and the mixture was stirred at room temperature overnight. This resulted in a yield of ~80% of macroinitiator after precipitation. [30] This strategy however led to a large amount of ~40 % byproduct with a molecular weight of 5 kDa according to GPC analysis (**Figure S2.1**). The shoulder peak in GPC can be due to the presence of either mPEG-ABCPA or unreacted mPEG, or a combination of both. It is known that a DCC-activated ester can undergo a rearrangement reaction to yield an N-acyl iso-urea product, which is not reactive with the primary hydroxyl group of mPEG.[31] Therefore, there is a possibility that the ABCPA reacts with only one mPEG chain giving mPEG-ABCPA, with or without an acyl urea (**Scheme S2.1**), as a byproduct. Consequently, unreacted mPEG-OH (free mPEG) will also be present in the reaction solution. TAIC is a reagent that is used for the quantitative determination of hydroxy end-groups of polymers using ^{1}H-NMR. [32,33] Therefore, this reagent was used to quantify the amount of free mPEG in the obtained product. Analysis showed the presence of ~30% unreacted mPEG, leaving the remaining 10% of the 5 kDa byproduct to be mPEG-ABCPA. Further purification steps such as dialysis could not separate the byproducts from mPEG-ABCPA-mPEG.

Upon the use of MI contaminated with mPEG-ABCPA for the polymerization of HMPA-Bz, both the p(HPMA-Bz) homopolymer and the aimed mPEG-*b*-p(HPMA-Bz) block copolymer are formed (**Figure 2.1**). The presence of the homopolymer p(HPMA-Bz) is unwanted because it will be solubilized in the core of the micelles, which in turn will result in an increase in micellar size. Therefore, the MI synthesis was optimized to obtain a high yield of mPEG-ABCPA-mPEG and to minimize the amounts of the mPEG-ABCPA/mPEG byproducts.

In the new procedure, all reagents, including mPEG but except DCC were dissolved in DCM. Subsequently DCC dissolved in DCM was added dropwise.[34] This resulted in activation of the COOH groups in the presence of mPEG to allow reaction of its OH group with the active ester, thereby reducing the possibility for the formation of the inactive N-acyl iso-urea product. Furthermore, contrary to the other procedure, no DMF was used and the reaction was therefore conducted in the less polar solvent DCM.

The new procedure resulted in the successful synthesis of two different mPEG-ABCPA-mPEG macro-initiators ($mPEG_{5K}$ and $mPEG_{2K}$) which were obtained in a yield of ~90% and only contained ~5% of the mixture of 5 kDa mPEG-ABCPA/free mPEG (**Figure S2.1**). The amount of free mPEG was determined by ^{1}H-NMR using TAIC to be 4.2% (**Figure S2.2**). This shows that the MI only contained a trace amount of 0.8% mPEG-ABCPA. Therefore, the MI synthesized according to this new procedure was used for the synthesis of the different mPEG-*b*-p(HPMA-Bz) block copolymers.

Synthesis of mPEG-b-p(HPMA-Bz) block copolymers

Amphiphilic mPEG-*b*-p(HPMA-Bz) block copolymers with varying molecular weights of the hydrophobic and hydrophilic blocks were synthesized by free radical polymerization of HPMA-Bz using mPEG-ABCPA-mPEG macro-initiators ($mPEG_{5K}$ or $mPEG_{2K}$) (**Figure 2.1**) at different macro-initiator/monomer ratios (MI:M) (**Table 2.1**). The molecular weights (M_n, M_w) of the obtained polymers were determined by ^{1}H-NMR and GPC analysis. As reported earlier, an increasing trend of molecular weight was observed upon increasing the monomer to initiator ratio.[35]

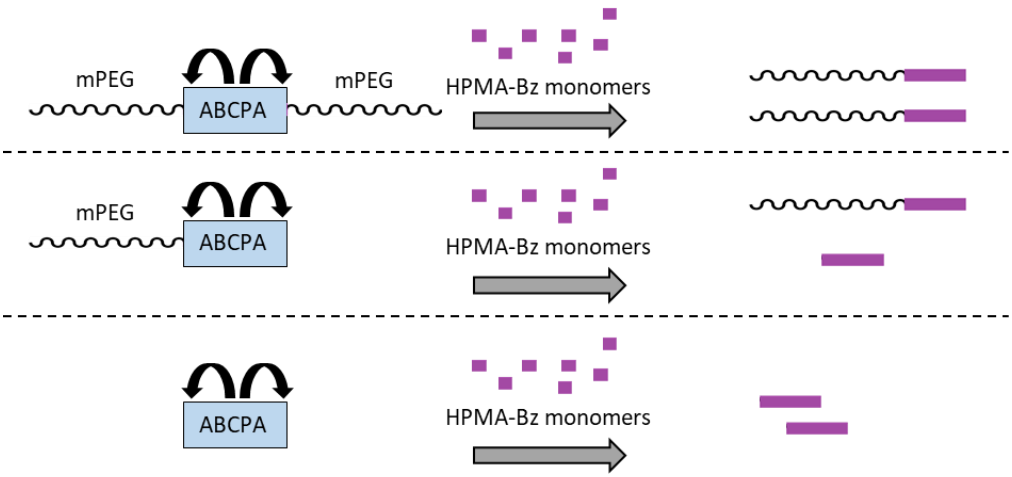

Figure 2.1. Schematic representation of the polymerization of mPEG-*b*-p(HPMA-Bz). Initiation by mPEG-ABCPA-mPEG results in the synthesis of mPEG-*b*-p(HPMA-Bz) diblock copolymers only. Initiation by mPEG-ABCPA will result in a mixture of block copolymer and homopolymer p(HPMA-Bz). Initiation by ABCPA will result in the formation of homopolymer only. It is hereby assumed that no chain transfer occurs.

Table 2.1. Characteristics of the synthesized mPEG-*b*-p(HPMA-Bz) block copolymers as determined by ^{1}H-NMR and GPC. M_n = number average molar mass, M_w = weight average molar mass and Đ = molar mass dispersity.

Polymer	MI:M	M_n by ^{1}H-NMR (kDa)	M_n by GPC (kDa)	M_w by GPC (kDa)	Đ (M_w/M_n) by GPC	Yield (%)
$mPEG_{5K}$-*b*-p(HPMA-Bz)$_{18.5K}$	1 : 200	23.5	18.9	21.1	1.12	72
$mPEG_{5K}$-*b*-p(HPMA-Bz)$_{9.6K}$	1 : 100	14.6	17.3	19.6	1.13	79
$mPEG_{5K}$-*b*-p(HPMA-Bz)$_{7.7K}$	1 : 75	12.7	16.4	18.7	1.14	81
$mPEG_{5K}$-*b*-p(HPMA-Bz)$_{4.7K}$	1 : 50	9.7	15.1	17.4	1.15	83
$mPEG_{5K}$-*b*-p(HPMA-Bz)$_{2.2K}$	1 : 25	7.2	12.8	14.8	1.16	83
$mPEG_{5K}$-*b*-p(HPMA-Bz)$_{1.0K}$	1 : 12.5	6.0	9.8	12.2	1.23	84
$mPEG_{2K}$-*b*-p(HPMA-Bz)$_{20.6K}$	1 : 200	22.6	13.5	19	1.42	59
$mPEG_{2K}$-*b*-p(HPMA-Bz)$_{10.9K}$	1 : 100	12.9	10.7	16	1.51	74
$mPEG_{2K}$-*b*-p(HPMA-Bz)$_{7.7K}$	1 : 75	9.7	8.5	17.1	1.57	53
$mPEG_{2K}$-*b*-p(HPMA-Bz)$_{5.3K}$	1 : 50	7.3	8.1	12.6	1.55	87
$mPEG_{2K}$-*b*-p(HPMA-Bz)$_{2.6K}$	1 : 25	4.6	5.7	8.2	1.45	82
$mPEG_{2K}$-*b*-p(HPMA-Bz)$_{1.2K}$	1 : 12.5	3.2	4.4	5.7	1.31	87

The average kinetic chain length for free radical chain polymerization is defined as the average number of monomers polymerized per initiated chain and is proportional to the monomer concentration $[M_0]$ divided by the square root of the initiator concentration $[I_0]^{-1/2}$.[36,37] Plotting the number average molecular weight (M_n) as measured by ^{1}H-NMR spectroscopic analysis against the average kinetic chain length indeed resulted in a linear correlation for both the $mPEG_{5K}$ and $mPEG_{2K}$ block copolymers (**Figure 2.2**) as also observed previously for the block copolymer mPEG-*b*-pHPMAmLac$_n$ (methoxy poly(ethylene glycol)-*b*-poly[N-(2-hydroxypropyl) methacrylamide-lactate]).[38]

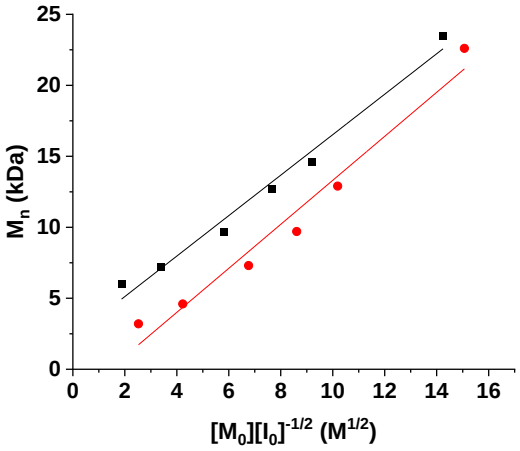

Figure 2.2. Linear correlation between the number average molecular weight (M_n) as measured by ^{1}H-NMR of mPEG-*b*-p(HPMA-Bz) as a function of the feed molar concentration of monomer divided by the square root of the feed molar concentration of initiator ($[M_0][I_0]^{-1/2}$) (black: mPEG$_{5k}$-*b*-p(HPMA-Bz)$_n$ with r^2 = 0.98; red: mPEG$_{2K}$-*b*-p(HPMA-Bz)$_n$ with r^2 = 0.97).

Residual solvent and kinetics of micelle formation

To get insight into the kinetics of micelle formation and the rate of removal of THF, in which the mPEG$_{5K}$-*b*-p(HPMA-Bz)$_{18.5K}$ polymer was dissolved at 20 mg/mL, the size of micelles was followed in time after direct addition of the THF/polymer solution to water (THF/water was 1:1 v/v). The hydrodynamic diameters of the micelles were measured using DLS, and THF content was measured using GC-headspace analysis directly after addition (0 h) and at regular time intervals up to 96 h (**Figure 2.3**). Directly after addition of the polymer solution to water, particles with a hydrodynamic diameter of approximately 80 nm and a polydispersity (PDI) value of less than 0.1 were formed. After 24 h, the micelles showed a decrease in size to 50 nm, and a residual THF content of ~3000 ppm was detected. At 25 h the micellar dispersion was spiked with an additional 50 volume percentage of THF, which resulted in an immediate increase in micelle size from 50 to 70 nm. It can therefore be concluded that there is a direct correlation between the remaining amount of THF and the hydrodynamic diameter of the micelles. It should be noted that the final micelle size of 50 nm was already reached at THF concentrations of less than 10^5 ppm. Addition of THF to the micellar dispersion

showed that the core of the micelles can become swollen by accommodating part of the added THF. After 48 h of evaporation, the residual THF content was ~3000 ppm. This is not sufficient to obtain a product within the acceptable range below 720 ppm according to the International Council of Harmonization of Technical Requirements for Registration of Pharmaceuticals for Human Use.[39] Therefore, the evaporation time was extended to 96 h and the micellar dispersion was also dialyzed against water to remove any residual THF. The final THF content after dialysis, as measured by GC headspace, was below the detection limit (10 ppm).

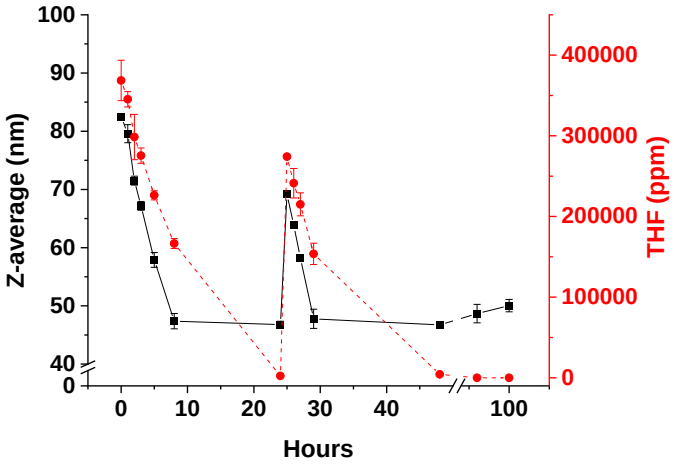

Figure 2.3. Average hydrodynamic diameter (black) of mPEG$_{5K}$-*b*-p(HPMA-Bz)$_{18.5K}$ micelles and THF concentration (red) of the micellar dispersion as a function of time. At 25 h the dispersion was spiked with THF. After a second overnight evaporation (48 h) and subsequent over weekend evaporation (96 h) the samples were dialyzed overnight, which is represented at time point 100 h in the graph.

Effect of the hydrophobic/hydrophilic block molecular weight of mPEG-b-p(HPMA-Bz) on the micelle size

To investigate the effect of the hydrophobic/hydrophilic block molecular weight of the polymers on the micelle size, micelles were prepared from the synthesized polymers of **Table 2.1**. The polymers were dissolved in THF at 20 mg/mL and used to prepare micelles through the nanoprecipitation method in water as described in the Experimental Details section. All $mPEG_{5K}$ block copolymers formed micelles as was demonstrated by cryo-TEM and DLS analysis.

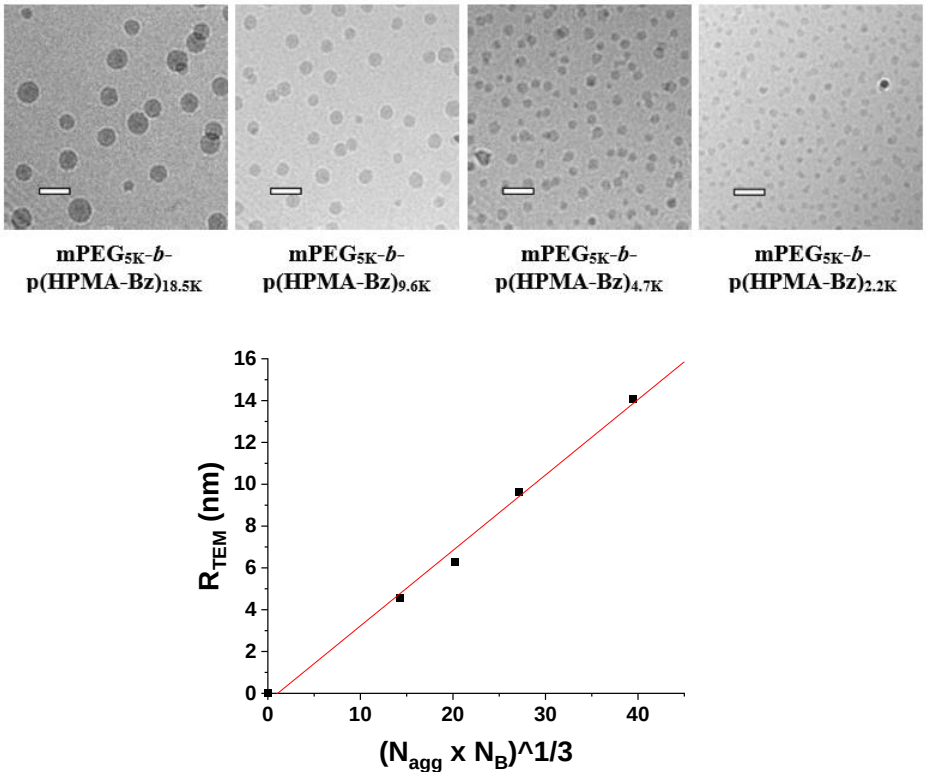

Figure 2.4. Cryo-TEM and AF4-MALS results. (Top) cryo-TEM images showing particle size variation upon molecular weight changes of the $mPEG_{5K}$ block copolymers used; scale bars correspond to 50 nm. (Bottom) the average micelle core diameter measured by cryo-TEM as a function of the cubic root of the product of the degree of polymerization (N_B) of the hydrophobic blocks of the copolymers as determined by ^{1}H-NMR, and the aggregation number (N_{agg}) of the corresponding micelles revealed by AF4-MALS, $r^2 = 0.99$.

Both the DLS and the cryo-TEM results showed that the micelle size proportionally increased from the smallest to largest molecular weights of the hydrophobic block from 30 to 48 nm for the hydrodynamic diameter and from 9 to 28 nm for the cryo-TEM diameter (**Figure 2.4** and **Figure S2.3**). The PDI values were lower than 0.1 pointing to a narrow size distribution, which is in agreement with the results of the TEM pictures. More precisely, the histograms of the TEM diameters based on ~100 to ~400 micelles (for $mPEG_{5K}$-*b*-$p(HPMA\text{-}Bz)_{18.5K}$ and $mPEG_{5K}$-*b*-$p(HPMA\text{-}Bz)_{2.2K}$ copolymer respectively) exhibited normalized standard deviations of 25% at most. The hydrated layer of the micelles was estimated by the difference of radii between the radius of hydration (R_h) and the radius as determined by TEM (R_{TEM}) and appeared to be constant for the four samples (approximately 10 nm; **Table 2.2**).

The radius of gyration (R_g), radius of hydration (R_h) and M_w of the micelles based on a selection of $mPEG_{5K}$ polymers of **Table 2.1** were determined by AF4-MALS (**Table 2.2**). The ratio of R_g/R_h is structure sensitive and provides information about the morphology of a system. The ratio for rigid spherical structures with a uniform density is $\sqrt{3/5} \approx 0.775$.[40–42] Structures with a dense core and a partly coiled less dense shell (core-shell structures) show a smaller R_g and therefore have R_g/R_h values lower than 0.775. [40–45] Based on the MALS data, the produced $mPEG_{5K}$-*b*-p(HPMA-Bz) micelles had a core-shell structure because the R_g/R_h ratios were between 0.59 and 0.64 and thus lower than that of typical rigid spheres. This core-corona structure was also confirmed using ^{1}H-NMR analysis of the micelles dispersed in deuterium oxide (D_2O) (**Figure S2.4**). The ^{1}H-NMR spectrum of mPEG-*b*-p(HPMA-Bz) block copolymer dissolved in DMSO-d_6 (**Figure S2.4**) showed resonances that can be assigned to the protons of both mPEG as the hydrophilic part (3.40-3.60 ppm) and p(HPMA-Bz) as the hydrophobic block (5.25 ppm and 7.25-8.25 ppm). The self-assembled structure of the mPEG-*b*-p(HPMA-Bz) block copolymer in D_2O only showed resonances belonging to the mPEG block of the copolymer while the peaks of the p(HPMA-Bz) block completely disappeared due to suppression of molecular motion of the hydrophobic part inside the core of the micelles. [46,47]

Table 2.2. Characteristics of mPEG$_{5K}$-*b*-p(HPMA-Bz) micelles prepared from a 20 mg/mL THF solution and determined by AF4-MALS; R_g = radius of gyration (nm); R_h = hydrodynamic radius (nm); R_{TEM} = radius as measured by TEM (nm); $M_{w(mic)}$ = weight average molecular weight of the micelles (10^6 Da); N_{agg} = the micelle aggregation number; σ^{-1} = mean surface area per molecule calculated by $\sigma^{-1} = d^2 = 4\pi R_h^2 / N_{agg}$ where d is the inter-chain distance (nm^2); H = shell brush height calculated by the de Gennes-Alexander model $H = N_A a_A (a_A/d)^{2/3}$ (nm).

Polymer	R_g	R_h	R_{TEM}	R_g/R_h	$M_{w(mic)}$	N_{agg}	$\sigma^{-1} = d^2$	H	R_h-R_{TEM}
mPEG$_{5K}$-*b*-p(HPMA-Bz)$_{18.5K}$	15	24	14.1	0.63	21.2	905	8.2	8.9	9.9
mPEG$_{5K}$-*b*-p(HPMA-Bz)$_{9.6K}$	12	20	9.6	0.59	7.5	513	9.3	8.4	10.4
mPEG$_{5K}$-*b*-p(HPMA-Bz)$_{4.7K}$	12	18	6.3	0.63	4.0	416	10.0	8.3	11.7
mPEG$_{5K}$-*b*-p(HPMA-Bz)$_{2.2K}$	10	15	4.6	0.64	2.1	291	10.0	8.4	10.4

AF4-MALS also revealed that the micelle aggregation number (N_{agg}), calculated by dividing the weight average molecular weight of the micelles ($M_{w(mic)}$) by the M_n of the polymer as determined by ^{1}H-NMR analysis, decreased with decreasing molecular weight of the hydrophobic block of the block copolymer. This was also observed in dissipative particle dynamic simulations of A-B diblock copolymers by Li et al. and Sheng et al. where the N_{agg} increases by either increasing the hydrophobic interaction energy through varying the repulsive parameter within the hydrophobic block B or decreasing the molecular weight of the hydrophilic block A.[48,49] In our system, the molecular weight of the hydrophobic block B was varied between 2.2 and 18.5 kDa, which corresponds to degrees of polymerization N_B between 10 and 68, while the molecular weight of the hydrophilic block A was kept at 5 kDa (N_A=114). However, even the lowest M_n of the hydrophobic block p(HPMA-Bz) of 2.2 kDa still provided sufficient hydrophobicity for micelle formation by creating a packed core structure. Already indicated by the disappearance of the B block peaks in ^{1}H NMR spectroscopy, this statement can also be proved by a polymer physics consideration. As shown in **Figure 2.4**, the TEM radii that reflect the hydrophobic cores of the micelles follow a power law with the product of N_B and N_{agg} of exponent 1/3, characteristic for a collapsed state of the B block chains.[50] On the opposite, the mPEG chains of the corona are highly swollen by water, making them invisible on the TEM images. The

surface area per mPEG chain was calculated by dividing the surface area of the micelles ($4\pi R_h^2$) by the number of molecules (N_{agg}) and assimilated with the square of the inter-chain distance (d), neglecting a geometrical pre-factor. This spacing between mPEG molecules remained approximately the same for all samples (d~3.0±0.1 nm) since both N_{agg} and R_h decreased simultaneously when N_B was decreased. When using de Gennes-Alexander theory of polymer brushes, the mPEG height was estimated by $H=N_A a_A (a_A/d)^{2/3}$. [51–53] The values obtained by this model are shown in **Table 2.2** and were found approximately constant H~8.5±0.3 nm, using N_A=114 and a Kuhn length per mPEG segment $a_A = 0.33$ nm obtained from the bond lengths and coarse grain simulations.[54] In agreement with the constant difference of ~10 nm that was observed between R_h and R_{TEM}, one can deduce that the mPEG chains forming the corona of the micelles are densely packed and in a stretched conformation (brush regime). However, there was no curvature effect on the brush height as there was no variation observed with the micelle core size, which corresponds to the "crew cut" regime of micelles rather than the "star-like" regime that would require longer hydrophilic blocks. [55] Of the $mPEG_{2K}$ copolymers only $mPEG_{2K}$-*b*-$p(HPMA\text{-}Bz)_{2.6K}$ and $mPEG_{2K}$-*b*-$p(HPMA\text{-}Bz)_{1.2K}$ formed clear micellar dispersions with a size of the micelles of 25 nm and PDI value lower than 0.2. On the other hand, the block copolymers with higher molecular weight of the hydrophobic block (between 5.3 and 20.6 kDa) (**Table 2.1**) aggregated after THF evaporation. Cryo-TEM analysis of $mPEG_{2K}$-*b*-$p(HPMA\text{-}Bz)_{20.6K}$ after nanoprecipitation confirmed that mainly aggregates were formed, yet showing an interesting internal structure appearing as densely packed spherical globules (**Figure S2.5**). Typically, the spherical micelle shape is stable if the core diameter does not exceed too much the dimensions of the corona, which is estimated at 3.3 nm using de Gennes-Alexander formula with $N_A = 45$ for $mPEG_{2K}$. This is the case when the right balance of hydrophilic to hydrophobic ratio is used. When increasing the hydrophobic content, this will eventually cause phase separation, as mentioned by Sheng et al.[49] In other words, the ratio between the hydrophilic and hydrophobic block influences the critical packing parameter, which in turn can predict whether either micelles or aggregates are formed. These scaling laws state that once the effective hydrophilic surface area at the aggregate solution interface is reached, the volume occupied by the hydrophobic chains in the aggregate core becomes too large to be able to form spherical micelles or vesicles.[56,57] Cylindrical and lamellar aggregates, but also aggregated precipitated structures will in these

cases be observed as is the case for the $mPEG_{2K}$ block copolymers with higher molecular weight of the hydrophobic block.

Critical micelle concentration determination

The critical micelle concentrations (CMCs) of the polymers of **Table 2.1** were determined using the commonly used pyrene method. Pyrene is a hydrophobic fluorescent molecule that shows a shift of the excitation wavelength (from 300 to 360 nm) as a result of its partitioning in the hydrophobic core of polymeric micelles. [58] **Figure 2.5** shows the CMC values for the block copolymers with a fixed hydrophilic mPEG block of 5 kDa and a varying molecular weight of the hydrophobic p(HPMA-Bz) block. For the polymer $mPEG_{5K}$-*b*-$p(HPMA\text{-}Bz)_{18.5K}$ (total M_w of 23.5 kDa), the CMC is 2.3 µg/mL. On the other hand, the block copolymer with the smallest hydrophobic block $mPEG_{5K}$-*b*-$p(HPMA\text{-}Bz)_{1.0K}$ (total M_w of 6 kDa) had a CMC of 16.4 µg/mL. This demonstrates that a block copolymer with only ~5 monomeric units in the hydrophobic block is already able to form micelles pointing to strong π-π stacking interactions. It was also shown that the CMCs of the polymers decreased with increasing molecular weight of the hydrophobic block. This trend has previously been reported in literature. [47,59,60] The CMCs of $mPEG_{2K}$-*b*-$p(HPMA\text{-}Bz)_{2.6K}$ and $mPEG_{2K}$-*b*-$p(HPMA\text{-}Bz)_{1.2K}$ are 5.1 and 7.4 µg/mL respectively (**Figure 2.5**). These CMCs are still lower compared to the $mPEG_{5K}$-*b*-$p(HPMA\text{-}Bz)_{2.2K}$ and $mPEG_{5K}$-*b*-$p(HPMA\text{-}Bz)_{1.0K}$, with a CMC of 10.2 and 16.4 µg/mL respectively, where the only difference between those polymers is the molecular weight of the hydrophilic mPEG block being 2 or 5 kDa. Therefore, as expected and previously shown for other systems, it can be concluded that both the size of the hydrophobic block and the hydrophilic/hydrophobic ratio determine the CMC value. [61,62]

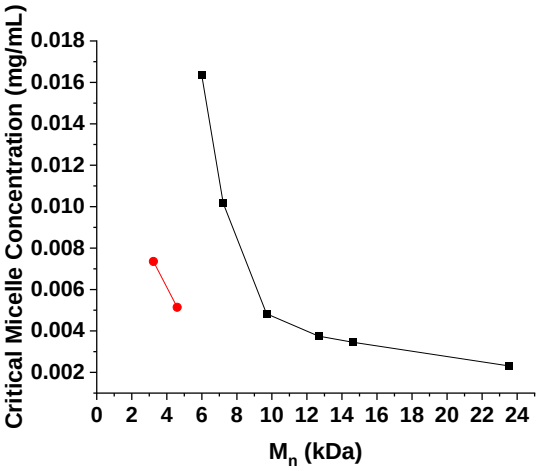

Figure 2.5. Critical micelle concentration as a function of polymer molecular weight. The black line shows the CMC of the polymers with a fixed mPEG of 5 kDa, whereas the red line shows the CMC of the polymers with a fixed mPEG of 2 kDa.

The effect of free homopolymer and free PEG on the size of micelles

To investigate the effect of homopolymer in the polymer mixture on micelle size, homopolymers p(HPMA-Bz) were synthesized with an M_n of 14.5, 11.2 and 5.5 kDa. Subsequently, known amounts of the p(HPMA-Bz)$_{14.5K}$ homopolymer together with mPEG$_{5K}$-*b*-p(HPMA-Bz)$_{18.5K}$ were dissolved in THF and added to water to obtain micelles with PDI values lower than 0.2. **Figure 2.6A** shows that with increasing amounts of homopolymer in the THF solution, the size of the obtained micelles increased proportionally. Since the p(HPMA-Bz)$_{14.5K}$ homopolymer is very hydrophobic it will very likely partition inside the hydrophobic core of the micelles resulting in an increase in micellar size. Similar results were observed for mPEG$_{5K}$-*b*-p(HPMA-Bz)$_{9.6K}$ and mPEG$_{5K}$-*b*-p(HPMA-Bz)$_{4.7K}$, upon addition of homopolymers with an M_n of 11.3 kDa and 5.5 kDa to the feed (**Figure 2.6B**). It also shows that the effect of the added homopolymer on the size of the micelles is larger for micelles made of polymers with a smaller hydrophobic domain. A possible explanation is that block copolymers with a smaller hydrophobic block are relatively more soluble in water, as also shown by a higher CMC, making them more susceptible to the conditions at which the mixing and solvent shifting occur. Additionally, the N_{agg} of the micelles is lower for the smaller polymers.

Therefore, incorporation of homopolymer in the core of the micelles based on lower polymer molecular weight increases the size of micelle more drastically.

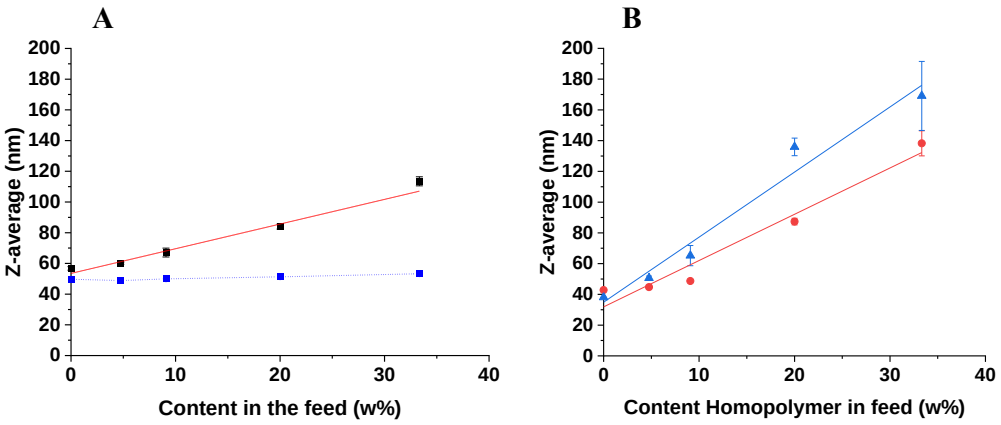

Figure 2.6. Average hydrodynamic diameter of mPEG$_{5K}$-*b*-p(HPMA-Bz)$_x$ polymers as a function of content feed. (**A**) mPEG$_{5K}$-*b*-p(HPMA-Bz)$_{18.5K}$ in black/red as a function of p(HPMA-Bz)$_{14.5K}$ homopolymer content in the feed, and in blue as a function of free mPEG$_{5K}$ content in the feed (n=3). (**B**) Red: mPEG$_{5K}$-*b*-p(HPMA-Bz)$_{9.6K}$ with p(HPMA-Bz)$_{11.3}$ and Blue: mPEG$_{5K}$-*b*-p(HPMA-Bz)$_{4.7K}$ with p(HPMA-Bz)$_{5.5}$.

Figure 2.6A and B and previous studies of Kataoka et al. [23] and Kimura et al. [63] show that the presence of homopolymer in the feed can be exploited to tailor the size of polymer micelles. Kataoka et al. mixed poly(glutamic acid) homopolymer with PEG–b-poly(glutamic acid) to control the size of micelles [23] and Kimura et al. used poly(L-lactic acid) homopolymer to control the size of (sarcosine)-b-(L-lactic acid) nano-particles. [63]

Besides p(HPMA-Bz), the block copolymer mixture might also contain less than 5% free mPEG as mentioned before. We therefore also examined the effect of free mPEG on the size of micelles by adding excess amounts of mPEG to the polymer mixture (**Figure 2.6A**). The presence of up to 40% of free mPEG did not result in changes in micelle size, which is probably due to the high solubility of mPEG$_{5K}$ in water.

The effect of polymer concentration and rate of addition on micelle size

Micelles were prepared by addition of THF with varying concentrations of $mPEG_{5K}$-*b*-$p(HPMA\text{-}Bz)_{18.5K}$ block copolymers. **Figure 2.7A** shows that the hydrodynamic diameter of the formed micelles decreased from approximately 80 to 50 nm with increasing polymer concentration in THF. Concomitantly, the micelles had a smaller size distribution at higher initial polymer concentrations, as indicated by the decreasing indices from 0.3 to less than 0.1. Although less obvious, similar results were observed for $mPEG_{5K}$-*b*-$p(HPMA\text{-}Bz)_{9.6K}$ and $mPEG_{5K}$-*b*-$p(HPMA\text{-}Bz)_{4.7K}$ of which the sizes changed from approximately 50 to 42 nm and from approximately 42 to 36 nm, respectively, upon increasing the polymer concentration in THF (**Figure 2.7A**). These results suggest that the self-assembly is based on a nucleation-controlled process where the size of micelles is dependent on the nucleation rate. A larger number of nuclei will thereby result in smaller micelles. [64] This trend was also observed in the study of Caron et al. where higher initial concentration of squalenoyl prodrug in the organic phase yielded smaller sized self-assemblies. [65] The concentration dependency on the resulting micelle size was also confirmed in another experiment where the final concentration of the polymer in the water phase after THF evaporation was fixed at 10, 20 and 30 mg/mL, but the ratio of organic solvent to water was reduced from 1:1 to 0.3:1 using less THF (0.3, 0.6 and 1 mL) to dissolve the same amount of polymer (**Figure 2.7B**). Higher initial polymer concentrations in the organic phase upon mixing with the water phase led to higher supersaturation and consequently to more nuclei and smaller micelles. Also, at higher THF content the supersaturation state is lower, decreasing nucleus formation. Therefore, as expected, smaller micelles were obtained at 0.3:1 compared to 1:1 volume ratio. [66] Furthermore, the size of the micelles reached a minimum at approximately 50-55 nm suggesting a critical particle size was obtained and increasing the concentration did not affect the size anymore. [67]

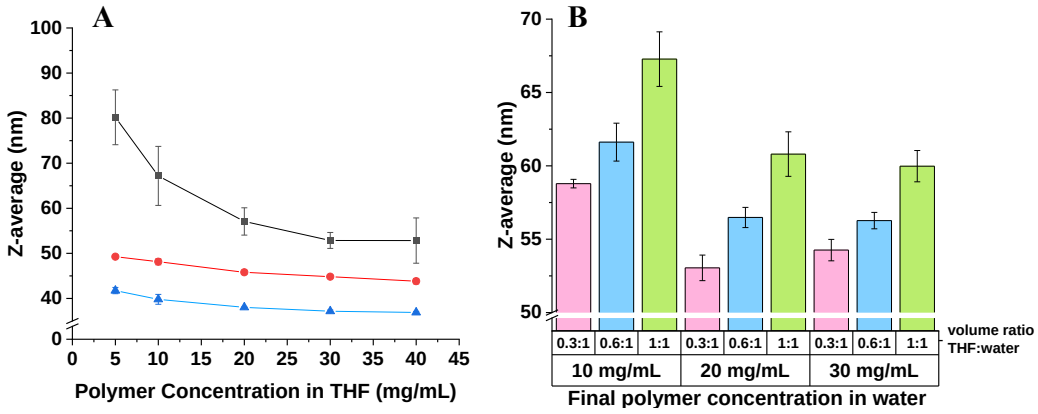

Figure 2.7. Hydrodynamic diameters of micelles as a function of polymer concentration. (**A**) The ratio of THF added to water was 1:1; Black: mPEG$_{5K}$-*b*-p(HPMA-Bz)$_{18.5K}$, Red: mPEG$_{5K}$-*b*-p(HPMA-Bz)$_{9.6K}$ and Blue: mPEG$_{5K}$-*b*-p(HPMA-Bz)$_{4.7K}$; (**B**) The effect of changing the concentration of polymer in THF using different THF to water volume ratios. The final polymer concentrations were 10, 20 and 30 mg/mL (n=3).

As the nucleation rate is dependent on supersaturation and is also affected by the quality of mixing, different rates of addition of organic polymer solution to aqueous phase were used to manipulate the supersaturation state. Thus, micelles were prepared at different addition rates of the polymer solution to water and by fast addition of water to the organic phase (**Figure 2.8**). The hydrodynamic diameters of mPEG5K-b-p(HPMA-Bz)$_{18.5K}$ micelles after THF evaporation were 82 and 62 nm with PDI values of less than 0.1 and 0.2 at addition rates of 0.15 and 1.5 mL/min, respectively. Also, the sizes of the micelles upon rapid addition of the polymer solution to the water phase, or the water phase to the polymer solution were 58 and 56 nm, respectively, with PDI values of less than 0.1, reaching the minimal micelle size. This is similar to the finding reported by Aliabadi et al. in which no significant difference in size of MePEO-b-PCL micelles prepared by addition of water to acetone, or acetone to water was observed. [68] As expected, similar results were observed using mPEG$_{5K}$-*b*-p(HPMA-Bz)$_{9.6K}$ and mPEG$_{5K}$-*b*-p(HPMA-Bz)$_{4.7K}$ polymers (**Figure 2.8**). However, the PDI values of the micellar dispersions were higher (0.35 and 0.45) at 0.15 ml/min rate of addition. Generally, during nanoprecipitation, both nucleation and particle growth occur in the water/THF mixture even before complete mixing. So, when the polymer solution is added slowly to water, there is a continuous change in the composition of the mixture

which results into less homogeneous supersaturation. Fast addition of THF to water, on the other hand, results in a fast mixing which in turn is associated with rapid supersaturation causing the formation of smaller nuclei and thus smaller and more monodisperse micelles. [69]

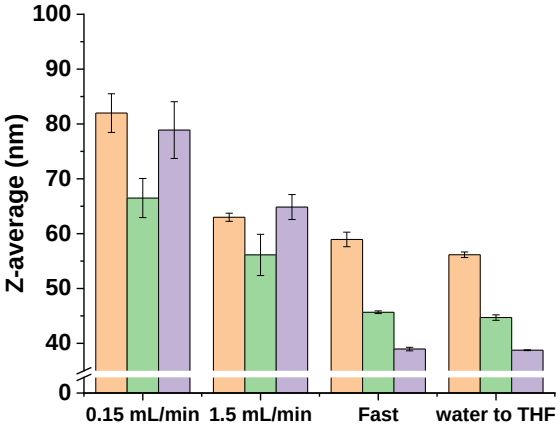

Figure 2.8. The effect of addition rate of the polymer solution in THF to the aqueous phase on micelle size; Orange bars: mPEG$_{5K}$-*b*-p(HPMA-Bz)$_{18.5K}$, Green bars: mPEG$_{5K}$-*b*-p(HPMA-Bz)$_{9.6K}$ and Purple bars: mPEG$_{5K}$-*b*-p(HPMA-Bz)$_{4.7K}$; the samples were stirred during and until 1 minute after addition of the polymer solution to aqueous buffer (n=3).

The effect of different solvents and buffers on micelle size

The effect of the type of organic solvent on the size of HPMA-Bz micelles was also investigated. THF, acetonitrile, acetone, ethanol, 1,4-dioxane, DMSO and DMF were used because of their miscibility with water and ability to dissolve the mPEG-*b*-p(HPMA-Bz) block copolymers. The polymer concentrations in organic solvent were fixed at 20 mg/mL to avoid the effect of polymer concentration on the nanoprecipitation process. In the case of ethanol, the polymer was only soluble at temperatures above ~60˚C and thus the micelle preparation was conducted using polymer solutions and water at 70˚C. Subsequently the solvents were removed by either evaporation (for THF, acetonitrile and acetone) or, in case of the less volatile solvents dioxane, DMSO, DMF and ethanol, by dialysis. As depicted in **Figure 2.9A**, the use of DMSO and DMF resulted into large micelles, 175 and 75 nm, respectively, compared to the micelles formed using THF, which were 50 nm. Acetone, acetonitrile and dioxane resulted in smaller micelles of approximately 45 nm

with PDI values lower than 0.2. Generally, solvents with a lower viscosity such as THF, acetone and acetonitrile mix faster with water which causes more uniform supersaturation, leading to smaller micelles.[69] On the other hand, solvents with relatively higher viscosity and surface tension (DMF and DMSO) have slower mixing rates with water, resulting in the growth of micelles and larger self-assemblies. In line with our observations, Kissel et al. reported that nanoparticles prepared using acetone were smaller than particles prepared in THF (140 and 180 nm respectively) due to its lower viscosity and higher diffusion rate in water.[70]

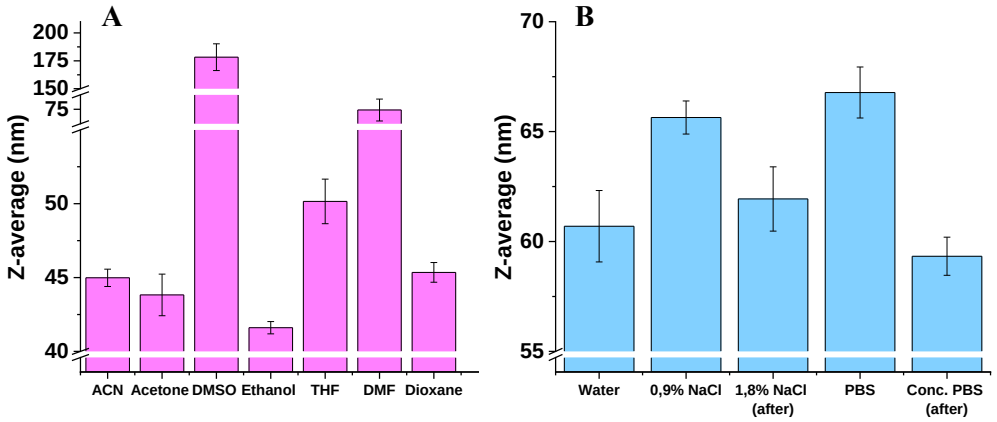

Figure 2.9. The effect of different solvents and aqueous phases on the hydrodynamic diameter of mPEG$_{5K}$-*b*-p(HPMA-Bz)$_{18.5K}$ micelles. (**A**) The effect of different solvents. (**B**) the effect of different aqueous phases; in the graph, bars depicted with (after), were samples prepared in water and later concentrated solutions of salts were added (n=3).

The effect of the composition of the aqueous phase on the size of the obtained micelles was evaluated by addition of a 20 mg/mL polymer solution in THF to different aqueous phases. The micelles were slightly larger when they were made in either PBS or 0.9% NaCl solution (85 and 80 nm respectively). Addition of salt to water increases the viscosity of the aqueous phase which in turn affects the mixing of solvent and non-solvent and thus nanoprecipitation of micelles in line with previous studies.[71] However, once the micelles were formed in water and the aqueous phase was subsequently adjusted by adding concentrated 1.8 % NaCl solution or twice concentrated PBS, the size of micelles did not change (**Figure 2.9B**) showing that the micellar structures are thermodynamically stable after formation.

CONCLUSION

The results of this study demonstrate that the self-assembly of mPEG-*b*-p(HPMA-Bz) polymers into micelles can be easily tailored in size. This size-control relies on both the molecular weight of the polymers and the processing methods which change the saturation conditions. In short it can be said that reducing the micelle size can be accomplished by controlling the polymerization step and optimizing the polymer molecular weight by using higher hydrophilic to hydrophobic ratios. The size dependency coming from those ratios, fits excellently into the de Gennes-Alexander theory and scaling law. Reducing the homopolymer content as a potential byproduct of block copolymer synthesis will also optimize the production of smaller micelles. Moreover, in terms of processing conditions, the use of organic solvents with faster mixing quality with water and applying higher rates of addition yield smaller and more homogenous micelles. This systematic study is of great importance as it indicates which parameters during the micelle formation process are critical to allow reproducible formation of micelles with a desired size.

ACKNOWLEDGEMENTS

Mahsa Bagheri and Aida Varela-Moreira are thanked for their experimental contributions and fruitful discussions. Dr. Olivier Sandre, Dr. Bart Metselaar and Dr. René van Nostrum are acknowledged for the useful discussions. Dr Alexander Mason and Imke Welzen-Pijpers are acknowledged for their efforts to provide cryo-TEM images.

We are also grateful for the financial support received from the European Union's Horizon 2020 research and innovation program Marie Sklodowska-Curie Innovative Training Networks (ITN) under grant No. 676137.

MATERIALS AND METHODS

Materials

4-(Dimethylamino)pyridine (DMAP), p-toluenesulfonic acid, 4,4-azobis(4-cyanopentanoic acid) (ABCPA), DL-1-amino-2-propanol, methacryloyl chloride, benzoyl chloride, poly(ethylene glycol) methyl ether (mPEG) 2 kDa, N,N'-dicyclohexylcarbodiimide (DCC), trichloroacetyl isocyanate (TAIC), bovine serum albumin and pyrene were obtained from Sigma-Aldrich (Darmstadt, Germany) and used without further purification. mPEG 5 kDa was obtained from Polysciences (Warrington, USA) and dried in a vacuum oven overnight at 70 °C. Easivial PEG standards for GPC analysis were obtained from Agilent (Santa Clara, USA). All solvents were purchased from commercial suppliers and used as received.

^{1}H-NMR

The MI sample was prepared by dissolving 20 mg product in 700 µL $CDCl_3$. To determine the unreacted mPEG-OH content, TAIC was added to the sample and analyzed again after 20 minutes using ^{1}H-NMR spectroscopy. After reaction with TAIC, the signal of the methylene group neighboring the terminal hydroxyl group shifts from 4.2 to 4.4 ppm and the amount of unreacted mPEG-OH could subsequently be determined based on the peak areas. [29,32]

The synthesized polymers samples were prepared by dissolving 20 mg of polymer in 700 µL DMSO-d6.

All samples were analyzed using a 400 MHz NMR with a 5 mm PABBO BB probe from Bruker.

GPC

MI and synthesized polymers samples were prepared by dissolving approximately 5 mg in 1 mL DMF containing 10 mM LiCl. They were analyzed by GPC, to determine the number average molecular weight (M_n), weight average molecular weight (M_w) and molar mass dispersity (Đ), using a PSS PFG analytical linear S column and PEGs of narrow molecular weights as calibration standards as described previously. Samples of 20 µL were injected, the eluent was DMF containing 10 mM LiCl, the elution rate was 0.7 mL/min,

the temperature was 40˚C and detection was done using a refractive index detector. [38]

Dynamic light scattering (DLS)

The size of the formed micelles was determined by DLS using a Malvern Zetasizer nano series ZS90 with a measurement angle of 90° and a temperature of 25 °C. Unless stated differently, the concentration of the micellar dispersions was 20 mg/mL.

Gas chromatography headspace analysis (GC-headspace)

GC-headspace was conducted to determine the residual solvent contents in the different micellar dispersions using a Shimadzu GC-2010 equipped with a Flame Ionization Detector and Shimadzu HS-20 headspace auto-sampler. A 30 m x 0.32 mm capillary column with a film thickness of 0.25 µm was used. An internal standard stock solution was prepared by dissolving 150 µL 2-propanol (analytical standard) in water in a volumetric 100 mL flask. 1 mL of this solution was transferred into a 100 mL volumetric flask and diluted to the 100 mL volume with DMF. Samples were prepared by taking 50 µL of micellar dispersion and dissolving it in 1 mL DMF, and subsequently 4 mL internal standard stock solution was added. The flow rate of nitrogen was 1.8 mL/min. All measurements were done in triplicate.

Cryogenic transmission electron microscopy (cryo-TEM) analysis

Cryo-TEM measurements were performed on selected micelles. Samples were prepared on Quantifoil R 2/2 grids. In short, 3 µL micellar dispersion was pipetted onto the grid and blotted for 3 seconds using a fully automated vitrification robot (MARK III) at 100% relative humidity. The grid was subsequently plunged and frozen in liquid ethane. Micrographs were taken using a FEI Tecnai G2 Sphere (200 kV electron source) equipped with LaB6 filament utilizing a cryoholder or a FEI Titan (300 kV electron source) equipped with an autoloader station.

Analysis of the micelles by Asymmetric Flow Field-Flow Fractionation connected to Multi-Angle Light Scattering detector (AF4-MALS)

The radius of gyration (R_g) and weight-average molecular weight (M_w) of some selected micelles was determined using a Wyatt Dualtec AF4 instrument connected to a Shimadzu LC-2030 Prominence-I system with a Shimadzu LC-

2030 auto-sampler. Fractionation was performed on an AF4 short channel with a 10 kDa membrane of regenerated cellulose and a spacer of 350 µm. The AF4 was connected to a light scattering detector (Wyatt DAWN HELEOS II) installed at 16 different angles ranging from 12.9 to 157.8˚ using a laser operating at 664.5 nm and a refractive index detector (Wyatt Optilab). Bovine serum albumin dissolved in phosphate buffer saline (PBS) pH 7.4 with a concentration of 5 mg/mL was used for calibration. The data were analyzed using ASTRA software. Also, to be able to calculate the M_w of micelles using the Zimm plot method [72], the refraction index increment (dn/dc) of the polymers was measured in water by injection of 600 µL of precisely weighted samples in the range of 6 to 15 mg/ml and using a flow rate of 0.6 mL/min in an Optilab Rex detector (Wyatt technology).

Critical micelle concentration (CMC) determination

The CMC of the different block copolymers in water was determined using pyrene as a fluorescent probe. [35,58] Samples were prepared by dissolving the polymers in THF at different concentrations of which 500 µL was added to 4.5 mL 120 mM ammonium acetate buffer pH 5.0. This was followed by solvent evaporation. The final polymer concentrations ranged from 1.9×10^{-6} to 1.0 mg/mL. A 15 µL solution of pyrene in acetone (0.18 mM) was added to the polymer solution in buffer and the solvent was allowed to evaporate overnight. Fluorescence excitation spectra of pyrene between 300 and 360 nm were recorded with an emission wavelength at 390 nm at 37 °C using a UV spectrometer (Jasco FP-8300 Fluorescence Spectrometer). The excitation and emission band slits were 4 and 2 nm, respectively. The intensity ratio of I_{338}/I_{333} was plotted against the polymer concentration to calculate the CMC.

Optimized macro-initiator (MI) synthesis

mPEG-ABCPA-mPEG macro-initiators were synthesized through an esterification of mPEG (molecular weight 2.0 or 5.0 kDa) and ABCPA, using DCC as a coupling reagent and 4-(dimethylamino) pyridinium 4-toluenesulfonate (DPTS; which was made by separately dissolving DMAP and p-toluenesulfonic acid in THF and mixing the two solutions using a 1:1 molar equivalence) as a catalyst (**Scheme 2.1**). [34] One equivalent ABCPA, 2 equivalents mPEG and 0.3 equivalents of DPTS (or 0.280 g ABCPA, 10 g mPEG, 0.094 g DPTS, respectively) were dissolved in 50 mL dry DCM and put on ice. Next, 3 equivalents of DCC (0.619 g DCC) were dissolved in 50

mL DCM and dropwise added to the mPEG solution under nitrogen atmosphere. After addition of DCC, the ice bath was removed allowing the reaction mixture to reach room temperature. After 16 h at room temperature, the reaction mixture was filtered to remove the precipitated 1,3-dicyclohexyl urea and the solvent was removed *in vacuo*. The product was dissolved in water, stirred for 2 h and dialyzed against water for 72 h at 4˚C. The sample was freeze-dried to obtain a fluffy white product with a yield of ~90% (^{1}H-NMR and GPC data can be found in **Figure S2.1** and **S2.2** respectively).

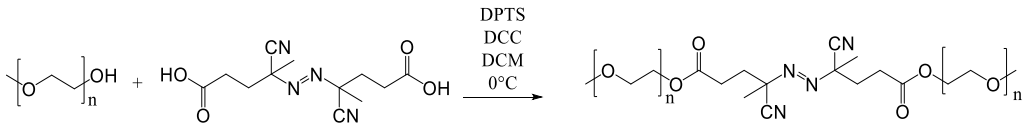

Scheme 2.1. Synthesis of mPEG-ABCPA-mPEG macro-initiator.

Polymer synthesis

mPEG-*block*-poly(*N*-2-benzoyloxypropyl methacrylamide) (mPEG-*b*-p(HPMA-Bz)) block copolymers (^{1}H-NMR can be found in **Figure S2.4**) were synthesized via free radical polymerization as described earlier using mPEG-ABCPA-mPEG as a macro-initiator and N-(2-benzoyloxypropyl methacrylamide) (HPMA-Bz) as the monomer. [28,35,73]mPEG-*b*-p(HPMA-Bz) block copolymers with different molecular weights of the hydrophobic and hydrophilic block were synthesized either by using $mPEG_{2K}$-ABCPA-$mPEG_{2K}$ or $mPEG_{5K}$-ABCPA-$mPEG_{5K}$ as a macro-initiator and by varying the molar feed ratios of macro-initiator:monomer (1:200, 1:100, 1:75, 1:50, 1:25, 1:12.5 mol/mol) (**Scheme 2.2**). In short, the selected macro-initiator and monomer amounts were dissolved at a total concentration of 0.3 g/mL in 20 mL of acetonitrile. The polymerization was conducted at 70˚C in a nitrogen atmosphere for 24 h. The resulting polymers were precipitated in cold diethyl ether and collected after centrifugation. Homopolymers of p(HPMA-Bz) were synthesized and collected in the same way using ABCPA as initiator and HPMA-Bz as monomer. The feed ratios of initiator:monomer were 1:200 (mol/mol), 1:100 (mol/mol) and 1:50 (mol/mol) with a total concentration of 0.3 g/mL in 10 mL acetonitrile to obtain a total of 2 g homopolymer after precipitation in cold diethyl ether and centrifugation.

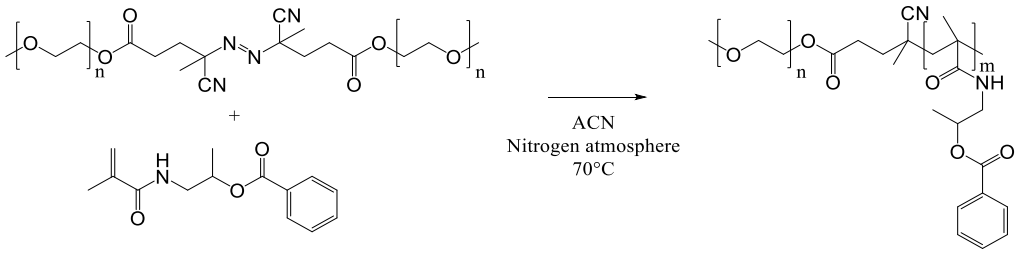

Scheme 2.2. Synthesis of mPEG-*b*-p(HPMA-Bz)

Micelle preparation

mPEG-*b*-p(HPMA-Bz) micelles were prepared in triplo by a nanoprecipitation of the polymer dissolved in THF, using water as non-solvent. First, the polymers were dissolved in THF and the obtained solutions were pipetted into MilliQ at a 1:1 volume ratio while stirring. Subsequently, THF was evaporated overnight at room temperature, resulting in the formation of micelles. To investigate the effect of polymer concentration on micellar sizes, samples were prepared using 5, 10, 20, 30, 40 mg/mL of polymer solution. Additionally, an experiment was carried out where the volume ratio of solvent-to-water was decreased from 1:1 to 0.6:1 and 0.3:1. Addition of the polymer/solvent solution to water was performed rapidly using a pipette while stirring. The final polymer concentrations in water were 10, 20 and 30 mg/mL. Thus, in total nine different conditions were tested. In the remainder of the experiments the polymer concentration was fixed at 20 mg/mL, unless mentioned otherwise. Besides THF, the following solvents were also used: acetonitrile, acetone, 1,4-dioxane, dimethylformamide (DMF), dimethylsulfoxide (DMSO) and ethanol. For the less/non-volatile solvents (dioxane, DMSO, DMF and ethanol), the residual solvent was removed by dialysis using a Spectra/Por dialysis membrane with a molecular weight cut off of 6-8 kDa. Moreover, the aqueous phase was varied: water, 0.9% NaCl solution, PBS (containing 3.1 g Na_2HPO_4, 0.3 g NaH_2PO_4, 8.2 g NaCl in 1 L pH 7.4) and 120 mM ammonium acetate buffer pH 5.0 were used. The addition rates were varied by introducing the polymer solution in THF into the aqueous phase using a peristaltic pump (Pharmacia LKB pump P-1, made in Sweden) at 0.15 and 1.5 mL/min while stirring using a magnetic stirrer. Also, the effect of adding MilliQ to the polymer solution in THF in a 1:1 volume ratio was investigated.

The effect of the presence of p(HPMA-Bz) homopolymer and the presence of free mPEG on the size of polymeric micelles

Samples of 20 mg mPEG-*b*-p(HPMA-Bz) and 0, 1, 2, 5 and 10 mg p(HPMA-Bz) were dissolved in 1 mL THF corresponding with weight fractions of 0, 5, 9, 20 and 33 w% of the homopolymer. Other samples of 20 mg mPEG-*b*-p(HPMA-Bz) and 0, 1, 2, 5 and 10 mg $mPEG_{5K}$ were dissolved in 1 mL THF corresponding with weight fractions of 0, 5, 9, 20 and 33 w% of the $mPEG_{5K}$. Addition of the polymer solution to water was performed rapidly using a pipette while stirring. THF was evaporated overnight at room temperature, resulting in the formation of micelles.

REFERENCES

(1) Duncan, R.; Vicent, M. J. *Adv. Drug Deliv. Rev.* **2013**, *65* (1), 60–70.
(2) Hare, J. I.; Lammers, T.; Ashford, M. B.; Puri, S.; Storm, G.; Barry, S. T. *Adv. Drug Deliv. Rev.* **2017**, *108*, 25–38.
(3) Kunjachan, S.; Ehling, J.; Storm, G.; Kiessling, F.; Lammers, T. *Chem. Rev.* **2015**, *115* (19), 10907–10937.
(4) Björnmalm, M.; Thurecht, K. J.; Michael, M.; Scott, A. M.; Caruso, F. *ACS Nano* **2017**, *11* (10), 9594–9613.
(5) van Elk, M.; Murphy, B. P.; Eufrásio-da-Silva, T.; O'Reilly, D. P.; Vermonden, T.; Hennink, P. W. E.; Duffy, G. P.; Ruiz-Hernández, E. *Int. J. Pharm.* **2016**, *515* (1–2), 132–164.
(6) Deng, C.; Jiang, Y.; Cheng, R.; Meng, F.; Zhong, Z. *Nano Today* **2012**, *7* (5), 467–480.
(7) Mikhail, A. S.; Allen, C. *J. Control. Release* **2009**, *138* (3), 214–223.
(8) Cabral, H.; Kataoka, K. *J. Control. Release* **2014**, *190*, 465–476.
(9) Cagel, M.; Tesan, F. C.; Bernabeu, E.; Salgueiro, M. J.; Zubillaga, M. B.; Moretton, M. A.; Chiappetta, D. A. *European Journal of Pharmaceutics and Biopharmaceutics*. Elsevier April 1, 2017, pp 211–228.
(10) Houdaihed, L.; Evans, J. C.; Allen, C. *Mol. Pharm.* **2017**, acs.molpharmaceut.7b00188.
(11) Varela-Moreira, A.; Shi, Y.; Fens, M. H. A. M.; Lammers, T.; Hennink, W. E.; Schiffelers, R. M. *Mater. Chem. Front.* **2017**, *1* (8), 1485–1501.
(12) Cabral, H.; Miyata, K.; Osada, K.; Kataoka, K. *Chem. Rev.* **2018**, *118* (14), 6844–6892.
(13) Yuan, X.; Jiang, M.; Zhao, H.; Wang, M.; Zhao, Y.; Wu, C. *Langmuir* **2001**, *17* (20), 6122–6126.
(14) Shi, Y.; Lammers, T.; Storm, G.; Hennink, W. E. *Macromol. Biosci.* **2016**, 1–11.
(15) Kang, N.; Perron, M. È.; Prud'Homme, R. E.; Zhang, Y.; Gaucher, G.; Leroux, J. C. *Nano Lett.* **2005**, *5* (2), 315–319.
(16) van Nostrum, C. F. *Soft Matter* **2011**, *7* (7), 3246.
(17) Fang, J.; Nakamura, H.; Maeda, H. *Adv. Drug Deliv. Rev.* **2011**, *63* (3), 136–151.
(18) Maeda, H.; Wu, J.; Sawa, T.; Matsumura, Y.; Hori, K. *J. Control. Release* **2000**, *65* (1–2), 271–284.
(19) Torchilin, V. *Adv. Drug Deliv. Rev.* **2011**, *63* (3), 131–135.
(20) Rizzo, L. Y.; Theek, B.; Storm, G.; Kiessling, F.; Lammers, T. *Curr. Opin. Biotechnol.* **2013**, *24* (6), 1159–1166.
(21) Bharali, D. J.; Mousa, S. A. *Pharmacol. Ther.* **2010**, *128* (2), 324–335.
(22) Wang, J.; Mao, W.; Lock, L. L.; Tang, J.; Sui, M.; Sun, W.; Cui, H.; Xu, D.; Shen, Y. *ACS Nano* **2015**, *9* (7), 7195–7206.
(23) Cabral, H.; Matsumoto, Y.; Mizuno, K.; Chen, Q.; Murakami, M.; Kimura, M.; Terada, Y.; Kano, M. R.; Miyazono, K.; Uesaka, M.; Nishiyama, N.; Kataoka, K. *Nat. Nanotechnol.* **2011**, *6* (12), 815–823.
(24) Sun, Q.; Ojha, T.; Kiessling, F.; Lammers, T.; Shi, Y. *Biomacromolecules* **2017**, *18* (5), 1449–1459.
(25) Huang, K.; Ma, H.; Liu, J.; Huo, S.; Kumar, A.; Wei, T.; Zhang, X.; Jin, S.; Gan, Y.;

Wang, P.; He, S.; Liang, X. *ACS Nano* **2012**, *6* (5), 4483–4493.
(26) Dreher, M. R.; Liu, W.; Michelich, C. R.; Dewhirst, M. W.; Yuan, F.; Chilkoti, A. *J. Natl. Cancer Inst.* **2006**, *98* (5), 335–344.
(27) Priwitaningrum, D. L.; Blondé, J. B. G.; Sridhar, A.; van Baarlen, J.; Hennink, W. E.; Storm, G.; Le Gac, S.; Prakash, J. *J. Control. Release* **2016**, *244*, 257–268.
(28) Shi, Y.; Van Der Meel, R.; Theek, B.; Oude Blenke, E.; Pieters, E. H. E.; Fens, M. H. A. M.; Ehling, J.; Schiffelers, R. M.; Storm, G.; Van Nostrum, C. F.; Lammers, T.; Hennink, W. E. *ACS Nano* **2015**, *9* (4), 3740–3752.
(29) Talelli, M.; Rijcken, C. J. F.; Oliveira, S.; Van Der Meel, R.; Van Bergen En Henegouwen, P. M. P.; Lammers, T.; Van Nostrum, C. F.; Storm, G.; Hennink, W. E. *J. Control. Release* **2011**, *153* (1), 93–102.
(30) Neradovic, D.; Van Nostrum, C. F.; Hennink, W. E. *Macromolecules* **2001**, *34* (22), 7589–7591.
(31) Hermanson, G. T. In *Bioconjugate Techniques*; Academic Press: Boston, 2013; pp 259–273.
(32) De Vos, R.; Goethals, E. J. *Polym. Bull.* **1986**, *15*, 547–549.
(33) Postma, A.; Davis, T. P.; Donovan, A. R.; Li, G.; Moad, G.; Mulder, R.; O'Shea, M. S. *Polymer* **2006**, *47* (6), 1899–1911.
(34) Lo, C. L.; Lin, S. J.; Tsai, H. C.; Chan, W. H.; Tsai, C. H.; Cheng, C. H. D.; Hsiue, G. H. *Biomaterials* **2009**, *30* (23–24), 3961–3970.
(35) Naksuriya, O.; Shi, Y.; van Nostrum, C. F.; Anuchapreeda, S.; Hennink, W. E.; Okonogi, S. *Eur. J. Pharm. Biopharm.* **2015**, *94* (2015), 501–512.
(36) Su, W. F. In *Principles of polymer design and synthesis*; Springer-Verlag Berlin Heidelberg: Berlin, 2013; pp 137–183.
(37) Odian, G. In *Principles of polymerization*; John Wiley & Sons, Inc.: New Jersey, 2004; pp 198–349.
(38) Hu, Q.; Rijcken, C. J. F.; van Gaal, E.; Brundel, P.; Kostkova, H.; Etrych, T.; Weber, B.; Barz, M.; Kiessling, F.; Prakash, J.; Storm, G.; Hennink, W. E.; Lammers, T. *J. Control. Release* **2016**, *244*, 314–325.
(39) ICH Harmonised Guidelines, Impurities: Guideline for Residual Solvents Q3c(R6) Step 4.
(40) Ma, C.; Pan, P.; Shan, G.; Bao, Y.; Fujita, M.; Maeda, M. *Langmuir* **2015**, *31* (4), 1527–1536.
(41) Nie, T.; Zhao, Y.; Xie, Z.; Wu, C. *Macromolecules* **2003**, *36* (23), 8825–8829.
(42) Nguyen, V. T. A.; De Pauw-Gillet, M. C.; Sandre, O.; Gauthier, M. *Langmuir* **2016**, *32* (50), 13482–13492.
(43) Giacomelli, C.; Schmidt, V.; Aissou, K.; Borsali, R. *Langmuir* **2010**, *26* (20), 15734–15744.
(44) Kale, T. S.; Klaikherd, A.; Popere, B.; Thayumanavan, S. *Langmuir* **2009**, *25* (17), 9660–9670.
(45) De Graaf, A. J.; Boere, K. W. M.; Kemmink, J.; Fokkink, R. G.; Van Nostrum, C. F.; Rijkers, D. T. S.; Van Der Gucht, J.; Wienk, H.; Baldus, M.; Mastrobattista, E.; Vermonden, T.; Hennink, W. E. *Langmuir* **2011**, *27* (16), 9843–9848.
(46) Li, W.; Nakayama, M.; Akimoto, J.; Okano, T. *Polymer* **2011**, *52* (17), 3783–3790.
(47) Soga, O.; Van Nostrum, C. F.; Ramzi, A.; Visser, T.; Soulimani, F.; Frederik, P. M.; Bomans, P. H. H.; Hennink, W. E. *Langmuir* **2004**, *20* (21), 9388–9395.

(48) Li, Z.; Dormidontova, E. E. *Macromolecules* **2010**, *43* (7), 3521–3531.
(49) Sheng, Y. J.; Wang, T. Y.; Chen, W. M.; Tsao, H. K. *J. Phys. Chem. B* **2007**, *111* (37), 10938–10945.
(50) Williams, C.; Brochard, F.; Frisch, H. L. *Annu. Rev. Phys. Chem.* **1981**, *32* (1), 433–451.
(51) Alexander, S. *J. Phys.* **1977**, *38* (8), 983–987.
(52) de Gennes, P. G. *Adv. Colloid Interface Sci.* **1987**, *27* (3–4), 189–209.
(53) de Gennes, P. G. *Macromolecules* **1980**, *13* (5), 1069–1075.
(54) Lee, H.; De Vries, A. H.; Marrink, S. J.; Pastor, R. W. *J. Phys. Chem. B* **2009**, *113* (40), 13186–13194.
(55) Daoud, M.; Cotton, J. P. *J. Phys. Paris* **1982**, *43* (3), 531–538.
(56) Mai, Y.; Eisenberg, A. *Chem. Soc. Rev.* **2012**, *41* (18), 5969–5985.
(57) Zhulina, E. B.; Adam, M.; Larue, I.; Sheiko, S. S.; Rubinstein, M. *Macromolecules* **2005**, *38* (12), 5330–5351.
(58) Zhao, C.; Winnik, M. A.; Riess, G.; Croucher, M. D. *Langmuir* **1990**, *6* (11), 514–516.
(59) Astafieva, I.; Zhong, X. F.; Eisenberg, A. *Macromolecules* **1993**, *26* (26), 7339–7352.
(60) Zhang, Z. G.; Yin, H. *J. Zhejiang Univ. Sci.* **2005**, *6 B* (3), 219–221.
(61) Torchilin, V. P. *J. Control. Release* **2001**, *73* (2–3), 137–172.
(62) Ashok, B.; Arleth, L.; Hjelm, R. P.; Rubinstein, I.; Önyüksel, H. *J. Pharm. Sci.* **2004**, *93* (10), 2476–2487.
(63) Makino, A.; Hara, E.; Hara, I.; Ozeki, E.; Kimura, S. *Langmuir* **2013**.
(64) Zhang, C.; Pansare, V. J.; Prud'Homme, R. K.; Priestley, R. D. *Soft Matter* **2012**, *8* (1), 86–93.
(65) Caron, J.; Maksimenko, A.; Wack, S.; Lepeltier, E.; Bourgaux, C.; Morvan, E.; Leblanc, K.; Couvreur, P.; Desmaële, D. *Adv. Healthc. Mater.* **2013**, *2* (1), 172–185.
(66) Aubry, J.; Ganachaud, F.; Addad, J. P. C.; Cabane, B. *Langmuir* **2009**, *25* (4), 1970–1979.
(67) Johnson, B. K.; Prud'homme, R. K. *Phys. Rev. Lett.* **2003**, *91* (11), 1–4.
(68) Aliabadi, H. M.; Elhasi, S.; Mahmud, A.; Gulamhusein, R.; Mahdipoor, P.; Lavasanifar, A. *Int. J. Pharm.* **2007**, *329* (1–2), 158–165.
(69) Lepeltier, E.; Bourgaux, C.; Couvreur, P. *Adv. Drug Deliv. Rev.* **2014**, *71*, 86–97.
(70) Beck-Broichsitter, M.; Rytting, E.; Lebhardt, T.; Wang, X.; Kissel, T. *Eur. J. Pharm. Sci.* **2010**, *41* (2), 244–253.
(71) Wei Huang; Chenming Zhang. *Biotechnol. J.* **2017**, *13* (1), 1–19.
(72) Zimm, B. H. *J. Chem. Phys.* **1948**, *16* (12), 1099–1116.
(73) Shi, Y.; Van Steenbergen, M. J.; Teunissen, E. A.; Novo, L.; Gradmann, S.; Baldus, M.; Van Nostrum, C. F.; Hennink, W. E. *Biomacromolecules* **2013**, *14* (6), 1826–1837.

SUPPLEMENTARY FIGURES AND TABLES

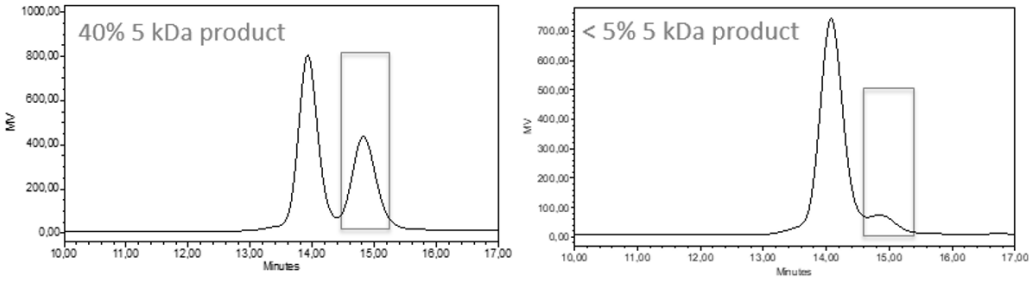

Figure S2.1. GPC chromatograms of mPEG$_{5K}$-ABCPA-mPEG$_{5K}$ macro-initiator. Left: the chromatogram of the macroinitiator containing ~40% of mPEG/mPEG-ABCPA (traditional synthesis). Right: the chromatogram of the macroinitiator with less than 5% free mPEG (optimized synthetic route).

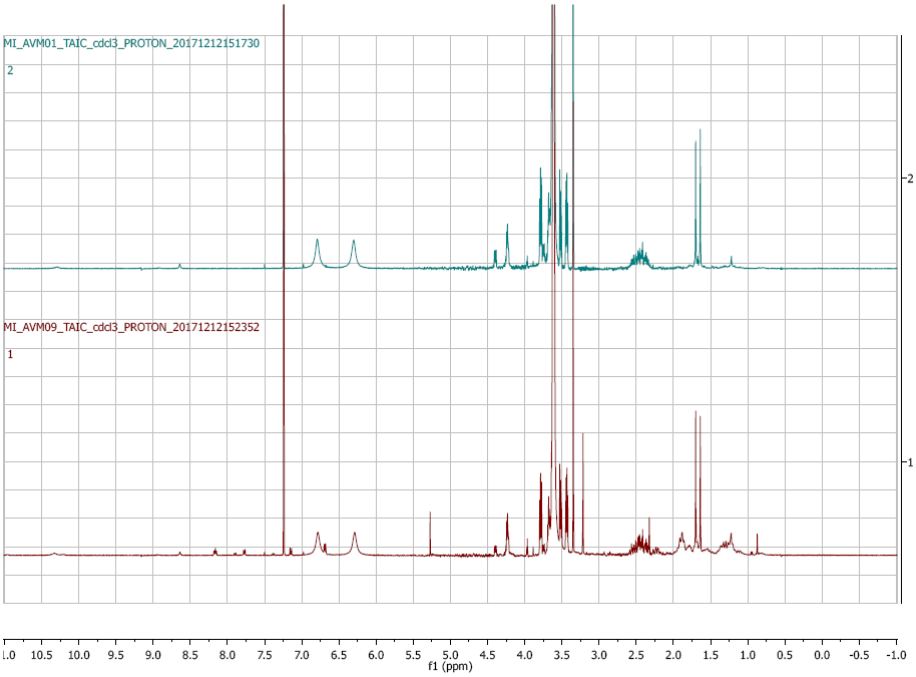

Figure S2.2. ^{1}H-NMR results of the mPEG5K-ABCPA-mPEG5K macro-initiators using TAIC. (Top) The spectrum of the macroinitiator containing ~40% of free mPEG/ mPEG-ABCPA (**Figure S2.1**). The product contains 30% mPEG according to ^{1}H-NMR with TAIC reagent. (Bottom) The spectrum of the macroinitiator containing less than 5% of free mPEG/mPEG-ABCPA (**Figure S2.1**). The product contains 4.2% mPEG according to ^{1}H-NMR with TAIC reagent.

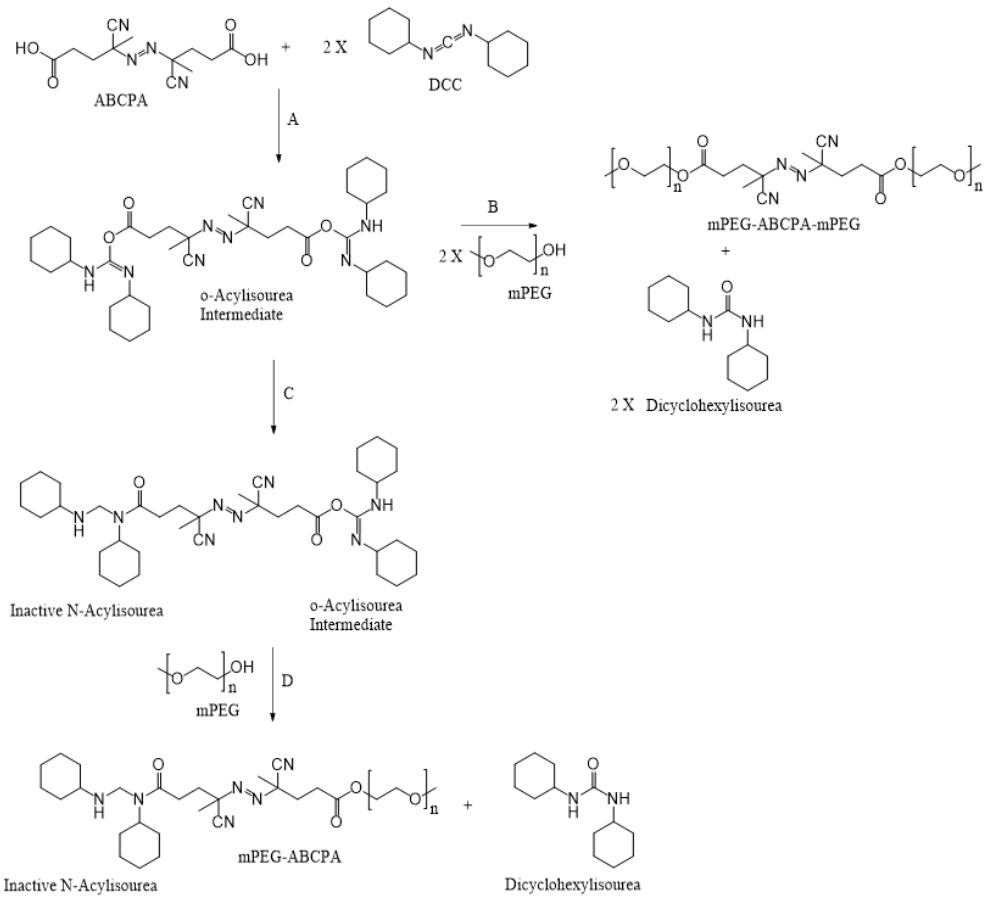

Scheme S2.1. Reaction A shows the activation of the ABCPA initiator. Reaction B shows the subsequent coupling of mPEG with the activated ABCPA resulting in the formation of mPEG-ABCPA-mPEG and dicyclohexylisourea. Note that activation of ABCPA and coupling of mPEG to ABCPA can occur at both carboxylic acids subsequently but also at the same time. Reaction C shows the rearrangement of the activated ABCPA resulting in inactive N-acylisourea. Reaction D shows the subsequent coupling of mPEG with the partly inactivated ABCPA resulting in the formation of mPEG-ABCPA and dicyclohexylisourea.

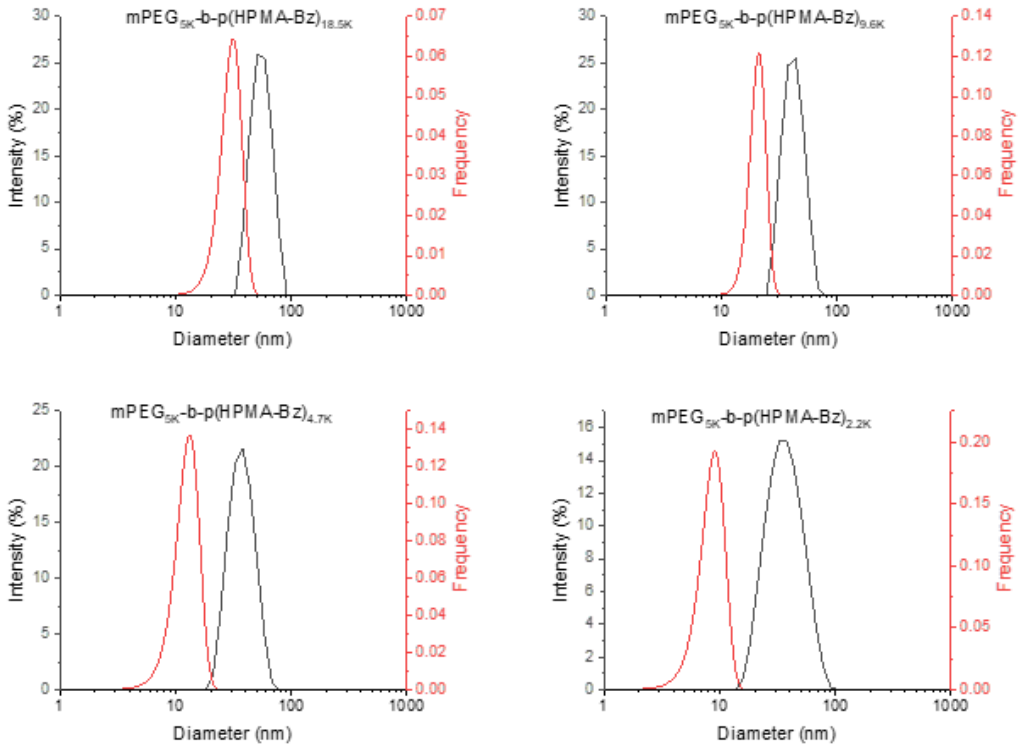

Figure S2.3. Histograms of diameters. (Black) measured by DLS and depicted by intensity. (Red) measured by TEM and depicted by frequency. This was done for the four studied micelle samples of mPEG$_{5K}$-*b*-p(HPMA-Bz)$_{18.5K}$, mPEG$_{5K}$-*b*-p(HPMA-Bz)$_{9.6K}$, mPEG$_{5K}$-*b*-p(HPMA-Bz)$_{4.7K}$ and mPEG$_{5K}$-*b*-p(HPMA-Bz)$_{2.2K}$.

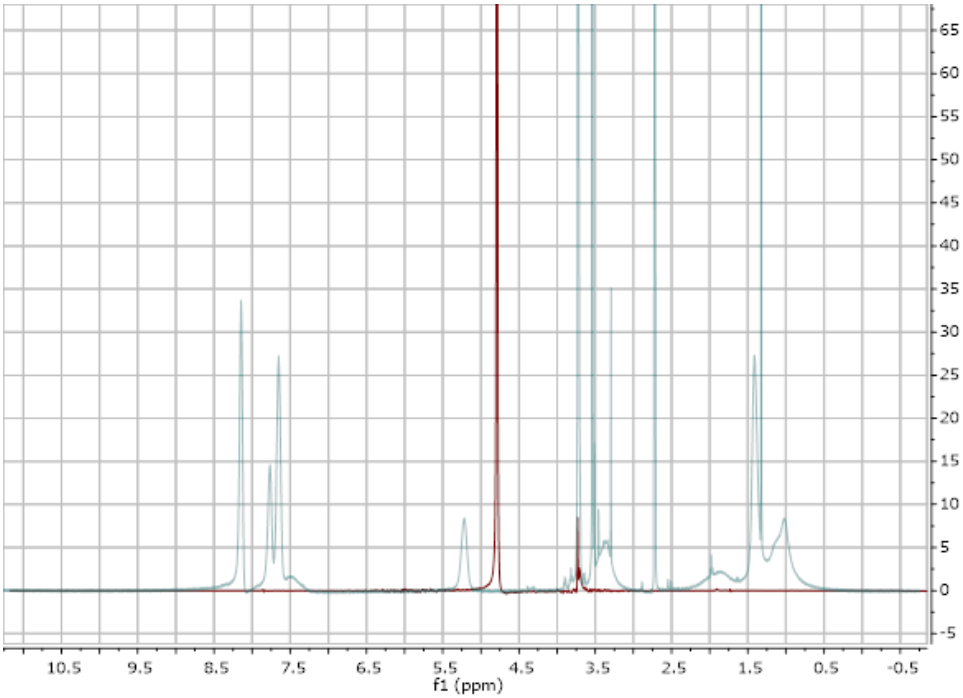

Figure S2.4. ^{1}H-NMR spectra. (Blue) mPEG-*b*-p(HPMA-Bz) copolymer in DMSO-d_6 and (red) micelle dispersion in D_2O at 25°C.

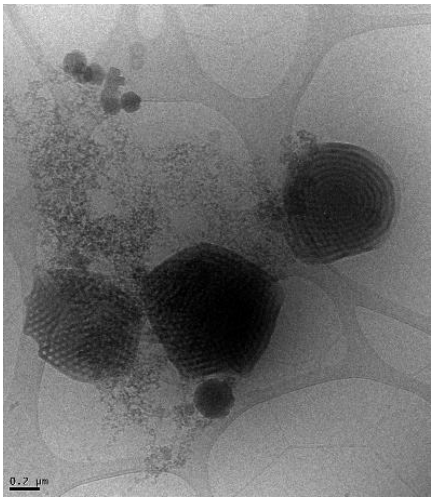

Figure S2.5. Cryo-TEM image of the mPEG$_{2K}$-*b*-p(HPMA-Bz)$_{20.6K}$ aggregates; scale bar corresponds to 0.2 µm.

Chapter 3

Tuning Size and Morphology of mPEG-*b*-p(HPMA-Bz) Block Copolymer Self-Assemblies Using Microfluidics

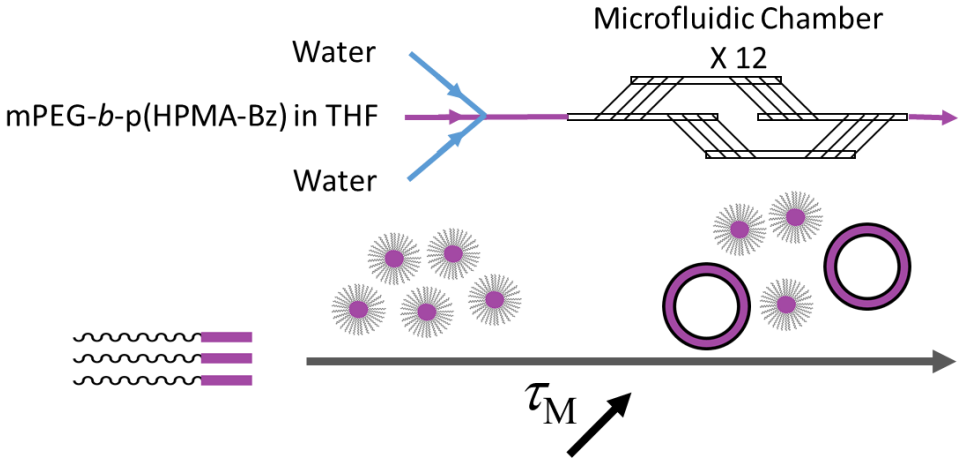

ABSTRACT.

The aim of this study was to investigate the preparation of poly(ethylene glycol)-*b*-poly(*N*-2-benzoyloxypropyl methacrylamide) mPEG-*b*-p(HPMA-Bz) block copolymer nanoparticles with tailored sizes and morphologies using microfluidics by changing the process and formulation parameters. For this purpose, four block copolymers with a fixed hydrophilic block of mPEG 5kDa and a varying molecular weight of the hydrophobic p(HPMA-Bz) block (17.5, 10.0, 5.2 and 2.7 kDa) were used. The polymers were dissolved in THF and nanostructures were formed by nanoprecipitation upon contact with water as the selected non-solvent, under well-defined flow conditions, in a commercially available microfluidic mixing chip. It was shown that upon using the block copolymer with the largest hydrophobic block (17.5 kDa), decreasing polymer concentration and increasing mixing time by decreasing flow rates led to an increase in particle size and even formation of polymer vesicles (polymersomes) along with micelles. In this case, the hydrodynamic diameter ranged from approximately 55 to 90 nm as determined by dynamic light scattering (DLS). For the block copolymer with the smallest hydrophobic block (2.7 kDa), regardless of the used concentration, with decreasing flow rates the overall nanoparticle size increased from 35 to 70 nm. Using the slowest flow rates, polymersomes were also formed. For the block copolymers with hydrophobic blocks of 10 and 5.2 kDa mostly micelles were formed at the different applied flow rates with negligible size difference for the different polymer concentrations. In conclusion, this study demonstrates that the self-assembly of mPEG-*b*-p(HPMA-Bz) block copolymers can be easily tailored in size and morphology using microfluidics, which therefore is an attractive option for further scaled-up production activities.

INTRODUCTION

During the past decades, polymeric based drug delivery nanoparticles, in particular polymeric micelles, have received growing interest for tumor targeting and other therapeutic purposes. [1–3] In general, polymeric micelles are core-shell structures composed of amphiphilic block copolymers. The shell consists of a brush of the hydrophilic block chains, usually poly(ethylene glycol) (PEG), which provides stealth-like properties against non-specific protein adsorption and offers good colloidal stability in physiological conditions. The hydrophobic core, in its turn, can be used to accommodate poorly water-soluble drugs. [4–6] A careful design of the topological features of the polymeric micelles is of importance to achieve efficacy of treatment e.g. regarding pharmacokinetics and tumor penetration.[7–9] Particle size is particularly relevant in this regard.

Various methods are available to prepare polymeric micelles such as emulsion-based and solvent displacement procedures. The latter is also referred to as nanoprecipitation, which renders tailorable characteristics such as size and size distribution.[10] The nanoprecipitation method is a simple, fast and straightforward technique to produce polymer-based nanoparticles. In short, an amphiphilic block copolymer (in combination with a drug) is dissolved in a water-miscible organic solvent. The obtained solution is then added to an aqueous phase, which acts as a non-solvent for the hydrophobic block and leads to the formation of (drug-loaded) nanoparticles. In the final step, the organic solvent is removed by evaporation or dialysis. [11–14]

The conventional nanoprecipitation method is performed in batch mode *i.e.* in traditional glassware, which is simple and efficient. Nevertheless, it has its limitations regarding uniformity and reproducibility of mixing. For instance, temperature or concentration inhomogeneity during mixing can have a substantial effect on the final size and structure of the particles.[10] Such issues might be particularly relevant with a block copolymer such as poly(ethylene glycol)-*b*-poly(*N*-2-benzoyloxypropyl methacrylamide) (mPEG-*b*-p(HPMA-Bz)), since the benzyl groups have shown to provide strong π- π stacking interactions and its self-assembly most likely leads to kinetically trapped nanoparticles rather than a dynamic micelle state.[15] Even for a block copolymer without aromatic groups such as poly(ethylene glycol)-*block*-poly(butyl acrylate) (mPEG-*b*-PBMA), previously reported simulations demonstrated that its self-assembly is controlled by kinetics and the applied

process conditions rather than thermodynamics.[16] In this case, with a moderately hydrophobic block, the introduction of charges in the hydrophilic block can drive the self-assembly towards dynamic micelles.[17]

Microfluidics is a technology that handles minute volumes of solutions in microscale fluidic devices in a precise and controlled way.[18,19] Small dimensions lead to a much higher surface to volume ratio of the solutions to be mixed than what is achieved in macroscopic vessels, which in turn drastically reduces the mixing time of the solvent and non-solvent.[20,21] This controlled and tunable mixing has a critical impact on the kinetically controlled nanoprecipitation process, facilitating control over size and size distribution of the formed self-assemblies.[22] For instance, Xu et al. described a lab-made coaxial flow chip enabling encapsulation of hydrophobic drugs with high efficiency in poly(lactic-*co*-glycolic acid) (PLGA) nanoparticles. [23] Furthermore, it is important to remark that microfluidics has a great potential in scaling up production of nanomedicines due to its continuous flow process, which is a major advantage for the production of formulations when moving to clinical (trial) applications.[24–26]

Although there is still some variability in outcome, most of the previously published studies showed that, when using microfluidics, fine-tuning of the flow rates and the ratio of organic solvent to the aqueous buffer enables control over both final particle size and polydispersity (PDI) value.[26–31] As an example, for the preparation of chitosan nanoparticles using microfluidics, varying the flow rates of the polymeric to alkaline water solutions resulted in the formation of smaller nanoparticles of 63 and 102 nm at respectively the shortest and longest applied mixing time in the microfluidic device, as compared to 161 nm nanosized particles using bulk production.[27] In the same study, it was also observed that the nanoparticles obtained from microfluidics had a narrower size distribution over all applied mixing times compared to the particles prepared using a bulk procedure. Similarly, Bally et al., reported that increasing the flow rates of non-solvent to the polymer solution and thus a faster and more efficient mixing resulted in smaller poly(methyl methacrylate)-based nanoparticles as compared to particles prepared in a batch process at similar solvent to non-solvent ratios (100 and 245 nm respectively).[28] In general, microfluidic devices offer control over flow rates, and therewith mixing times, which is of utmost importance to tailor particle size.[26,29–31]

In ***Chapter 2***, we reported on the preparation of size-tunable micelles based on poly(ethylene glycol)-*block*-poly(N-2-benzoyloxypropyl methacrylamide) (mPEG-*b*-p(HPMA-Bz)) in batch mode.[32] That study showed that the obtained micelles exhibited crew-cut structures and that their sizes were sensitive to the mixing rate of solvents and non-solvents, emphasizing the need for a system with robust mixing features. Therefore, in this chapter, a microfluidic mixing device was used to investigate the effects of process and formulation parameters on the size of mPEG-*b*-p(HPMA-Bz) micelles. This is of great importance with our aim of achieving a robust method for the production of small (< 100 nm) and well-defined polymeric nanoparticles eventually suitable for drug delivery purposes. More precisely, a commercial glass chip from Dolomite Inc. was used, which belongs to the herringbone-type micromixers employing chaotic laminar flow.[33] This set-up had previously shown its suitability for achieving morphological control via the assembly of a block copolymer with poly(ɣ-benzyl-*L*-glutamate) as the hydrophobic block and elastin-like polypeptide (ELP) as the hydrophilic block on the same chip.[34]

RESULTS AND DISCUSSION

Synthesis of mPEG-b-p(HPMA-Bz) block copolymers

Amphiphilic mPEG-*b*-p(HPMA-Bz) block copolymers were synthesized through free radical polymerization with varying feed ratios of macro-initiator mPEG-ABCPA-mPEG to monomer HPMA-Bz (MI:M). The number- and weight- average molar masses (M_n and M_w respectively), the degree of polymerization ($N_{HPMA\text{-}Bz}$) and the molar mass dispersity (Đ) of the obtained block copolymers were determined by ^{1}H-NMR and GPC analysis (**Table 3.1**).

Table 3.1. Characteristics of the synthesized mPEG$_{5K}$-*b*-p(HPMA-Bz)$_X$ block copolymers as determined by ^{1}H-NMR and GPC. M:MI = monomer to macro-initiator ratio (mol/mol), M_n = number average molar mass (kDa), M_w = weight average molar mass (kDa), Đ = molar mass dispersity, $N_{HPMA-Bz}$ = degree of polymerization, f_{PEG} = calculated hydrophilic weight fraction (wt%) and $\emptyset_{PEG}$ = hydrophilic volume fraction (vol%).

Block copolymer	M:MI	M_n	GPC			$N_{HPMA-Bz}$	f_{PEG}	$\emptyset_{PEG}$
			M_n	M_w	Đ			
A: mPEG$_{5K}$-*b*-p(HPMA-Bz)$_{17.1K}$	200	22.1	15.8	20.7	1.31	69	23	24
B: mPEG$_{5K}$-*b*-p(HPMA-Bz)$_{10.0K}$	100	15.0	13.2	17.5	1.32	40	33	35
C: mPEG$_{5K}$-*b*-p(HPMA-Bz)$_{5.2K}$	50	10.2	10.8	14.0	1.30	21	49	50
D: mPEG$_{5K}$-*b*-p(HPMA-Bz)$_{2.7K}$	25	7.7	8.9	11.0	1.24	11	65	66

Furthermore, powder mass densities were measured by helium pycnometry. The values for HPMA-Bz monomer and p(HPMA-Bz) polymer were 1.1796±0.002 and 1.1944±0.0012 g·cm^{-3}, respectively. On the other hand, according to literature, PEG has a mass density of 1.13 g·cm^{-3}. [35] With this information the hydrophilic volume fraction ($\emptyset_{\mathrm{PEG}}$) could be estimated (**Table 3.1**) by applying the following equation where f_{PEG} is the calculated hydrophilic weight fraction, d_{PEG} is the mass density of PEG and $d_{\mathrm{p(HPMA-Bz)}}$ is the mass density of the p(HPMA-Bz) polymer:

$$\emptyset_{\mathrm{PEG}} = \frac{f_{\mathrm{PEG}}/d_{\mathrm{PEG}}}{\left[f_{\mathrm{PEG}}/d_{\mathrm{PEG}} + (1-f_{\mathrm{PEG}})/d_{\mathrm{p(HPMA-Bz)}}\right]}$$

Interestingly, the volume fractions $\emptyset_{\mathrm{PEG}}$ were not very different from the weight fractions f_{PEG}. Based on the phase diagram reported by Jain and Bates for the low glass transition temperature (T_g) poly(butadiene)-*b*-poly(ethylene glycol) as a function of the degree of polymerization of the hydrophobic block and the hydrophilic fraction $f_{PEG,}$ [36] the expected equilibrium morphologies of the self-assemblies were vesicles for block copolymer A (mPEG$_{5K}$-*b*-p(HPMA-Bz)$_{17.1K}$), a blend of vesicles and cylinders for block copolymer B (mPEG$_{5K}$-*b*-p(HPMA-Bz)$_{10.0K}$), only cylinders for block copolymer C

(mPEG$_{5K}$-*b*-p(HPMA-Bz)$_{5.2K}$), and spherical micelles for block copolymer D (mPEG$_{5K}$-*b*-p(HPMA-Bz)$_{2.7K}$).

The effect of mixing time on the size and morphology of mPEG-b-p-(HPMA-Bz) nanoparticles

The effect on the size and morphology of mPEG-*b*-p(HPMA-Bz) block copolymer nanoparticles formed by the solvent shift method (nanoprecipitation) was studied using microfluidics. By applying total flow rates (Q_{tot}) ranging from 100 to 1600 µL/min the mixing time (τ_M) in the micromixer was varied from 1570 to 42 ms according to the data provided by the manufacturer (**Table 3.2**).

Table 3.2. Flow rates and their approximated mixing times as calculated using the information from **Figure 3.10**.

O_{tot} (µL/min)	τ_M (ms)
100	1570
200	634
350	305
500	192
1600	42

Figure 3.1A demonstrates that block copolymer A (mPEG$_{5K}$-*b*-p(HPMA-Bz)$_{17.1K}$), with the largest hydrophobic block and lowest f_{PEG} (23 %), at a polymer concentration of 5 mg/mL assembled into particles increased in size from 55 to 90 nm when the flow rate decreased from 1600 to 100 µL/min. The PDI values for the different nanoparticles were all below 0.2, thereby demonstrating homogeneity in the assembly process. **Figure 3.1A** also shows that the total flow rate dependency was less pronounced upon increasing the block copolymer A concentration to 20 mg/mL. These results can be explained by the nucleation-controlled self-assembly process as the size of the nanoparticle is dependent on the nucleation rate. This is in line with the results from our previous study regarding nanoprecipitation in bulk. [32] In short, the addition of antisolvent reduces the solubility of block copolymers and induces supersaturation. [37] The nucleation rate is dependent on the supersaturation degree of the block copolymers, which is in its turn affected by the used concentration and mixing rate of the polymer-containing solvent and anti-

solvent. Slower flow rates result in longer mixing times, which provide a more gradual change in the composition of all the components (solvent, unimers and chain aggregates). This eventually results in less homogeneous supersaturation and slow nucleation and therefore provides a longer growth time of the nanoparticles. Faster flow rates, on the other hand, ensure shorter mixing times. This is associated with rapid supersaturation and the formation of more numerous nuclei, which eventually results in smaller and more monodisperse nanoparticles according to the classical nucleation and growth model. [11]

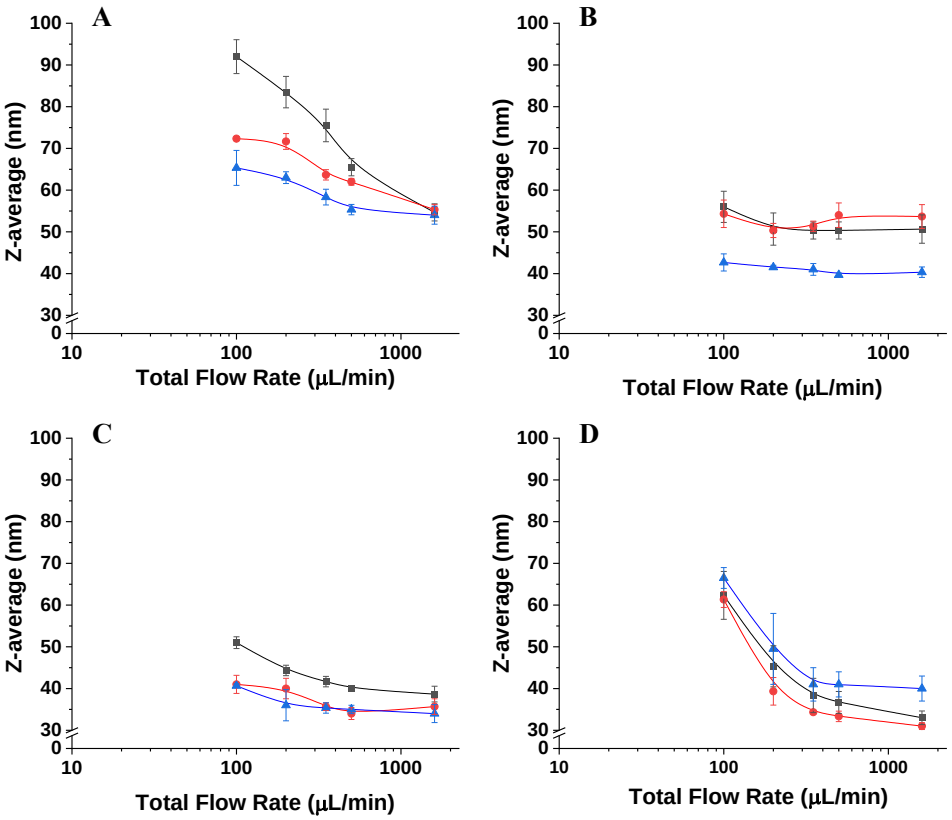

Figure 3.1. Average hydrodynamic diameter of mPEG$_{5K}$-*b*-p(HPMA-Bz)$_X$ nanoparticles as a function of flow rate. (A) mPEG$_{5K}$-*b*-p(HPMA-Bz)$_{17.1K}$, **(B)** mPEG$_{5K}$-*b*-p(HPMA-Bz)$_{10.0K}$, **(C)** mPEG$_{5K}$-*b*-p(HPMA-Bz)$_{5.2K}$ and **(D)** mPEG$_{5K}$-*b*-p(HPMA-Bz)$_{2.7K}$. Black square: 5 mg/mL, red circle: 10 mg/mL and blue triangle: 20 mg/mL block copolymer concentration in THF.

The Z-average hydrodynamic diameters of self-assemblies based on the block copolymers with larger hydrophilic weight fraction f_{PEG}, (mPEG$_{5K}$-*b*-p(HPMA-Bz)$_{10.0K}$ (B) and mPEG$_{5K}$-*b*-p(HPMA-Bz)$_{5.2K}$ (C), did not change significantly when different polymer concentrations or flow rates were used (**Figure 3.1B and C**). However, self-assembly of block copolymer D with the smallest hydrophobic block and thus the highest f_{PEG} (65 %), mPEG$_{5K}$-*b*-p(HPMA-Bz)$_{2.7K}$, resulted in an increase in nanoparticle size from 30 to 65 nm upon decreasing the flow rate regardless of the polymer concentration (**Figure 3.1D**). Along with an increase in particle size, the PDI values also increased moderately upon decreasing the flow rates (**Figure 3.2**).

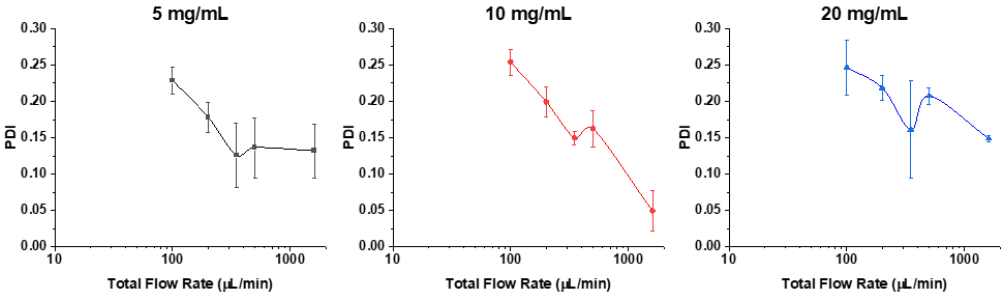

Figure 3.2. PDI values of block copolymer D mPEG$_{5K}$-*b*-p(HPMA-Bz)$_{2.7K}$ nanostructures as a function of mixing time. The three different concentrations are depicted in separate graphs.

Morphology of mPEG-b-p-(HPMA-Bz) nanoparticles

To get insight into the morphology of the formed nanoparticles based on the largest block copolymer A mPEG$_{5K}$-*b*-p(HPMA-Bz)$_{17.1K}$, the radius of gyration (R_g), hydrodynamic radius (R_h) and size distribution (fractograms) were determined using AF4-MALLS (**Table 3.3**). Interestingly, the R_g/R_h ratio and the weight average molecular weight of the nanoparticles ($M_{w(np)}$) deduced from a Zimm plot gradually increased upon decreasing the flow rate. At the two lower block copolymer concentrations in THF, 5 and 10 mg/mL, R_g/R_h ratios of ~1 were observed for the slowest flow rate (100 µL/min) *i.e.* longest mixing time (1570 ms). However, this was not observed for the highest polymer concentration studied (20 mg/mL) at which R_g/R_h ratios close to 0.8 were measured at all flow rates.

Table 3.3. Characteristics of block copolymer A ($mPEG_{5K}$-*b*-$p(HPMA\text{-}Bz)_{17.1K}$) nanoparticles as determined by AF4-MALLS. ρ = concentration (mg/mL); Q_{tot} = flow rate (µL/min); R_g = radius of gyration (nm); R_h = hydrodynamic radius (nm); $M_{w(np)}$ = weight average molecular weight of the nanoparticles (10^3 kDa); N_{agg} = nanoparticle aggregation number.

ρ	Q_{tot}	R_g	R_h	R_g/R_h	$M_{w(np)}$	N_{agg}
5	100	46	45	1.03	187	8500
5	200	35	39	0.90	142	6400
5	350	32	36	0.89	131	5900
5	500	30	37	0.82	150	6800
5	1600	21	26	0.81	36	1600
10	100	34	33	1.03	79	3600
10	200	24	30	0.82	64	2900
10	350	24	28	0.86	42	1900
10	500	22	28	0.78	39	1800
10	1600	17	25	0.69	26	1200
20	100	24	28	0.85	42	1900
20	200	22	26	0.82	34	1600
20	350	20	27	0.73	69	3100
20	500	21	28	0.76	36	1600
20	1600	20	25	0.78	34	1500

The R_g/R_h ratio (or shape factor ρ) is structure sensitive and therefore provides information about the morphology of nanoparticles. [38] In particular, it has been shown that the R_g/R_h ratios for structures with a dense core and less dense shell (core-shell structures) are lower than 0.775.[39–43] On the other hand, particles with a rigid spherical structure have in theory R_g/R_h ratios of ~ $\sqrt{3/5}$ or ~0.775.[39,40] For spherical vesicles like polymersomes, the scattering mass is concentrated on the surface of the sphere yielding a R_g/R_h ratio near 1. [44,45] Therefore, the AF4-MALLS results for block copolymer A ($mPEG_{5K}$-*b*-$p(HPMA\text{-}Bz)_{17.1K}$) nanoparticles indicate that polymer vesicles (polymersomes) were formed at slower flow rates, instead of the filled micelles that were formed at higher concentrations and faster flow rates.

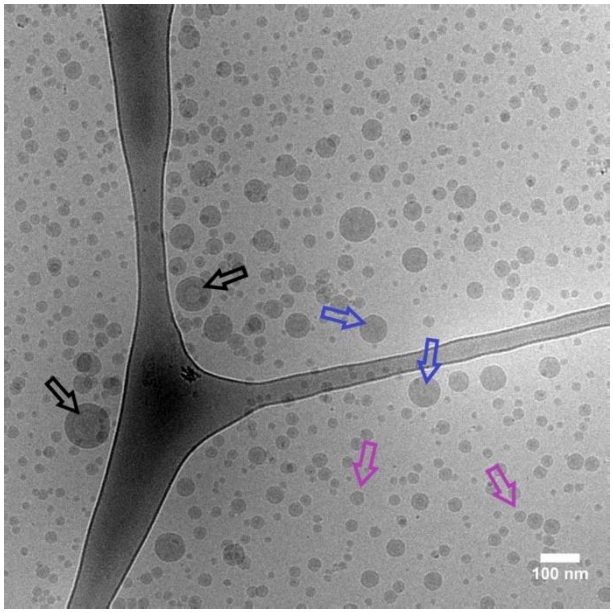

Figure 3.3. Cryo-TEM overview picture of block copolymer A (mPEG$_{5K}$-*b*-p(HPMA-Bz)$_{17.1K}$) nanoparticles. Nanoparticles were prepared at a block copolymer concentration of 5 mg/mL in THF and a total flow rate of 100 µL/min. Black arrows point to vesicles such as polymersomes, blue arrows point to bigger micelles and the purple arrows point to smaller filled micelles. Scalebar indicates 100 nm.

Cryo-TEM analysis of some selected samples was used to corroborate the AF4-MALLS results regarding the nanoparticle morphology of block copolymer A (mPEG$_{5K}$-*b*-p(HPMA-Bz)$_{17.1K}$) nanoparticles. **Figure 3.3** provides an overview of all the observed morphologies. It was shown that for the two lowest concentrations (5 and 10 mg/mL) using slower flow rates, larger micelles and also polymersomes were formed. Interestingly, at the fastest flow rate of 1600 µL/min, regardless of the used concentration, only rigid micelles were formed with a diameter of around 35 nm as measured by cryo-TEM (**Figure 3.4**). The hydrodynamic diameters for these samples were around 55 nm as measured by DLS (**Figure 3.1A**). This apparent discrepancy in diameters can be easily explained. Indeed, cryo-TEM only allows visualization the core of the micelles where the aromatic benzyl groups are localized which provide a high scattering density for electrons, whereas DLS includes the hydrated mPEG corona, which is much transparent to the electron beam. **Figure 3.4** also demonstrates that only micelles were formed at 20 mg/mL, independent of the used flow rates.

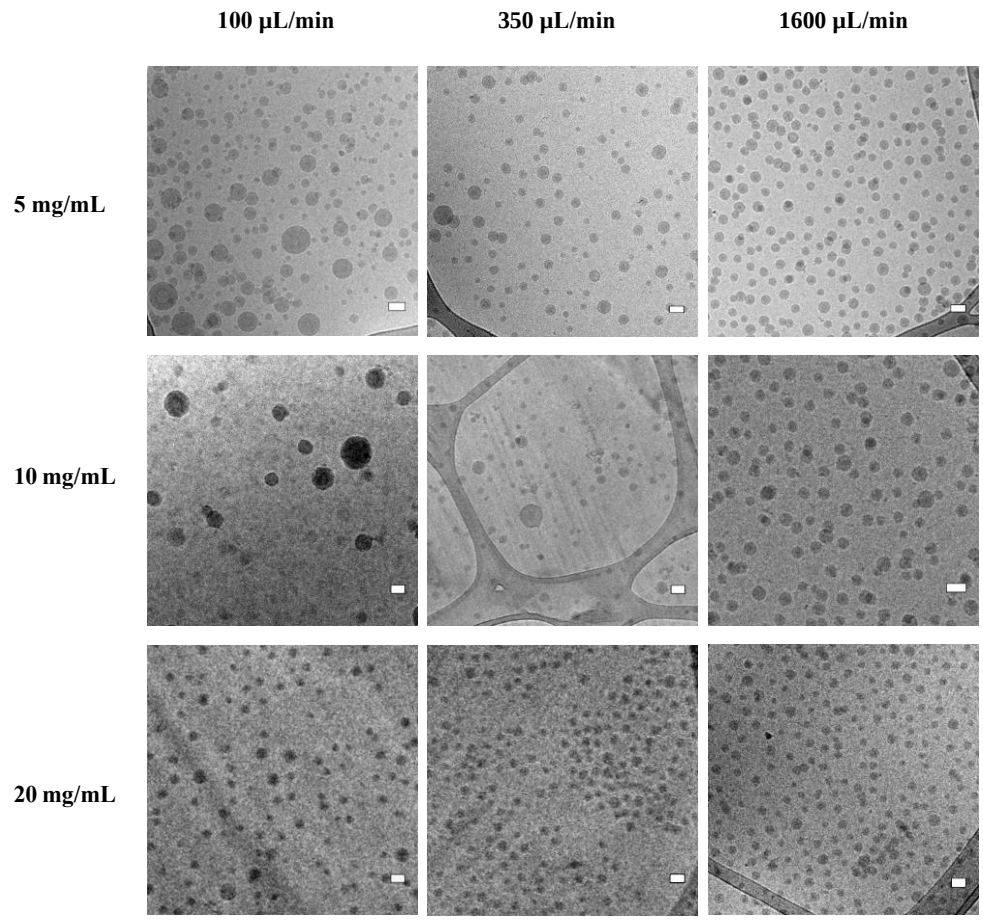

Figure 3.4. Cryo-TEM pictures of mPEG$_{5K}$-*b*-p(HPMA-Bz)$_{17.1K}$ nanoparticles. Nanoparticles were prepared using different block copolymer concentrations in THF (5, 10 and 20 mg/mL) and flow rates (100, 350 and 1600 µL/min). Scale bars indicate 50 nm.

The fractograms of the AF4-MALLS of the 5 mg/mL samples for block copolymer A revealed only one peak for the particles prepared at the fastest flow rates (500 and 1600 µL/min) and one peak with a tail at higher retention times for particles prepared at microfluidic flow rates below 350 µL/min, which could not be separated even by adjusting the fractionation method (**Figure 3.5A**). This observation is in agreement with the cryo-TEM results, which showed that at slower microfluidic flow rates mostly micelles with a size around 30-35 nm were formed together with some bigger objects of 50-

100 nm, presumably micelles and even polymersomes (**Figure 3.4**). This transition from homogenous small micelles of 30-35 nm diameter at high microfluidic flow rates to more polydisperse particles where small micelles coexist with larger micelles and vesicles is rather gradual. This explains the tail in the chromatographic fractogram by AF4-MALLS.

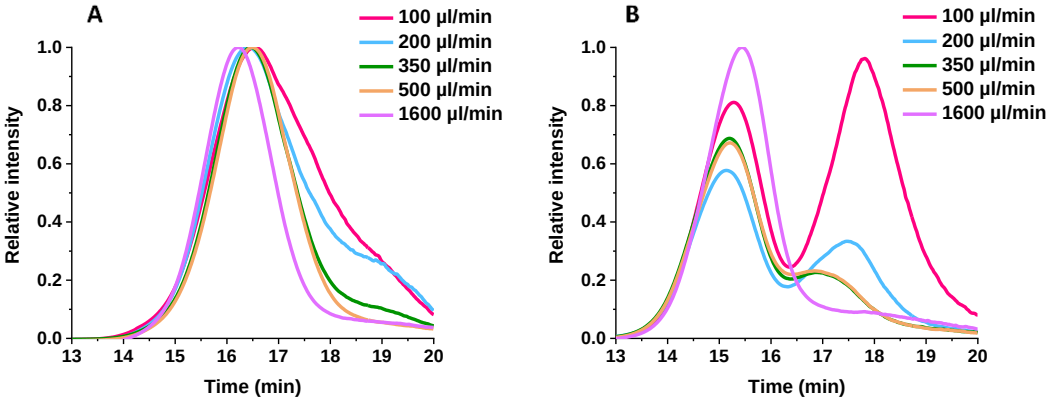

Figure 3.5. Fractograms of nanoparticles obtained at varying microfluidic flow rates measured with AF4-MALLS. A: block copolymer A (mPEG$_{5K}$-*b*-p(HPMA-Bz)$_{17.1K}$) at concentration of 5 mg/mL and B: block copolymer D (mPEG$_{5K}$-*b*-p(HPMA-Bz)$_{2.7K}$) with a concentration of 5 mg/mL.

AF4-MALLS results of the samples prepared from the smallest block copolymer D (mPEG$_{5K}$-*b*-p(HPMA-Bz)$_{2.7K}$) showed strikingly different fractograms compared to the largest block copolymer A (**Figure 3.5B).** At slower microfluidic flow rates, two distinct peaks corresponding to two populations of nanoparticles were observed, whereas for the shortest mixing time, only one peak and therefore one population was detected.

The R_g and R_h of the mPEG$_{5K}$-*b*-p(HPMA-Bz)$_{2.7K}$ nanoparticles were determined for the separate populations by AF4-MALLS (**Table 3.4**). Interestingly, the average R_g/R_h ratios of the nanoparticles of the first peaks were all around 0.7, which points to solid spherical structures (~0.775). On the other hand, the nanoparticles of the second peaks showed higher R_g/R_h values with some even approaching ~1 suggesting the presence of polymersomes. Moreover, the $M_{w(np)}$ of the nanoparticles corresponding to the second peak were considerably higher compared to the first peak, between 10-150 MDa and around 3 MDa, respectively. The results for the first peak are comparable with the values previously reported for micelles from the same polymer

prepared in batch mode. [32] These results demonstrate that, independent of polymer concentration, two separate particle populations of very distinct morphologies were formed when flow rates were decreased and thus mixing times increased. The formation of other morphologies was also substantiated by the increasing PDI values as measured by DLS (**Figure 3.2**).

Table 3.4. Characteristics of block copolymer D (mPEG$_{5K}$-*b*-p(HPMA-Bz)$_{2.7K}$) nanoparticles as determined by AF4-MALLS. ρ = concentration (mg/mL); Q_{tot} = flow rate (µL/min); R_g = radius of gyration (nm); R_h = hydrodynamic radius (nm); $M_{w(np)}$ = weight average molecular weight of the nanoparticles (10^3 kDa); N_{agg} = nanoparticle aggregation number.

ρ	Q_{tot}	Peak 1					Peak 2				
		R_g	R_h	R_g/R_h	$M_{w(np)}$	N_{agg}	R_g	R_h	R_g/R_h	$M_{w(np)}$	N_{agg}
5	100	13	17	0.76	3.1	400	54	54	0.99	98	12700
5	200	13	17	0.80	3.2	420	46	51	0.91	68	8800
5	350	13	17	0.77	3.3	430	34	40	0.85	91	11800
5	500	12	17	0.68	3.5	450	32	39	0.82	171	22200
5	1600	11	17	0.63	3.4	450	-	-	-	-	-
10	100	10	16	0.65	2.5	320	53	56	0.93	70	9000
10	200	11	16	0.67	2.9	380	47	76	0.62	11	1500
10	350	11	17	0.63	3.2	420	26	39	0.65	625	81200
10	500	12	16	0.71	2.6	340	-	39	-	-	-
10	1600	13	17	0.77	2.8	360	-	-	-	-	-
20	100	12	16	0.75	2.3	300	59	54	1.09	147	19100
20	200	13	16	0.81	2.3	300	47	45	1.04	145	18780
20	350	11	16	0.71	2.5	320	48	45	1.06	66	8500
20	500	13	16	0.81	2.3	300	31	36	0.87	104	13600
20	1600	11	16	0.75	2.5	320	-	-	-	-	-

These results are in accordance with the cryo-TEM results of a selection of mPEG$_{5K}$-*b*-p(HPMA-Bz)$_{2.7K}$ nanoparticles (**Figure 3.6**). It was shown that mostly small filled micelles with a size around 15-20 nm and a few bigger polymersome structures were formed.

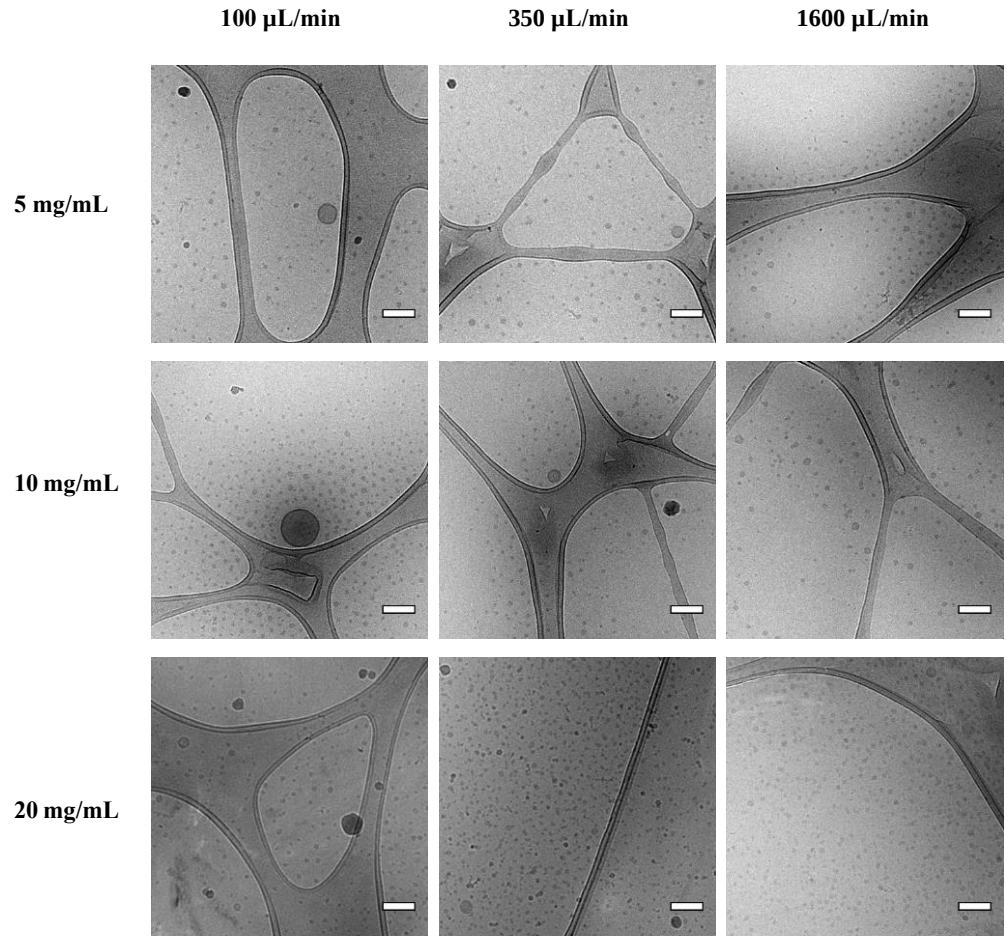

Figure 3.6. Cryo-TEM pictures of mPEG$_{5K}$-*b*-p(HPMA-Bz)$_{2.7K}$ nanoparticles prepared using different concentrations (5, 10 and 20 mg/mL) and different flow rates (100, 350 and 1600 µL/min). Scalebars indicate 100 nm.

The R_g/R_h ratios as determined by AF4-MALLS of block copolymer B (mPEG$_{5K}$-*b*-p(HPMA-Bz)$_{10.0K}$) nanoparticles showed a main value near 0.775 and a second peak with values between 1.13 and 1.73 (**Table 3.5**), demonstrating that not only rigid micelles were formed but also other structures like vesicles depending on the used concentration and flow rate.

Table 3.5. Characteristics of block copolymer B mPEG$_{5K}$-*b*-p(HPMA-Bz)$_{10.0K}$ nanoparticles as determined by AF4-MALLS. ρ = concentration (mg/mL); Q_{tot} = flow rate (µL/min); R_g = radius of gyration (nm); R_h = hydrodynamic radius (nm); $M_{w(np)}$ = weight average molecular weight of the nanoparticles (10^3 kDa); N_{agg} = nanoparticle aggregation number.

ρ	Q_{tot}	Peak 1					Peak 2				
		R_g	R_h	R_g/R_h	$M_{w(np)}$	N_{agg}	R_g	R_h	R_g/R_h	$M_{w(np)}$	N_{agg}
5	100	19	25	0.77	16	1060	-	-	-	-	-
5	200	18	25	0.72	16	1060	-	-	-	-	-
5	350	17	23	0.72	15	1000	-	-	-	-	-
5	500	14	22	0.63	13	880	73	49	1.49	232	1550
5	1600	13	22	0.59	13	860	84	52	1.62	263	1750
10	100	15	21	0.72	12	770	52	46	1.13	1263	8420
10	200	13	20	0.65	11	720	70	46	1.52	585	3900
10	350	14	20	0.69	11	730	80	48	1.67	1717	1145
10	500	14	21	0.69	12	780	-	51	-	-	-
10	1600	14	20	0.67	11	730	85	49	1.73	1441	9610
20	100	14	20	0.69	9.6	640	-	-	-	-	-
20	200	16	21	0.75	9.9	660	-	-	-	-	-
20	350	14	20	0.70	9.6	640	-	-	-	-	-
20	500	11	20	0.56	9.9	660	-	-	-	-	-
20	1600	13	20	0.65	9.9	660	-	-	-	-	-

Cryo-TEM measurements were in accordance with these results and showed that mostly small filled micelles were formed with a size around 30 and a few bigger polymersome structures (**Figure 3.7**).

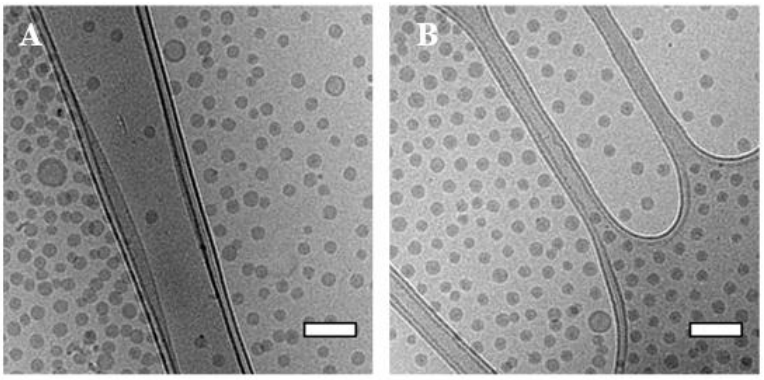

Figure 3.7. Cryo-TEM pictures of block copolymer B mPEG$_{5K}$-*b*-p(HPMA-Bz)$_{10.0K}$ nanoparticles. Nanoparticles were prepared at a concentration of 10 mg/mL and flow rates **(A)** 100 µL/min and **(B)** 350 µL/min. Scale bars indicate 100 nm.

The R_g/R_h ratios of block copolymer C (mPEG$_{5K}$-*b*-p(HPMA-Bz)$_{5.2K}$) nanoparticles showed a main value near 0.775 and a second peak with values between 0.92 and 1.38 (**Table 3.6**), demonstrating that not only rigid micelles were formed but also other structures like vesicles depending on the used flow rate.

Table 3.6. Characteristics of block copolymer C mPEG$_{5K}$-*b*-p(HPMA-Bz)$_{5.2K}$ nanoparticles as determined by AF4-MALLS. ρ = concentration (mg/mL); Q_{tot} = flow rate (µL/min); R_g = radius of gyration (nm); R_h = hydrodynamic radius (nm); $M_{w(np)}$ = weight average molecular weight of the nanoparticles (10^3 kDa); N_{agg} = nanoparticle aggregation number.

ρ	Q_{tot}	Peak 1					Peak 2				
		R_g	R_h	R_g/R_h	$M_{w(np)}$	N_{agg}	R_g	R_h	R_g/R_h	$M_{w(np)}$	N_{agg}
5	100	12	20	0.61	6.5	640	-	-	-	-	-
5	200	11	18	0.63	5.2	510	41	44	0.93	96	9400
5	350	11	18	0.64	5.3	520	35	38	0.92	48	4700
5	500	11	19	0.56	5.9	580	-	-	-	-	-
5	1600	11	18	0.65	5.3	520	-	-	-	-	-
10	100	14	17	0.80	4.5	440	58	42	1.38	210	2020
10	200	13	17	0.77	4.7	460	-	-	-	-	-
10	350	11	17	0.66	4.3	420	-	-	-	-	-
10	500	13	17	0.76	4.3	420	-	-	-	-	-
10	1600	12	17	0.72	4.6	450	-	-	-	-	-
20	100	12	17	0.73	4.1	400	87	116	0.75	25	2500
20	200	10	16	0.60	3.6	360	-	-	-	-	-
20	350	11	16	0.68	3.9	380	-	-	-	-	-
20	500	11	17	0.67	3.9	390	-	-	-	-	-
20	1600	10	16	0.63	3.6	360	-	-	-	-	-

Cryo-TEM measurements were in accordance with these results and showed that mostly small filled micelles were formed with a size around 21 nm and a few bigger polymersome structures (**Figure 3.8**).

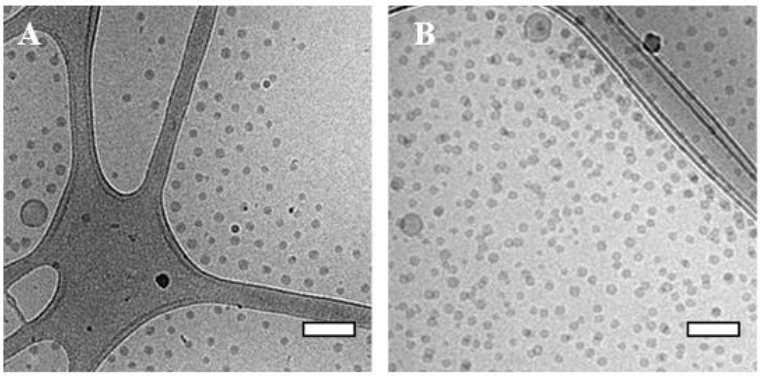

Figure 3.8. Cryo-TEM pictures of block copolymer C mPEG$_{5K}$-*b*-p(HPMA-Bz)$_{5.2K}$ nanoparticles. Nanoparticles were prepared at a concentration of 5 mg/mL and flow rates **(A)**100 µL/min and **(B)** 350 µL/min. Scale bars indicate 100 nm.

In the case of mPEG$_{5K}$-*b*-p(HPMA-Bz), with a hydrophobic block of high T_g (**Figure 3.11**) and aromatic side-groups providing strong π-π interactions, nanoprecipitation at fast mixing rates leads to frozen self-assemblies as soon as water and THF are mixed. The occurrence of different morphologies can be explained by the competition between the kinetic process and the thermodynamically favorable structure. Therefore, by using a microfluidic mixing device and performing nanoprecipitation at mixing times τ_M that could be tuned between 42 and 1600 ms, snapshots of the kinetic process of block copolymer self-assembly were captured.

The mechanism that is best applicable to vesicle formation from mPEG-*b*-p(HPMA-Bz) block copolymers depends on the size of the hydrophobic block. For the largest block copolymer A (mPEG$_{5K}$-*b*-p(HPMA-Bz)$_{17.1K}$) vesicles are expected to be formed at the thermodynamic state, from the packing parameter model with a hydrophilic fraction f_{PEG}~23% and a hydrophobic block length $N_{HPMA\text{-}Bz}$ ~69 [46,47]. It is envisioned that the vesicles are formed through a mechanism as described in detail by He & Schmid. [48] They stated that vesicles form *via* self-assembly of micelles that subsequently undergo an internal reorganization to yield vesicular membranes. It was shown that under dilute conditions, first spherical micelles were formed that continue to grow through a path reminiscent of Ostwald ripening into larger micelles. These subsequently transform into semi-vesicles through a flip-flop motion of chains that brings the hydrophilic PEG chains inward and drives solvent diffusion inside and eventually reach full vesicle morphologies. The fact that the

different sizes and shapes of the particles could not be separated on AF4-MALLS as described above emphasizes a gradual growth of micelles and eventually a rearrangement into a lamellar structures. Therefore, this explains why the fractogram of samples prepared from block copolymer A ($mPEG_{5K}$-*b*-$p(HPMA\text{-}Bz)_{17.1K}$) at slower microfluidic flow rates was broader and becomes narrower at faster microfluidic flow rates. The cryo-TEM pictures confirmed the proposed mechanism, and all three structures (micelles, larger micelles and vesicles) were observed for particles prepared at the slowest flow rates and the lowest concentration (**Figure 3.3**).

From these results, it is apparent that in order to prepare dispersions with only spherical micelles, three factors are important. The first factor is the hydrophobic to hydrophilic ratio, here determined by f_{PEG}. In this research, it was shown that nanoparticles resulting from all block copolymers resulted mainly into spherical micelles at high concentrations and/or at fast flow rates. Although their equilibrium morphology corresponds in theory to vesicles for block copolymer A, a blend of vesicles and of cylindrical (worm-like) micelles for block copolymer B, only cylinders for block copolymer C and spherical micelles for block copolymer D. Vesicles were only detected as a small secondary populations at low concentrations and/or slow flow rates. The second important factor is the used polymer concentration which determines the supersaturation condition. It was for example observed for block copolymer A ($mPEG_{5K}$-*b*-$p(HPMA\text{-}Bz)_{17.1K}$) that nanoprecipitation at high supersaturation condition as a results of using high polymer concentrations is needed in order to obtain only spherical micelles. The third important factor is the flow rate of solvents or mixing time during the nanoprecipitation process, which also has an influence on supersaturation conditions. For both block copolymer A and D ($mPEG_{5K}$-*b*-$p(HPMA\text{-}Bz)_{17.1K}$ and $mPEG_{5K}$-*b*-$p(HPMA\text{-}Bz)_{2.7K}$ respectively) it was found that higher flow rates led to faster and better mixing and therefore resulted in the formation of micelles only. On the contrary, the lower flow rates led to slower mixing conditions (with mixing time up to 1.6 sec), which favors the apparition of self-assemblies with a R_g/R_h ratio around 1. This is a characteristic of vesicles and was even observed for block copolymer D whose hydrophilic fraction $f_{PEG} \sim 65$ % and hydrophobic block length $N_{HPMA\text{-}Bz} \sim 11$ and indicates a preference for the formation of spherical micelles at thermal equilibrium. It is hypothesized that vesicle formation proceeds in the case of block copolymer D through a different mechanism. It was proposed that upon mixing a block copolymer solution with a non-solvent for one block, first spherical micelles that aggregate through

coalescence and grow into larger cylindrical micelles which later fuse into flat membranes that eventually close up on themselves and entrap solvent to yield vesicles. [46,47,49] Such scenario of block copolymer self-assembly from micelles to vesicles through cylinders was confirmed with numerical simulation as described by Campos-Villalobos et al.. [16] This is ascribed to a plasticizing effect of THF, enabling chain mobility even at a temperature below the T_g.

In general, for reliable nanoprecipitation of mPEG-*b*-p(HPMA-Bz) block copolymers into spherical micelles, a high nucleation rate should be created. This could be achieved by providing high supersaturation conditions by applying fast mixing rates and using high polymer concentrations. The intrinsic propensity of the block copolymers to form other morphologies, based on their hydrophobic to hydrophilic ratio, were hereby overwritten. Only at lower mixing rates and lower concentrations these thermodynamically more favorable morphologies became apparent. Finally, after one year, all the samples showed no visible precipitation and evolution when remeasured using DLS, indicating that the formed nanoparticles are stable.

CONCLUSION

This study demonstrates that the self-assembly of mPEG-*b*-p(HPMA-Bz) block copolymers into nanoparticles can be easily tailored in size and morphology using microfluidics. This control relies partly on the hydrophobic to hydrophilic ratio of the block copolymers and mostly on the processing methods which change the supersaturation conditions. In general, mPEG-*b*-p(HPMA-Bz) block copolymers formed micelles when both concentration and total flow rate were high. Lowering both concentration and flow rate resulted in a considerable effect on the resulting size and morphology of mPEG-*b*-p(HPMA-Bz) self-assembled nanoparticles. Even polymersomes were formed for block copolymers which supposedly self-assemble into spherical micelles at the thermodynamic state. However, other time-resolved experiments such X-ray or neutron scattering techniques are necessary to definitively describe the pathway from unimers to self-assemblies. Importantly, microfluidics is a very suitable method to prepare spherical micelles in a scalable and reproducible manner. For future scale-up work, using microfluidics is preferred over batch-wise production as it offers more control over the size and morphology of the nanoparticles that are produced.

ACKNOWLEDGEMENTS

Mahsa Bagheri is thanked for her experimental contributions and fruitful discussions. Dr. Coralie Lebleu, Dr. Olivier Sandre and Dr. René van Nostrum are acknowledged for the useful discussions. Dr Alexander Mason and Imke Welzen-Pijpers are acknowledged for their tremendous efforts to provide cryo-TEM images. Mr Eric Laurichesse from Centre de Recherche Paul Pascal (CNRS, Univ. Bordeaux, France) and Dr Esra Aydinlioglu (LCPO) are kindly acknowledged for the helium pycnometry experiments to measure polymer mass density.

We are also grateful for the financial support received from the European Union's Horizon 2020 research and innovation program Marie Sklodowska-Curie Innovative Training Networks (ITN) under grant No. 676137. Also, the financial support from the CPER CAMPUSB project funded by the French state and the Region Nouvelle Aquitaine is gratefully acknowledged for acquisition of the Dolomite micromixer system.

MATERIALS AND METHODS

Materials

N-(2-benzoyloxypropyl) methacrylamide (HPMA-Bz) and mPEG-ABCPA-mPEG macroinitiator (each mPEG block with a molecular weight of 5.0 kDa) were synthesized and characterized using previously published protocols.[32,50,51] PTFE and cellulose acetate syringe disc filters (both 0.22 μm) and bovine serum albumin (BSA) were obtained from Merck (Darmstadt, Germany). PEG standards for gel permeation chromatography (GPC) analysis were obtained from Agilent (Santa Clara, USA). All solvents were purchased from commercial suppliers and used as received.

Instrumentation: Laminar chaotic mixing microfluidic system

The core of the microfluidic system consists of a commercial herringbone micromixer glass chip (Part No. 3200401 purchased from Dolomite Center Ltd, Royston, UK). According to the manufacturer, the chip consists of two independent channels with 12 mixing steps with a depth and width alternating between 125 × 350 μm and 50 × 125 μm, creating lamination of the entering flows and even swirling of the flow streams. The whole microfluidic system is constituted of two pressure pumps and two flowmeters (range 30 – 1000 μL/min) connected to a computer to control the pumps with the provided software (Mitos Flow Control Center 2.5.17 software), PTFE tubing, ETFE T-connector, a micromixer chip and a fast camera from Dolomite Microfluidics® (**Figure 3.9**). Pump A was linked to the chip through inlets 1 + 3 using the T-connector, whereas the pump B was connected directly to inlet 2.

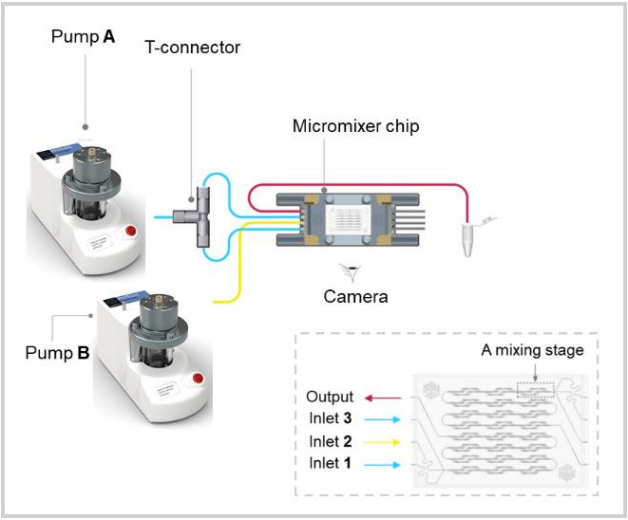

Figure 3.9. Scheme of the microfluidic system used in the present study (from Dolomite Inc., UK).

Flow rate calibration as a function of applied pressure and mixing time calculation was done as described in the manual provided by the supplier (**Figure 3.10** and **Table 3.2**)

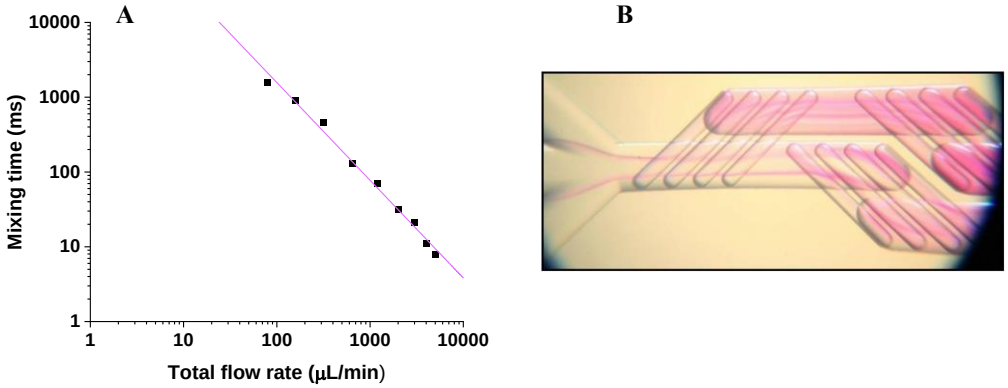

Figure 3.10. (A) Mixing time τ_M (ms) of NaOH and phenolphthalein solutions plotted against total flowrates Q_{tot} (µL/min) for 1:1 ratio at each pump and extrapolated to the following equation $\boldsymbol{mixing\ time\ (\tau_M) = 6.4133 \cdot 10^4\ Q_{tot}^{1.306}}$. **(B)** The photograph shows the calibration experiment of the mixing time using two identical flowrates of respectively phenolphthalein and NaOH solutions. Data and photograph were taken from the specifications on the manufacturer's website. [52]

Dynamic light scattering (DLS)

The hydrodynamic diameter of the self-assemblies was determined by DLS analysis using a Malvern Zetasizer nano series ZS90 with a measurement angle of 173° and a temperature of 25 °C. Prior to measuring, the samples were filtered using a 0.22 μm cellulose acetate disk filter to remove any dust and large particles.

Cryogenic transmission electron microscopy (cryo-TEM) analysis

Cryo-TEM analysis on selected samples was performed using a CryoTitan (Thermo Fisher Scientific) equipped with a field emission gun and autoloader and operated at 300 kV acceleration voltage in low-dose bright-field TEM mode. Samples for cryo-TEM were prepared by glow-discharging the grids (Lacey carbon coated, R2/2, Cu, 200 mesh, EM sciences) in a Cressington 208 carbon coater for 40 seconds. Then, 4 μL of the nanoparticle dispersion was pipetted onto the grid and blotted in a Vitrobot MARK III at room temperature and 100% humidity. The grid was blotted for 3 seconds (offset -3) and subsequently frozen in liquid ethane. Cryo-TEM images were acquired with zero loss energy filtering mode (Gatan GIF 2002, 20eV energy slit) on a CCD camera (Gatan model 794).

Analysis of the micelles by Asymmetric Flow Field-Flow Fractionation connected to Multi-Angle Light Scattering detector (AF4-MALS)

The R_g and R_h were determined using a Wyatt Dualtec AF4 instrument connected to a Shimadzu LC-2030 Prominence-I system with a Shimadzu LC-2030 auto-sampler. The fractionation was accomplished on an AF4 short channel with a spacer of 350 μm and a 10 kDa membrane of regenerated cellulose. The AF4 was attached to a light scattering detector (Wyatt DAWN HELEOS II) that was installed at 16 different angles ranging from 12.9 to 157.8˚ using a laser operating at 664.5 nm and a refractive index detector (Wyatt Optilab). BSA (5 mg/mL) dissolved in phosphate buffer saline (PBS) (0.01 M phosphate buffer, 0.0027 M potassium chloride and 0.137 M sodium chloride, pH 7.4, at 25°C) was used for calibration. The data were analyzed using the provided ASTRA software. The refractive index increment (dn/dc) of the polymers was measured by injection of 600 μL of precisely weighted samples in the range of 6 to 15 mg/mL and using a flow rate of 0.6 mL/min in an Optilab Rex detector (Wyatt technology). The results of the dn/dc measurements were used to calculate the molecular weight $M_{w(np)}$ of the

scattering nanoparticles using a Zimm plot and to deduce the aggregation number N_{agg} by dividing the $M_{w(np)}$ by the weight-averaged molar mass of the polymer chains.[53]

Differential scanning calorimetry

Differential scanning calorimetry (DSC) was performed using a Discovery DSC (TA Instruments, New Castle, DE, USA) calibrated with indium. Samples (5-10 mg) were heated with a ramp of 2 °C/min up to 170 °C (modulated), kept isothermal for 2 min, cooled down at 1 ◦C/min to −90 °C (modulated), isothermal for 10 min, and subsequently heated at 2 °C /min up to 170 °C (modulated). The second heating cycle was used to obtain the glass transition temperature (T_g). T_g was determined by taking the point of inflection of the step change observed in the reversing heat flow curve. For all polymers the T_g is around 98 °C.

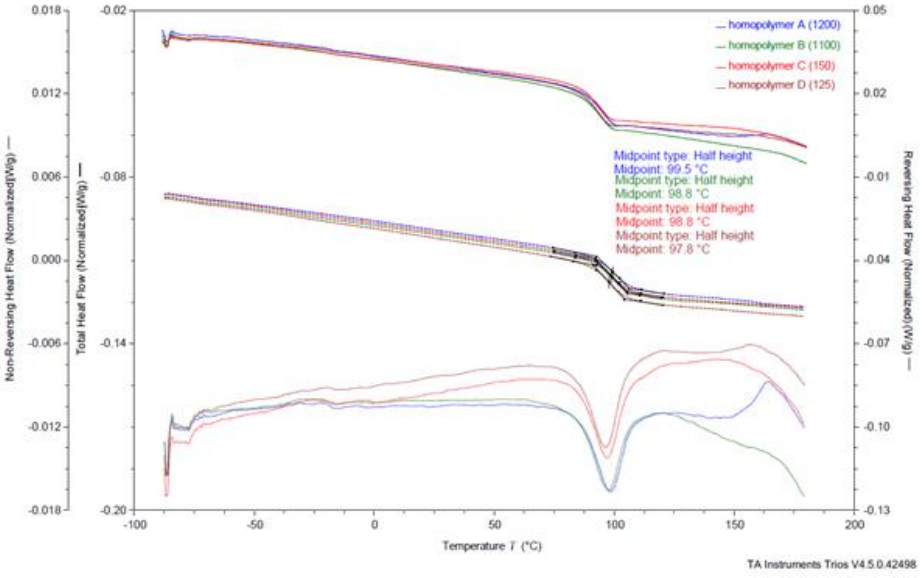

Figure 3.11. Thermograms of p(HPMA-Bz) homopolymers corresponding to the different molecular weight block copolymers recorded by DSC.

Polymer synthesis

mPEG-*b*-p(HPMA-Bz) block copolymers were synthesized by free radical polymerization as described previously (**Scheme 3.1**).[32,50,54] In short, a 4,4-azobis(4-cyanopentanoic acid) (ABCPA) containing macro-initiator, mPEG-ABCPA-mPEG, and HPMA-Bz were dissolved in acetonitrile at varying feed ratios (1:25, 1:50, 1:100, 1:200 mol/mol respectively). Under a nitrogen atmosphere, the polymerization was conducted at 70˚C for 24 h. The formed polymer was collected by precipitation in excess of ice-cold diethyl ether, followed by filtration and drying under vacuum. The synthesized block copolymers were analyzed by GPC and ^{1}H-NMR spectroscopy.

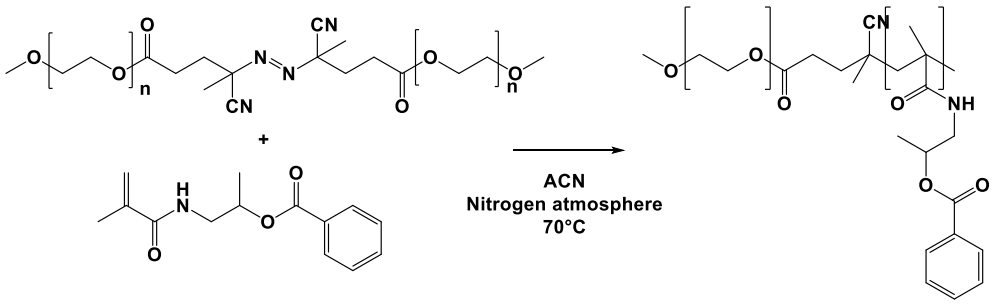

Scheme 3.1. Synthesis of mPEG-*b*-p(HPMA-Bz).

Preparation of nanoparticles based on mPEG-b-p(HPMA-Bz) using microfluidics

The different mPEG-*b*-p(HPMA-Bz) block copolymers were dissolved in THF (concentrations were 5, 10 and 20 mg/mL) and ultrapure water was used as a non-solvent. Both solutions were filtered prior to use with cellulose acetate 0.22 µm and PTFE 0.22 µm syringe filters, respectively. Pump **A** was filled with ultrapure water and pump **B** with the block copolymer solution in THF. The polymer solution and water were mixed at a 1:1 volume ratio at different total flow rates Q_{tot} (100, 200, 350, 500 and 1600 µL/min) and the obtained dispersions were collected at the output into a glass vial until a total volume of 2 mL was obtained. THF was removed by evaporation for 16 hours by leaving the vial uncapped in a fume hood, which leads to less than 1 vol% of THF remaining according to our previous study. [32] The formed nanoparticles, prepared in triplo, were characterized using DLS, AF4-MALLS and cryo-TEM.

REFERENCES

(1) Bobo, D.; Robinson, K. J.; Islam, J.; Thurecht, K. J.; Corrie, S. R. *Pharm. Res.* **2016**, *33* (10), 2373–2387.
(2) van der Meel, R.; Lammers, T.; Hennink, W. E. *Expert Opin. Drug Deliv.* **2017**, *14* (1), 1–5.
(3) Mi, P.; Cabral, H.; Kataoka, K. *Adv. Mater.* **2020**, *32* (13), 1–29.
(4) Varela-Moreira, A.; Shi, Y.; Fens, M. H. A. M.; Lammers, T.; Hennink, W. E.; Schiffelers, R. M. *Mater. Chem. Front.* **2017**, *1* (8), 1485–1501.
(5) Deng, C.; Jiang, Y.; Cheng, R.; Meng, F.; Zhong, Z. *Nano Today* **2012**, *7* (5), 467–480.
(6) Cabral, H.; Miyata, K.; Osada, K.; Kataoka, K. *Chem. Rev.* **2018**, *118* (14), 6844–6892.
(7) Wang, J.; Mao, W.; Lock, L. L.; Tang, J.; Sui, M.; Sun, W.; Cui, H.; Xu, D.; Shen, Y. *ACS Nano* **2015**, *9* (7), 7195–7206.
(8) Sun, Q.; Ojha, T.; Kiessling, F.; Lammers, T.; Shi, Y. *Biomacromolecules* **2017**, *18* (5), 1449–1459.
(9) Cabral, H.; Matsumoto, Y.; Mizuno, K.; Chen, Q.; Murakami, M.; Kimura, M.; Terada, Y.; Kano, M. R.; Miyazono, K.; Uesaka, M.; Nishiyama, N.; Kataoka, K. *Nat. Nanotechnol.* **2011**, *6* (12), 815–823.
(10) Pagels, R. F.; Edelstein, J.; Tang, C.; Prud'homme, R. K. *Nano Lett.* **2018**, *18* (2), 1139–1144.
(11) Lepeltier, E.; Bourgaux, C.; Couvreur, P. *Adv. Drug Deliv. Rev.* **2014**, *71*, 86–97.
(12) Beck-Broichsitter, M.; Rytting, E.; Lebhardt, T.; Wang, X.; Kissel, T. *Eur. J. Pharm. Sci.* **2010**, *41* (2), 244–253.
(13) Zhang, C.; Pansare, V. J.; Prud'Homme, R. K.; Priestley, R. D. *Soft Matter* **2012**, *8* (1), 86–93.
(14) Aubry, J.; Ganachaud, F.; Addad, J. P. C.; Cabane, B. *Langmuir* **2009**, *25* (4), 1970–1979.
(15) Nicolai, T.; Colombani, O.; Chassenieux, C. *Soft Matter* **2010**, *6* (14), 3111–3118.
(16) Campos-Villalobos, G.; Siperstein, F. R.; Charles, A.; Patti, A. *J. Colloid Interface Sci.* **2020**, *572*, 133–140.
(17) Lejeune, E.; Drechsler, M.; Jestin, J.; Müller, A. H. E.; Chassenieux, C.; Colombani, O. *Macromolecules* **2010**, *43* (6), 2667–2671.
(18) Valencia, P. M.; Pridgen, E. M.; Rhee, M.; Langer, R.; Farokhzad, O. C.; Karnik, R. *ACS Nano* **2013**, *7* (12), 10671–10680.
(19) Chen, R.; Wulff, J. E.; Moffitt, M. G. *Mol. Pharm.* **2018**, *15* (10), 4517–4528.
(20) Liu, D.; Zhang, H.; Fontana, F.; Hirvonen, J. T.; Santos, H. A. *Lab Chip* **2017**, *17* (11), 1856–1883.
(21) Liu, D.; Cito, S.; Zhang, Y.; Wang, C. F.; Sikanen, T. M.; Santos, H. A. *Adv. Mater.* **2015**, *27* (14), 2298–2304.
(22) Chiesa, E.; Dorati, R.; Modena, T.; Conti, B.; Genta, I. *Int. J. Pharm.* **2018**, *536* (1), 165–177.
(23) Xu, J.; Zhang, S.; MacHado, A.; Lecommandoux, S.; Sandre, O.; Gu, F.; Colin, A. *Sci. Rep.* **2017**, *7* (1), 1–12.
(24) Ding, S.; Anton, N.; Vandamme, T. F.; Serra, C. A. *Expert Opin. Drug Deliv.* **2016**,

13 (10), 1447–1460.
(25) Martins, J. P.; Torrieri, G.; Santos, H. A. *Expert Opin. Drug Deliv.* **2018**, *15* (5), 469–479.
(26) Liu, D.; Zhang, H.; Fontana, F.; Hirvonen, J. T.; Santos, H. A. *Adv. Drug Deliv. Rev.* **2018**, *128*, 54–83.
(27) Soleimani, S.; Hasani-Sadrabadi, M. M.; Majedi, F. S.; Dashtimoghadam, E.; Tondar, M.; Jacob, K. I. *Colloids Surfaces B Biointerfaces* **2016**, *145*, 802–811.
(28) Bally, F.; Garg, D. K.; Serra, C. A.; Hoarau, Y.; Anton, N.; Brochon, C.; Parida, D.; Vandamme, T.; Hadziioannou, G. *Polymer* **2012**, *53* (22), 5045–5051.
(29) Keßler, S.; Drese, K.; Schmid, F. *Polymer* **2017**, *126*, 9–18.
(30) Hamdallah, S. I.; Zoqlam, R.; Erfle, P.; Blyth, M.; Alkilany, A. M.; Dietzel, A.; Qi, S. *Int. J. Pharm.* **2020**, *584* (January).
(31) Lebleu, C.; Rodrigues, L.; Guigner, J. M.; Brûlet, A.; Garanger, E.; Lecommandoux, S. *Langmuir* **2019**, *35* (41), 13364–13374.
(32) Bagheri, M.; Bresseleers, J.; Varela-Moreira, A.; Sandre, O.; Meeuwissen, S. A.; Schiffelers, R. M.; Metselaar, J. M.; Van Nostrum, C. F.; Van Hest, J. C. M.; Hennink, W. E. *Langmuir* **2018**, *34* (50), 15495–15506.
(33) Sundararajan, P.; Stroock, A. D. *Annu. Rev. Chem. Biomol. Eng.* **2012**, *3* (1), 473–496.
(34) Le Fer, G.; Portes, D.; Goudounet, G.; Guigner, J. M.; Garanger, E.; Lecommandoux, S. *Org. Biomol. Chem.* **2017**, *15* (47), 10095–10104.
(35) Nelson, A.; Cosgrove, T. *Langmuir* **2004**, *20* (6), 2298–2304.
(36) Jain, S.; Bates, F. S. *Science* **2003**, *300* (5618), 460–464.
(37) D'Addio, S. M.; Prud'homme, R. K. *Adv. Drug Deliv. Rev.* **2011**, *63* (6), 417–426.
(38) Kunz, D.; Thurn, A.; Burchard, W. *Colloid Polym. Sci.* **1983**, *261* (8), 635–644.
(39) Ma, C.; Pan, P.; Shan, G.; Bao, Y.; Fujita, M.; Maeda, M. *Langmuir* **2015**, *31* (4), 1527–1536.
(40) Nie, T.; Zhao, Y.; Xie, Z.; Wu, C. *Macromolecules* **2003**, *36* (23), 8825–8829.
(41) Nguyen, V. T. A.; De Pauw-Gillet, M. C.; Sandre, O.; Gauthier, M. *Langmuir* **2016**, *32* (50), 13482–13492.
(42) Giacomelli, C.; Schmidt, V.; Aissou, K.; Borsali, R. *Langmuir* **2010**, *26* (20), 15734–15744.
(43) Kale, T. S.; Klaikherd, A.; Popere, B.; Thayumanavan, S. *Langmuir* **2009**, *25* (17), 9660–9670.
(44) Abdelmohsen, L. K. E. A.; Rikken, R. S. M.; Christianen, P. C. M.; van Hest, J. C. M.; Wilson, D. A. *Polymer* **2016**, *107*, 445–449.
(45) Chécot, F.; Brûlet, A.; Oberdisse, J.; Gnanou, Y.; Mondain-Monval, O.; Lecommandoux, S. *Langmuir* **2005**, *21* (10), 4308–4315.
(46) Antonietti, M.; Förster, S. *Adv. Mater.* **2003**, *15* (16), 1323–1333.
(47) Nagarajan, R. *Langmuir* **2002**, *18* (1), 31–38.
(48) He, X.; Schmid, F. *Macromolecules* **2006**, *39* (7), 2654–2662.
(49) Mai, Y.; Eisenberg, A. *Chem. Soc. Rev.* **2012**, *41* (18), 5969–5985.
(50) Bresseleers, J.; Bagheri, M.; Storm, G.; Metselaar, J. M.; Hennink, W. E.; Meeuwissen, S. A.; Van Hest, J. C. M. *Org. Process Res. Dev.* **2019**, *23*, 2707–2715.
(51) Shi, Y.; Van Steenbergen, M. J.; Teunissen, E. A.; Novo, L.; Gradmann, S.; Baldus, M.; Van Nostrum, C. F.; Hennink, W. E. *Biomacromolecules* **2013**, *14* (6), 1826–1837.
(52) Micromixer Chip https://www.dolomite-microfluidics.com/product/micromixer-chip/

(accessed May 26, 2020).
(53) Zimm, B. H. *J. Chem. Phys.* **1948**, *16* (12), 1099–1116.
(54) Shi, Y.; Van Der Meel, R.; Theek, B.; Oude Blenke, E.; Pieters, E. H. E.; Fens, M. H. A. M.; Ehling, J.; Schiffelers, R. M.; Storm, G.; Van Nostrum, C. F.; Lammers, T.; Hennink, W. E. *ACS Nano* **2015**, *9* (4), 3740–3752.

Chapter 4

Scale-up of the Manufacturing Process to Produce Docetaxel-Loaded mPEG-*b*-p(HPMA-Bz) Block Copolymer Micelles for Pharmaceutical Applications

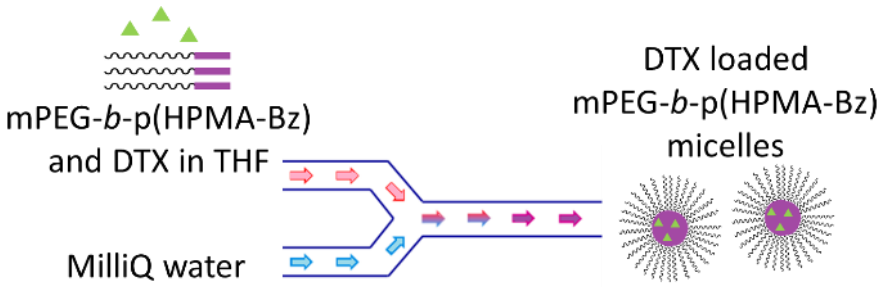

This work has been published as:

Bresseleers, J.; Bagheri, M.; Storm, G.; Metselaar, J. M.; Hennink, W. E.; Meeuwissen, S. A.; Van Hest, J. C. M. *Org. Process Res. Dev.* **2019**, *23*, 2707–2715.

ABSTRACT

In this chapter an efficient, scalable and good manufacturing practice (GMP) compatible process was developed for the production of docetaxel-loaded poly(ethylene glycol)-*b*-poly(*N*-2-benzoyloxypropyl methacrylamide) (mPEG-*b*-p(HPMA-Bz)) micelles. First, the synthesis of the mPEG-*b*-p(HPMA-Bz) block copolymer was optimized through step-by-step investigation of the batch synthesis procedures. This resulted in the production of 1 kg of mPEG-*b*-p(HPMA-Bz) block copolymer with a 5 kDa PEG block and an overall molecular weight of 22.5 kDa. Second, the reproducibility and scalability of micelle formation was investigated for both batch and continuous flow setups by assessing critical process parameters. This resulted in the development of a new and highly efficient continuous flow process, which led to the production of 100 mL of unloaded micelles with a size of 55 nm. Finally, the loading of the micelles with the anti-cancer drug docetaxel was successfully fine-tuned to obtain precise control on the loaded micelle characteristics. As a result, 100 mL of docetaxel loaded micelles (20 mg/mL polymer and 5 mg/mL docetaxel in the feed) with a size of 55 nm were prepared. The drug encapsulation efficiency was 65 %, which amounted to a loading capacity of 14 %. The particles, which were stable for at least two months in water at room temperature, were produced with the newly developed continuous flow process. In conclusion, this study paves the way for efficient and robust large-scale production of docetaxel loaded micelles with high encapsulation efficiencies and stability, which is crucial for their applicability as a clinically relevant drug delivery platform.

INTRODUCTION

Long-standing developments in the field of nanomedicine have resulted in a range of promising nanocarrier formulations for drug delivery. [1–4] For example, polymeric micelles, which are core-shell nanoparticulate structures composed of amphiphilic polymers, have attracted much attention. Their hydrophobic core allows for the accommodation and potentially improved pharmacokinetics of poorly water-soluble drugs such as a number of chemotherapeutics used for cancer treatment. The hydrophilic shell of polymer micelles, often based on the hydrophilic polyethylene glycol (PEG), provides colloidal stability and stealth-like properties [5–10].

Despite promising preclinical results and their high pharmaceutical and economical potential [2,11], there are still some important hurdles that typically appear in the development process of nanomedicines. A main challenge that needs to be tackled is the scalable and reproducible production of not only the building blocks but also the drug-loaded assembled nanoparticles. Although scalability is an important aspect in the development of any new drug formulation, this challenge is even more prominent in the relatively new area of nanomedicine. The reasons for this are the complexity of the chemistry required (since nanoparticles are usually assemblies of multiple components), the manufacturing process and the quality control (which should all match with the standards of GMP) [12,13,14]. Besides that, the instability of the nanoparticles is also a typical issue that needs attention. During early experimentation and preclinical research programs, these crucial aspects are often not studied. This is reflected by very limited publications regarding scalability, reproducibility and process development towards GMP production of nanomedicines.

Recently, a highly promising polymer micelle formulation based on poly(ethylene glycol)-*block*-poly(*N*-2-benzoyloxypropyl methacrylamide) (mPEG-*b*-p(HPMA-Bz)) was reported. [15–17] These micelles demonstrated high drug loading for paclitaxel and docetaxel (DTX), drug retention and particle stability as a result of the π-π stacking and hydrophobic interactions enabled by the hydrophobic benzyl groups containing blocks in the core of the micelles. In this chapter, the chemotherapeutic drug DTX was chosen as a model drug for the loading of the micelles, since it is a clinically well-established drug that presents high therapeutic efficacy against a range of solid tumors. In general, the application of DTX is limited by dose depending neurotoxic side effects and its high hydrophobic nature. For the latter, solubility enhancers such as

Cremophor EL are used, which in turn are associated with hypersensitivity reactions. [18] In previous studies it was shown that DTX can be encapsulated with high efficiency, because of its high hydrophobicity and the presence of aromatic groups in its molecular structure contributing to the π-π stacking interactions in the core of the (mPEG-*b*-p(HPMA-Bz) micelles.[19]

The goal of the research described in this chapter was to develop an efficient, scalable and highly controlled process for the manufacturing of the newly developed DTX-loaded polymer micelles based on mPEG-*b*-p(HPMA-Bz), keeping GMP regulations in mind. This was achieved by first optimizing the 4-step synthesis of the mPEG-*b*-p(HPMA-Bz) building block with a fixed molecular weight of the mPEG of 5 kDa and an aimed molecular weight of the p(HPMA-Bz) block between 15-20 kDa. Subsequently, a thorough evaluation was performed of batch production versus continuous flow processes to enable the selection of the preferred preparation methodology for both unloaded and drug-loaded micelles at a large scale.

RESULTS AND DISCUSSION

In order to attain a clinically applicable nanomedicine formulation, all aspects of the production, from monomer synthesis to preparation of the drug loaded particles have to be done in a commercially feasible and reproducible manner. Synthesis was therefore performed on a kg scale. Furthermore, in the preclinical preparation protocol a number of adjustments had to be made to achieve this level of scalability. In the following sections the different steps are discussed in detail.

Monomer synthesis

HPMA synthesis

In a publication of Kopeček and Bažilová, HPMA was synthesized by reaction of methacryloyl chloride with 1-amino-2-propanol in acetonitrile at 0 ˚C. [20] In previous work we employed a Schotten-Baumann reaction overnight where 1-amino-2-propanol was stirred in a two-layer system of water and DCM while NaOH was titrated together with the methacryloyl chloride to neutralize the formed HCl, resulting in a ~80 % yield. [16,17,19]

In the present study, however, a new method was developed in which it was decided to perform the reaction in water only with an excess of NaOH. The presence of this excess neutralizes the formed HCl. An additional advantage of this method was that the reaction was completed in less than 3 hours instead of overnight. Additionally, after purification and work-up, this reaction resulted in an excellent yield of ~90 % and 99.9 % purity according to HPLC (**Figure S4.1 and S4.2**).

HPMA-Bz synthesis

HPMA-Bz was synthesized by reaction of HPMA and benzoyl chloride. The latter contained trace amounts of benzoyl anhydride, as detected by HPLC (**Figure S4.3**). During the HPMA-Bz synthesis, it was shown that even more benzoyl anhydride was formed, probably due to the reaction of benzoyl chloride with water present in the used DCM (**Figure S4.4**). This anhydride remained present during regular work-up procedures, and therefore an adequate extraction method was developed to remove this impurity from the solid HPMA-Bz. Multiple solvents were tested for a solid-liquid extraction process, including acetone, ACN, ethanol, methanol and heptane. It was found

that heptane was able to dissolve and extract the remaining anhydride from the product, because HPMA-Bz is essentially insoluble in this solvent. After a solid-liquid extraction, followed by filtration and drying of the powder, HPMA-Bz was obtained in a yield of ~85 % and a purity of 99.3 %, as determined by HPLC (**Figure S4.5**) and a content of 98.5 % as determined by content ^{1}H-NMR (**Figure S4.6**).

Macro-initiator synthesis

Following a recently optimized procedure [21], the mPEG-ABCPA-mPEG macro-initiator (MI) ($mPEG_{5K}$) was successfully synthesized on a large scale (450 g). The only difference with the previous method was that the product was precipitated in MTBE and collected through filtration instead of centrifugation. The total yield of the synthesized MI was very high (~97 %).

There is a possibility that the mono-functionalized initiator mPEG-ABCPA is formed upon MI synthesis, leading to the formation of unwanted p(HPMA-Bz) homopolymer during radical polymerization. This homopolymer will be solubilized in the core of the micelles, which in turn will result in an increase in micellar size. [21] Analysis of the synthesized MI by GPC showed that approximately 9 % impurity was present in the form of a molecular species with 5 kDa molecular weight, which corresponds to the mono-functionalized initiator mPEG-ABCPA and /or free mPEG (**Figure S4.7**). Analysis by ^{1}H-NMR using trichloroacetyl isocyanate (TAIC) as reactive agent, which allowed to detect the free OH group of unreacted PEG [22], showed that the impurity of the MI with free mPEG-OH also amounted to 9 %, indicating that the product only contained a trace amounts of mPEG-ABCPA (**Figure S4.8**). It was therefore envisioned that using this MI would result in only very low amounts of the homopolymer p(HPMA-Bz). However, there was also a possibility that non-functionalized ABCPA was present in the mixture which would give p(HPMA-Bz) upon polymerization. The detection limit of ABCPA within the MI sample was determined to be 0.1 wt %. Further HPLC analysis was not able to detect any ABCPA in the actual MI mixture and therefore indicated that only very low amounts of ABCPA were present (below 0.1 wt %), if present at all (**Figure S4.9**). The total yield of the synthesized MI was very high (~97 %).

Polymerization of HPMA-Bz using mPEG-ABCPA-mPEG as macro-initiator

The mPEG-*b*-p(HPMA-Bz) block copolymer was successfully synthesized on a scale of ~1.6 kg, using mPEG-ABCPA-mPEG as macro-initiator. After 2 precipitations in cold MTBE, mPEG-*b*-p(HPMA-Bz) was obtained with a yield of ~71 % with only trace amounts of residual monomer, as determined by ^{1}H-NMR (**Figure S4.10**).

Even though the formation of p(HPMA-Bz) homopolymer was reduced, due to the optimization of the procedure for the preparation of the mPEG-ABCPA-mPEG macro-initiator, some homopolymer could still be present in the mixture after polymerization. Therefore, a method was successfully developed to remove even trace amounts of p-(HPMA-Bz) homopolymer. This newly developed method can be found in the Materials and Methods section. Using a block copolymer sample deliberately contaminated with homopolymer, purification was obtained by precipitating a heated ethanol solution of the polymer mixture in water. It was shown by ^{1}H-NMR that the precipitate only contained 2 w% mPEG (**Figure S4.11**). This is 10 times smaller than envisioned for normally synthesized block copolymers and would give a block copolymer with an M_n of 222.3 kDa. This indicates that it was indeed mainly p(HPMA-Bz) homopolymer that precipitated. With this additional precipitation method, approximately 1 kg of the purified mPEG-b-p(HPMA-Bz) block copolymer (M_n 22.5 kDa) was eventually obtained.

The purified mPEG-b-p(HPMA-Bz) block copolymer product did not contain detectable residual monomer, as detected by ^{1}H-NMR and the molecular weights were determined by ^{1}H-NMR (M_n: 22.5 kDa) and GPC (M_n: 19.3 kDa and M_w: 21.6 kDa). (**Figure S4.12 and S4.13**)

Micelle preparation

In previous studies, the micelles were prepared through a nanoprecipitation method [16,21]. Purified mPEG-*b*-p(HPMA-Bz) was dissolved in THF and pipetted into water. This solution was left overnight in a fume hood for THF to spontaneously evaporate. For obvious reasons, when working on a large scale with multiple liters of solution, this is not a feasible method. An attempt was therefore made to remove the THF *in vacuo*, which unfortunately resulted in aggregation and visual precipitation of the polymeric material. As a result, it was decided to remove THF using dialysis. A simple dialysis was performed for the polymer THF/water solution against water in a dialysis bag with a cut-

off at 12-14 kDa. This resulted in the formation of micelles with an average diameter of ~57 nm and a narrow size distribution (PDI) lower than 0.1 according to DLS. This was in agreement with the solvent evaporation method that yielded sizes of ~55 nm and a PDI < 0.1. To replace the batch-wise dialysis process with a scalable procedure, continuous transient flow filtration (TFF) was explored.

Previous research in ***Chapter 2*** *and* ***Chapter 3*** showed that if supersaturation upon mixing is not obtained, micelle formation will result in poorly-defined micelles of varying sizes. [21] To reduce the risk in these variations and therefore ensure supersaturation of the mixture, the polymer was dissolved at high concentration (20 mg/mL) in THF and the ratio in which this solution was added to water was kept at 1:1 while collecting the micelle dispersions under continuous stirring. This was first tested on a small scale, collecting only 10 mL, and evaporating the THF overnight in a fume hood, which resulted in the formation of micelles with a mean size of 55 nm and a PDI lower than 0.1. With the continuous flow preparation, larger amounts of micellar dispersions were prepared, diluted, concentrated and purified by TFF. This resulted in the production of 100 mL of micellar dispersion in water with a concentration of 20 mg polymer per mL and a residual THF content below the detection limit of GC-headspace and therefore conform safety regulations. The mean size of the micelles was 55 nm and the PDI value was below 0.1, which is the same as the micelles produced using the batch setup (**Figure 4.4A**). The produced micelle dispersion was split in two parts which were stored at 4°C and at room temperature. After 2 months, no precipitation or changes in size and PDI were observed for both storage conditions. It is envisioned that even up to multiple liters can be prepared using this newly developed continuous flow method.

Preparation of docetaxel loaded micelles

For preparation of DTX-loaded mPEG-*b*-p(HPMA-Bz) micelles, mPEG-*b*-p(HPMA-Bz) was dissolved in THF (20 mg/mL) and subsequently DTX was added and dissolved (final concentration was 5 mg/mL) . The preparation method was first tested on a small scale in a fume hood. To this end, 1 mL of the polymer/DTX solution was added to 1 mL water, the THF was removed either by evaporation overnight in the fume hood or by dialysis against water. Both methods resulted in the formation of micelles with a mean size of 55 nm and PDIs below 0.1, which is a similar size and PDI as the non-loaded micelles (**Figure 4.4A**). Cryo-TEM imaging showed no difference between the

structures of the loaded versus the non-loaded micelles (**Figure 4.1**). The diameters of the micelles in the cryo-TEM images were smaller compared to the hydrodynamic diameters as detected by DLS. This is because using cryo-TEM imaging, only the micelle core is visualized. HPLC analysis showed that the encapsulation efficiency was ~85 % for the evaporated samples and ~65 % for the dialyzed samples (**Figure 4.2A**). The loading capacities were determined to be ~17.5 % and ~14 % respectively.

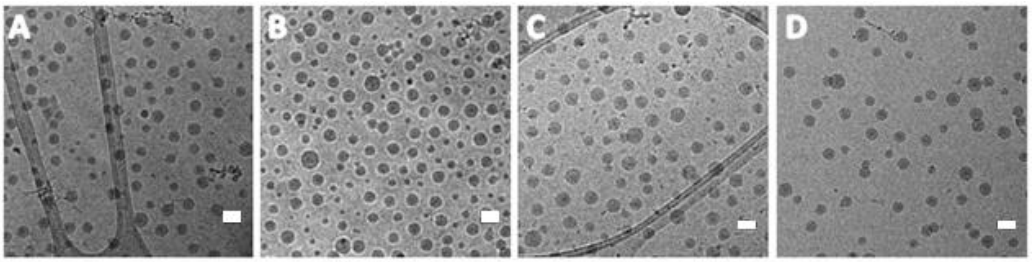

Figure 4.1. Cryo-TEM images of the mPEG-*b*-p(HPMA-Bz) micelles. Scale bars correspond to 50 nm. (**A**) unloaded and prepared in batch (average diameter 29 nm); (**B)** DTX loaded and prepared in batch (average diameter 28 nm); (C) unloaded and prepared using continuous flow (average diameter 28 nm); (**D**) DTX loaded and prepared using continuous flow (average diameter 27 nm).

One possible hypothesis for this difference in encapsulation efficiencies relies on the difference between the two work up methods that leads to a difference in the final concentration of DTX in the dispersions. During dialysis THF is passively replaced by water and therefore the micelle dispersion is diluted, whereas during evaporation THF is removed leaving a more concentrated dispersion. It is hypothesized that not all DTX is perfectly partitioned into the micellar cores with part of it located into the PEG corona. Once the micelle dispersion is then diluted during dialysis, the DTX that is present in the corona area will be released rapidly. In that case, visible precipitation of DTX is observed. For the micelles prepared using the evaporation method, this is not the case. It is envisioned that over time, the DTX that is present in the corona area will be slowly released. Eventually only DTX that is partitioned in the micelle cores will remain in the micelle dispersion and will be retained for a prolonged period of time.

$$Encapsulation\ efficiency\ (\%) = \frac{[measured\ DTX]}{[total\ added\ DTX]} \times 100$$

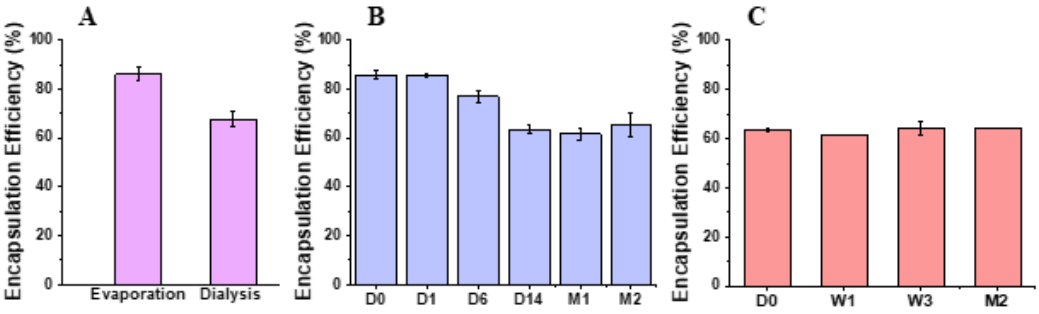

Figure 4.2. Encapsulation efficiencies of DTX-loaded micelles. (**A**) Using batch mode and the evaporation and dialysis protocols for work up. (**B**) Stability study at room temperature of the DTX-loaded micelles that were prepared using the solvent evaporation method. Time points are day 0 (D0), after 1 day (D1), after 6 days (D6), after 2 weeks (D14), after 1 month (M1), after 2 months (M2). (**C**) Stability study at room temperature of the DTX-loaded micelles that were produced using the dialysis work up. Time points are starting point (D0), after 1 week (W1), after 3 weeks (W3) and after 2 months (M2). Polymer concentration of each: 20 mg/mL.

The stability of the DTX-loaded micelles that were prepared using the solvent evaporation method, was followed upon incubation of the micellar dispersions at room temperature for two months. The micellar size distribution remained similar over this entire period, whereas the encapsulation efficiency decreased from ~85 % to ~65 % in 2 weeks (**Figure 4.2B**). This latter value resembles the DTX-loaded micelles that were produced using the dialysis method. On the contrary, looking into the stability of the DTX-loaded micelles produced in batch mode using dialysis, the encapsulation efficiency did not decrease over time (**Figure 4.2C**). This reinforces the hypothesis that not all DTX is partitioned in the micellar core and that a part is located in the PEG corona. For the samples obtained via the dialysis work up, as mentioned before, no decrease in encapsulation efficiency was observed over time, since all the DTX that was absorbed into the corona was already released due to the dilution factor. For the evaporation work up, this is not the case and the DTX that is located in the PEG corona will be released over time in the stability study. This result demonstrates that for reproducible micelle preparation a dialysis method is preferred.

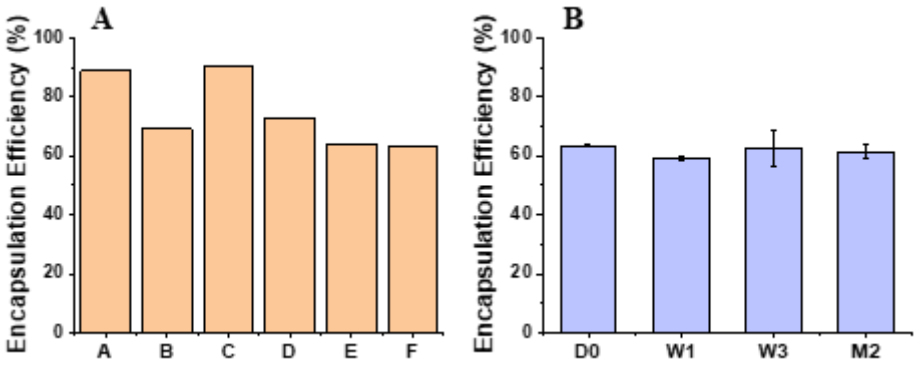

Figure 4.3. Encapsulation efficiencies of DTX. (**A**) EE after the different steps and controls during DTX-loaded micelle production using a continuous flow process. A: After overnight evaporation of THF; B: After dialysis against water; C: After filtration over a 0.2 µm disk filter and overnight evaporation; D: After diluting 10 times; E: after concentrating to a 20 mg/mL polymer solution; F: final DTX-loaded micelle product. (**B**) Stability study at room temperature of the DTX-loaded micelles produced in continuous flow. Time points are starting point (D0), after 1 week (W1), after 3 weeks (W3) and after 2 months (M2).

DTX-loaded micelles were also prepared using the newly developed continuous flow procedure. The DTX/polymer in THF solution was continuously added to MilliQ water at a 1:1 flow ratio with a total flow rate of 2 mL/min, using 2 piston pumps, until a total volume of 200 mL was obtained. Out of this dispersion two 1 mL samples were taken: THF was removed by overnight evaporation for one sample (**Figure 4.3A.A**), the other sample was dialyzed against water (**4.3A.B**). The remaining ~200 mL micelle dispersion was filtered over a 0.2 µm disk filter. A 1 mL sample was taken after filtration and THF was removed by overnight evaporation (**4.3A.C**). The micelle dispersion was then diluted 10 times (**4.3A.D**) and, by using TFF, concentrated to a 20 mg polymer solution per mL (**4.3A.E**). As a final purification step the micelle dispersion was washed with 4 diafiltration volumes, so 4 times with 100 mL MilliQ water to obtain the final DTX-loaded micelle product (**4.3A.F**) without any detectable residual THF as measured by GC-headspace. Analysis of the intermediate steps and the final product confirmed similar behavior regarding encapsulation efficiency as was observed for the small-scale productions. Once the micelle dispersion was further diluted with water, either by dialysis or simple addition of the water, the encapsulation efficiency dropped from approximately 85 to 65 %. Micelle size distributions did remain

constant with an average size of 55 nm and a PDI below 0.1, identical to those sizes obtained for the small-scale production methods (**Figure 4.4A**). Cryo-TEM imaging confirmed these results (**Figure 4.1**).

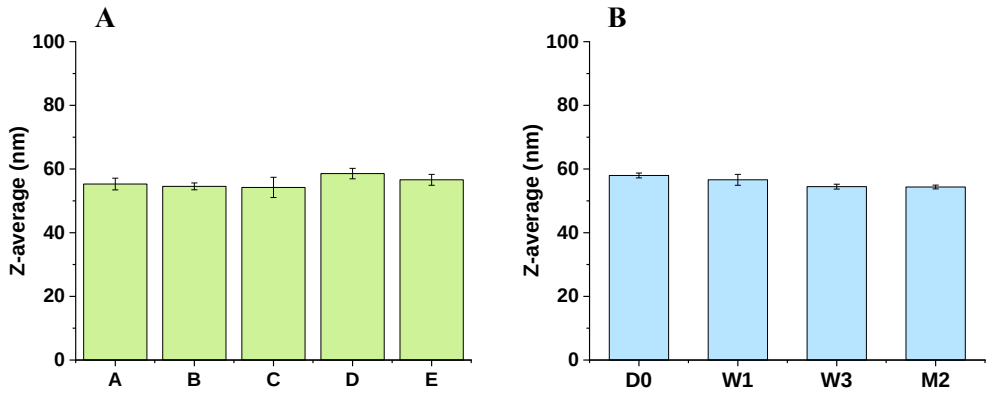

Figure 4.4. Average hydrodynamic diameters as measured by DLS. (**A**) A: micelles prepared using the nanoprecipitation method, followed by solvent evaporation, B: micelles prepared using the nanoprecipitation method followed by dialysis, C: micelles prepared using flow formation and TFF, D: DTX loaded micelles prepared using the nanoprecipitation method and evaporation, E: DTX loaded micelles prepared using flow formation and TFF. (**B**) Stability study at room temperature for the DTX-loaded micelles that were produced in continuous flow. Time points are starting point (D0), after 1 week (W1), after 3 weeks (W3) and after 2 months (M2).

The stability of the DTX-loaded micelles regarding drug retention, which were made using the continuous flow setup, was followed for a period of two months. After two months the micelle size distribution and encapsulation efficiency did not change significantly (**Figure 4.3B** and **Figure 4.4B**). This reinforces the hypothesis that upon micelle formation, not all DTX is solubilized in the micellar core and that part is present at the core-shell interface or even in the more hydrophilic mPEG corona. Most noteworthy, very stable particles with negligible DTX release during storage were produced on a large scale. The described continuous flow production process can be likely translated into a large-scale manufacturing process for the production of liters of loaded micelles suitable for clinical evaluation.

CONCLUSION

The goal of this study was to develop an efficient, scalable and highly controlled process for the manufacturing of DTX-containing nanoparticles based on polymer micelles assembled from the amphiphilic block copolymer mPEG-*b*-p(HPMA-Bz). The results demonstrate an excellent and optimized process for the large batch synthesis on ~ 1 kg scale of mPEG-*b*-p(HPMA-Bz) ($mPEG_{5K}$, M_n 22.5 kDa). It is important to know that the amount of polymer produced is sufficient for the production of enough micelle formulation to go through the first phase of clinical trials. Using this polymer, micelles were easily made by both batch and continuous flow setups. Comparison of the results and feasibility for larger scale production indicate a clear preference to using the continuous flow setup. Since the most important parameters for homogenous micelle formation are mixing and saturation conditions, polymer micelles were efficiently made in a reproducible manner regarding particle size using continuous flow processing. The loading of the mPEG-*b*-p(HPMA-Bz) with DTX was very efficient, with outstanding encapsulation efficiencies of ~65 % and a loading capacity of 14 %. Moreover, the drug-loaded micelles retained the encapsulated drug over a prolonged period of time. Most importantly, the production methodology described herein to produce the loaded nanoparticles can be readily translated for production under GMP conditions for future clinical trials.

ACKNOWLEDGMENT

Mahsa Bagheri is thanked for her experimental contributions and fruitful discussions. Dr. Bart Metselaar and Dr. Gert Storm are acknowledged for the useful discussions. Dr Alexander Mason and Imke Welzen-Pijpers are acknowledged for their efforts to provide cryo-TEM images.

We are also grateful for the financial support received from the European Union's Horizon 2020 research and innovation program Marie Sklodowska-Curie Innovative Training Networks (ITN) under grant No. 676137.

MATERIALS AND METHODS

Materials

DL-1-amino-2-propanol, methacryloyl chloride, sodium hydroxide (NaOH), sodium chloride (NaCl), magnesium sulphate ($MgSO_4$), benzoyl chloride, triethyl amine (TEA), benzoic anhydride, 4,4-azobis(4-cyanopentanoic acid) (ABCPA), N,N'-dicyclohexylcarbodiimide (DCC) and trichloroacetyl isocyanate (TAIC) were obtained from Sigma-Aldrich (Darmstadt, Germany) and used without further purification. Poly(ethylene glycol) methyl ether (mPEG) 5 kDa was obtained from Polysciences (Warrington, USA) and dried in a vacuum stove overnight at 70 °C. Docetaxel was obtained from Alfa Aesar (Kandel, Germany) and used without further purification. All solvents were purchased from commercial suppliers and used as received.

^{1}H-NMR

Approximately 20 mg of the product was dissolved in 700 µL and measured using a 400 MHz NMR with a 5 mm PABBO BB probe from Bruker. For HPMA, HPMA-Bz, mPEG-*b*-p(HPMA-Bz) and p(HPMA-Bz) DMSO-d6 and for the MI $CDCl_3$ was used as solvent.

The amount of unreacted mPEG-OH in the MI product was determined by TAIC. Five drops of TAIC were added to the NMR tube and after 20 minutes a ^{1}H-NMR spectrum was recorded. Using TAIC, the signal of the methylene group neighboring the terminal hydroxyl group was reported to shift from 4.2 to 4.4 ppm. [22] The amount of unreacted mPEG-OH was subsequently determined based on the peak areas. [17,23] The M_n of the block copolymer, before and after removal of the homopolymer, as well as the M_n of the removed homopolymer were determined using the following formula:

$$M_n = \left(integral\ at\ 8.0\ ppm/2\ * M_{w(HPMA-Bz)}\right) + 5000\ \ g/mol$$

Content ^{1}H-NMR

Content ^{1}H-NMR can be used to give information on the content or percentage of total compound present in an obtained product. This is done by adding a known amount of an internal standard with a distinct integration area compared to those of the tested compound. In our case for HPMA-Bz, approximately 20 mg of HPMA-Bz was dissolved in 700 µL DMSO-d6 and measured using a 400 MHz NMR with a 5 mm PABBO BB probe from Bruker. For determination of the content ~ 9 mg of maleic acid was added to the samples as an internal reference content standard (99.94 %). The content of the compound can be calculated using the following formula:

$$Px = \frac{I_x * N_{std} * M_x * W_{std}}{I_{std} * N_x * M_{std} * W_x} * P_{std}$$
$$= \frac{0.94 * 2 * 247.29\ g/mol * 9.62\ g}{2 * 1 * 116.07\ g/mol * 19.55\ g} * 99.94\% = 98.55\ \%$$

Where P_x is the content of the sample (%m/m), P_{std} is the content of the standard (%m/m), I_x is one of the integration areas of the HPMA-Bz sample (in our case the one at 5.59 ppm), I_{std} is the integration area of the standard at 6.28 ppm, N_x is the number of protons (1 proton) of the integrated peak at 5.59 ppm of the HPMA-Bz sample, N_{std} is the number of protons (2 protons) of the integrated peak of the standard, M_x is the molecular weight of the sample (247.29 g/mol), M_{std} is the molecular weight of the standard (116.07 g/mol), W_x is what was weighed of the sample (mg) and W_{std} is what was weighed of the standard (mg).

HPLC

HPMA, HPMA-Bz and DTX were analyzed via high performance liquid chromatography (HPLC) by injecting 1 µL, using an Agilent XDB-C18 (50 x 4.6 mm, 1.8 µm) column and a gradient flow of 1 mL/min, going from 95% of 0.1 % formic acid in water and 5% of 0.05 % formic acid in acetonitrile (ACN) to 95 % of 0.05 % formic acid in ACN and 5 % of 0.1% formic acid in water. Detection was done at 254 nm for HPMA and HPMA-Bz and at 230 nm for DTX. HPMA and HPMA-Bz samples were prepared by dissolving 20 mg in 1 mL ACN. For the determination of DTX loading, samples were prepared by dissolving 50 µL of filtered micelle dispersion in 950 µL ACN. This mixture

was vortexed to ensure complete disassembly of the micelles and a homogeneous distribution of DTX in the solution.

ABCPA was analyzed via HPLC by injecting 10 µL, using an XBridge C8 (50 x 4.6 mm, 5 µm) column and a gradient flow of 1 mL/min, going from 98% of 0.1 % formic acid in water and 2% of 0.05 % formic acid in acetonitrile (ACN) to 95 % of 0.05 % formic acid in ACN and 5 % of 0.1% formic acid in water. Detection was done at 210 nm. Samples were prepared by dissolving 20 mg of MI in 1 mL ACN.

GPC

The MI and the synthesized mPEG-*b*-p(HPMA-Bz) before and after homopolymer removal were analyzed by GPC to measure the number average molecular weight (M_n), weight average molecular weight (M_w) and molecular weight distribution using a PSS PFG analytical linear S column and PEGs of narrow molecular weights as calibration standards. The samples were prepared by dissolving approximately 5 mg in 1 mL DMF containing 10 mM LiCl. Samples of 20 µL were injected and eluted with DMF containing 10 mM LiCl as the eluent. The elution rate was 0.7 mL/min, with a temperature of 40 °C and the sample was detected using a refractive index detector.

Gas chromatography headspace analysis (GC-headspace)

To determine residual solvent in the micellar dispersions, GC-headspace was conducted. A Shimadzu GC-2010 equipped with a Flame Ionization Detector and Shimadzu HS-20 headspace auto-sampler was used together with a 30 m x 0.32 mm capillary column with a film thickness of 0.25 µm. For the internal standard, a stock solution was prepared by dissolving 150 µL 2-propanol (analytical standard) in water using a volumetric 100 mL flask. Of this solution,1 mL was transferred into another 100 mL volumetric flask and diluted to the 100 mL volume with DMF. The THF standard, used for calibration, was made by pipetting 300 µL in a 50 mL volumetric flask which was diluted to volume with DMF. 1 mL of this stock was transferred to a 100 mL volumetric flask and diluted to volume with DMF to get a THF concentration of 1067 ppm. 1 mL of this standard solution was mixed with 4 mL internal standard stock solution and put in a 20 mL GC-headspace vial. The samples were prepared dissolving 50 µL of micellar dispersion in 1 mL DMF. To this mixture, 4 mL internal standard stock solution was added and

the mixture was put in a 20 mL GC-headspace vial. The flow rate of nitrogen was 1.8 mL/min. All measurements were done in triplo.

DLS

For dynamic light scattering (DLS) measurements, a Malvern Zetasizer nano series ZS90 with a measurement angle of 173° and a temperature of 25 °C was used. Concentrations were approximately 20 mg/mL, without further diluting after production.

Cryogenic transmission electron microscopy (cryo-TEM) analysis

Cryo-TEM measurements were performed on loaded and unloaded, batch made and in flow made micelles. The samples were prepared on Quantifoil R 2/2 grids. In short, 3 µL of micellar dispersion was pipetted onto a grid and blotted for 3 seconds using a fully automated vitrification robot (MARK III) at 20 ˚C and 100% relative humidity. The grid was then rapidly plunged and frozen in liquid ethane. Micrographs were taken using a FEI Tecnai G2 Sphere (200 kV electron source) equipped with LaB6 filament utilizing a cryo-holder or a FEI Titan (300 kV electron source) equipped with an autoloader station.

Monomer synthesis

N-(2-Hydroxypropyl) methacrylamide (HPMA)

HPMA was synthesized through the reaction between DL-1-amino-2-propanol and methacryloyl chloride (**Scheme 4.1**) without adding more stabilizing antioxidant. The synthesis was performed by mixing 1 equivalent of DL-1-amino-2-propanol (1066 mL, 13.78 mol) with 1.2 equivalents of NaOH (1475 mL of 11.2 M NaOH) and 1500 mL water. This solution was stirred and brought to -10 °C. Then 1.05 equivalents of methacryloyl chloride (1400 mL, 14.46 mol, containing ~200 ppm monomethyl ether hydroquinone as stabilizer) were added dropwise in 90-120 minutes, whilst allowing the temperature to rise to 10 °C in the first 30 minutes. Thereafter the temperature was kept constant at 10 °C. After the addition of all the methacryloyl chloride, the temperature was allowed to reach room temperature and the reaction was stirred for another 30 minutes. The mixture was analyzed using thin layer chromatography (TLC; SiO_2, eluent: toluene/acetone 6/4, coloring agent: $KMnO_4$ stain) to verify complete conversion of the reaction. Once the reaction was completed, 3 liquid extractions with 1500 mL toluene each were

performed to remove apolar byproducts. The product was then isolated by a liquid extraction with 3 L dichloromethane (DCM). Then 5 more liquid extractions, each using 1500 mL of a DCM:methanol (9:1) mixture, were performed. Each extract was analyzed using TLC. The combined product layers were dried with $MgSO_4$, filtered and the product was obtained after solvent evaporation *in vacuo* at 30 °C. The product was recrystallized in acetone (100 g product in approximately 100 mL hot solvent) followed by slowly cooling down the solution to room temperature and then storing overnight at 2-7 °C. The HPMA crystals were collected through filtration, dried under vacuum to remove remaining acetone and analyzed by ^{1}H-NMR and HPLC (**Figure S4.1 and S4.2**).

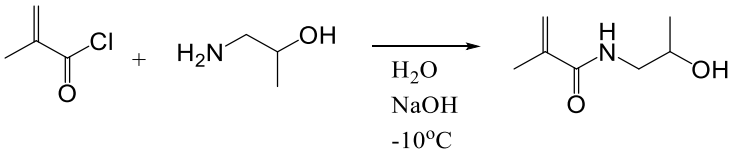

Scheme 4.1. Synthesis of HPMA

N-(2-benzoyloxypropyl) methacrylamide (HPMA-Bz)

HPMA-Bz was synthesized through the coupling reaction of HPMA and benzoyl chloride, (no stabilizer was added), and using triethyl amine (TEA) as a base (**Scheme 4.2**). One equivalent of HPMA (1041 g, 7.27 mol) and 1.43 equivalents of TEA (1457 mL, 10.4 mol) were dissolved in 1 L DCM. Once all the HPMA was dissolved, the homogeneous solution was cooled to 15 °C. Then 1.43 equivalents of benzoyl chloride (1207 mL, 10.4 mol) were added dropwise, whilst keeping the temperature at 15 °C. After complete addition of the benzoyl chloride, the mixture was allowed to reach room temperature and stirred overnight. The solution was filtered to remove the formed TEA HCl salt and unreacted HPMA was removed through extraction with 1 L water 3 times. The product-containing DCM layer was dried with $MgSO_4$, filtered and evaporated *in vacuo*. The obtained powder was stirred in 2 L heptane to remove benzoic anhydride. Both benzoic anhydride and benzoic acid are present in trace amounts in the benzoyl chloride starting material, but both are also formed by reaction of the benzoyl chloride with water to benzoic acid and as was shown by Dhimitruka *et al.* in the presence of TEA will eventually lead to the formation of benzoic anhydride. [24] The heptane was removed by filtration and the solid-liquid extraction cycle was repeated until all the benzoic

anhydride was removed as detected by HPLC (in general after two extractions). The product was dried *in vacuo* at 30 °C and analyzed via HPLC and ^{1}H-NMR. (**Figure S4.3 – S4.6**)

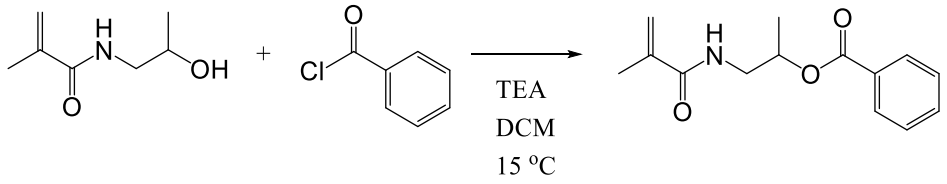

Scheme 4.2. Synthesis of HPMA-Bz

Macro-initiator (MI) synthesis

The mPEG-ABCPA-mPEG macro-initiator (MI) was synthesized, as previously described [21], through an esterification of one equivalent ABCPA and 2 equivalents of mPEG (**Scheme 4.3**). For this synthesis, 3 equivalents of DCC were used as a coupling reagent, and 0.3 equivalents of 4(-dimethylamino) pyridinium 4-toluenesulfonate (DPTS) were used as a catalyst. ABCPA, mPEG and DPTS (12 g ABCPA, 450 g mPEG, 4 g DPTS) were dissolved in 2.25 L DCM and the solution was brought to 0 °C and under a nitrogen atmosphere. Then 26 g of DCC was dissolved in 2.25 L DCM and added dropwise to the cooled solution. This mixture was left to react overnight at room temperature and subsequently filtered to remove precipitated 1,3-dicyclyhexylurea (DCU). The product was precipitated in cold methyl-tert-butylether (MTBE), collected through filtration and dried *in vacuo*. The product was then analyzed by GPC and ^{1}H-NMR. (**Figure S4.7 and S4.8**)

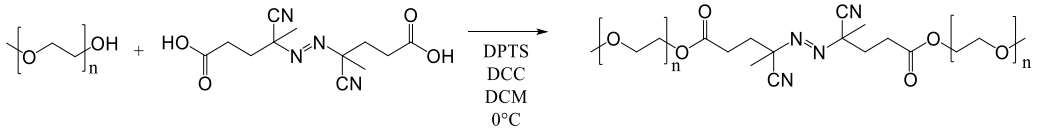

Scheme 4.3. Synthesis of mPEG-ABCPA-mPEG macro-initiator

Polymerization

mPEG-*block*-poly(*N*-2-benzoyloxypropyl methacrylamide) (mPEG-*b*-p(HPMA-Bz)) block copolymer was synthesized via free radical polymerization using mPEG-ABCPA-mPEG as macroinitiator (MI) and N-(2-benzoyloxypropyl methacrylamide) (HPMA-Bz) as monomer (**Scheme 4.4**),

as was described earlier. [15–17] The MI and monomer were dissolved in ACN at a total concentration of 300 g/L with a molar feed ratio of MI:HPMA-Bz (1:200 mol/mol). More specifically, 1367 g HPMA-Bz and 300 g MI were dissolved in 5.5 L ACN and the polymerization was conducted at 70 °C under a nitrogen atmosphere for 24 hours. The resulting mPEG-*b*-p(HPMA-Bz) block copolymer was collected through precipitation in cold MTBE (1 L of product in ACN to 5 L of MTBE) followed by filtration. To remove the unreacted monomer from the product, the polymer powder was dissolved in ACN (300 g/L) and reprecipitated in cold MTBE (1 L of product in ACN to 5 L of MTBE). After filtration the product was dried *in vacuo*.

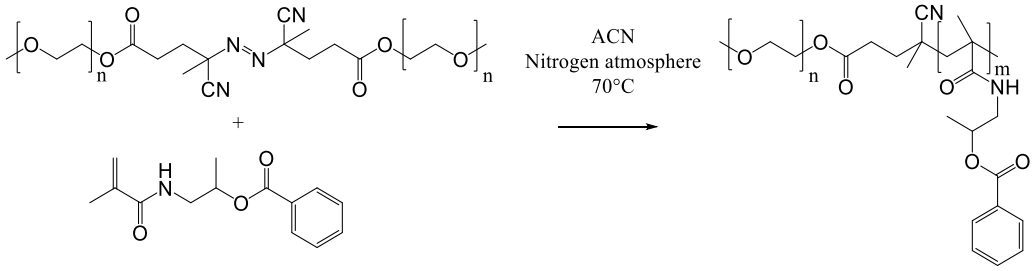

Scheme 4.4. Synthesis of mPEG-*b*-p(HPMA-Bz)

Poly(*N*-2-benzoyloxypropyl methacrylamide) p(HPMA-Bz) homopolymer was synthesized using the same procedure, via free radical polymerization using ABCPA as initiator and HPMA-Bz as monomer. They were dissolved in ACN at a total concentration of 0.3 g/ mL with a molar feed ratio of ABCPA:HPMA-Bz (1:200 mol/mol).). More specifically, 3 g HPMA-Bz and 0.017 g ABPCA were dissolved in 10 mL ACN and the polymerization was conducted at 70 °C under a nitrogen atmosphere for 24 hours. Workup was exactly the same as described for the mPEG-*b*-p(HPMA-Bz) block copolymer.

Homopolymer removal

The polymerization procedure of the mPEG-*b*-p(HPMA-Bz) block copolymer, as described in the previous section, might result also in the formation of p(HPMA-Bz) homopolymer. As pointed out and demonstrated in Chapter 2, this homopolymer will solubilize in the core of the micelles, leading to an increase in micelle size. [21] In order to maintain a highly controllable and

reproducible process for the production of micelles with a size of 50-60 nm, a procedure was developed to remove the p(HPMA-Bz) homopolymer from the polymer mixture.

mPEG-*b*-p(HPMA-Bz) spiked with 10 % p(HPMA-Bz) was dissolved in ethanol (2 g in 20 mL). Since the polymers did not dissolve in ethanol at ambient temperature, the mixture was heated to 70 °C. This heated solution was then rapidly added to room temperature water in a 1:1 volume ratio while continuously stirring. The precipitate was removed by centrifugation (15 min, 2886 g) and both the supernatant and the precipitate were dried in a vacuum oven at 40 °C overnight to obtain the purified mPEG-*b*-p(HPMA-Bz) from the supernatant. Both the product and the precipitate (homopolymer) were analyzed using GPC and ^{1}H-NMR. (**Figure S4.10 – S4.13**)

The described procedure above was also employed for the synthesized block copolymer to ensure no presence of homopolymer.

Micelle preparation in batch

mPEG-*b*-p(HPMA-Bz) micelles were prepared in batch by dissolving the homopolymer free mPEG-*b*-p(HPMA-Bz) in THF (20 mg/mL) and pipetting 1 mL into 1 mL MilliQ water as non-solvent. After THF evaporation overnight, this nanoprecipitation method results in the formation of micelles. Prior to analysis, the micelle dispersions were filtered through a 0.2 µm disk filter. Residual THF content was determined using GC-headspace. The size of the micelles was determined by Dynamic Light Scattering (DLS).

Instead of THF evaporation overnight, THF can also be removed by placing the 2 mL polymer/THF/MilliQ mixture in a regenerated cellulose dialysis bag with a cut-off at 12-14 kDa and dialyzing against MilliQ water overnight.

Micelle preparation in continuous flow

mPEG-*b*-p(HPMA-Bz) micelles were prepared in continuous flow by dissolving the homopolymer-free mPEG-*b*-p(HPMA-Bz) block copolymer in THF (20 mg/mL). A home-made setup consisting of two piston pumps was used, both at 1 mL/min, to pump both the polymer/THF mixture and MilliQ water via different inlets through a T-mixer to ensure rapid mixing (**Figure 4.5**). The outlet stream was collected in a flask and continuously stirred until a total of 200 mL was collected. The THF was removed through tangential flow

filtration (TFF) and replaced by MilliQ water using a Sius^{TM}-LS TFF Hystream, MWCO 100 kDa, 0.02 m^2 cassette. Due to a low compatibility of the membrane with THF, the micelle dispersion was diluted 10 times using MilliQ water prior to loading onto the membrane. Next, using the TFF setup, the micelle dispersion was concentrated to 20 mg/ml and the concentrated dispersion was further purified with 4 diafiltration volumes of water to ensure complete THF depletion. Eventually, this process resulted in the production of 100 mL of micellar dispersion with a concentration of 20 mg polymer per mL MilliQ. Residual THF content was determined using GC-headspace. The size of the micelles was determined by Dynamic Light Scattering (DLS).

Preparation of docetaxel loaded micelles

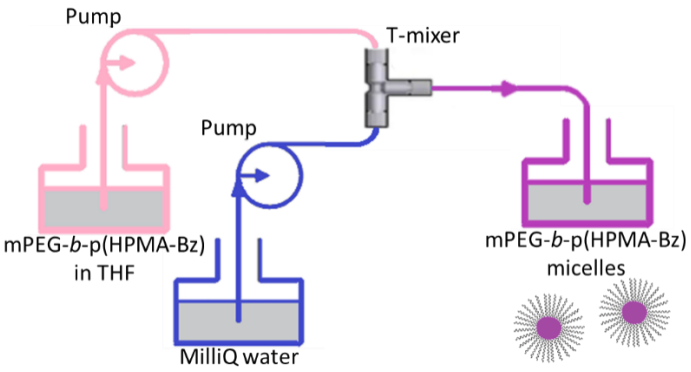

Figure 4.5. Schematic representation of the continuous flow setup.

DTX-loaded mPEG-*b*-p(HPMA-Bz) micelles were prepared using the same procedures as for the unloaded micelles described above, both in batch and in flow. DTX was co-dissolved with the polymer in THF (20 mg polymer and 5 mg DTX per mL THF). Using the batch setup, 1 mL of the polymer/DTX in THF was pipetted to 1 mL of MilliQ water. THF was removed by either evaporation overnight or overnight dialysis against MilliQ water using a regenerated cellulose dialysis bag with a cut-off at 12-14 kDa. Using the continuous flow setup, two piston pumps were used, both at 1 mL/min, to pump the polymer/DTX in THF mixture and MilliQ water through a T-mixer to ensure rapid mixing. The outlet stream was collected in a flask and continuously stirred until a total of 200 mL was collected. The THF was removed through TFF, as described above, resulting in the production of 100 mL of micellar dispersion with a concentration of 20 mg polymer per mL

MilliQ. The dispersion was first filtered through a 0.45 µm disk filter and then through a 0.2 µm disk filter to remove free DTX. The latter filtration step can also be used for sterilization purposes. The size of the DTX-loaded micelles was measured by DLS and the encapsulation efficiency of DTX in the micelles was determined by HPLC. Residual THF content was determined using GC-headspace.

Stability study

The stability of the unloaded and DTX-loaded micelles was determined by storing samples at 4 °C and at room temperature for a period up to 2 months. At different time points, samples of the stored micelle dispersions were filtered through a 0.2 µm disk filter to remove released/free DTX. The size of the DTX-loaded micelles was measured by DLS and the remaining DTX in the micelles was determined by HPLC.

REFERENCES

(1) van Elk, M.; Murphy, B. P.; Eufrásio-da-Silva, T.; O'Reilly, D. P.; Vermonden, T.; Hennink, P. W. E.; Duffy, G. P.; Ruiz-Hernández, E. *Int. J. Pharm.* **2016**, *515* (1–2), 132–164.
(2) Hare, J. I.; Lammers, T.; Ashford, M. B.; Puri, S.; Storm, G.; Barry, S. T. *Adv. Drug Deliv. Rev.* **2017**, *108*, 25–38.
(3) Duncan, R.; Vicent, M. J. *Adv. Drug Deliv. Rev.* **2013**, *65* (1), 60–70.
(4) Björnmalm, M.; Thurecht, K. J.; Michael, M.; Scott, A. M.; Caruso, F. *ACS Nano* **2017**, *11* (10), 9594–9613.
(5) Mikhail, A. S.; Allen, C. *J. Control. Release* **2009**, *138* (3), 214–223.
(6) Houdaihed, L.; Evans, J. C.; Allen, C. *Mol. Pharm.* **2017**, *14* (8), 2503–2517.
(7) Deng, C.; Jiang, Y.; Cheng, R.; Meng, F.; Zhong, Z. *Nano Today* **2012**, *7* (5), 467–480.
(8) Varela-Moreira, A.; Shi, Y.; Fens, M. H. A. M.; Lammers, T.; Hennink, W. E.; Schiffelers, R. M. *Mater. Chem. Front.* **2017**, *1* (8), 1485–1501.
(9) Cagel, M.; Tesan, F. C.; Bernabeu, E.; Salgueiro, M. J.; Zubillaga, M. B.; Moretton, M. A.; Chiappetta, D. A. *European Journal of Pharmaceutics and Biopharmaceutics*. Elsevier April 1, 2017, pp 211–228.
(10) Cabral, H.; Kataoka, K. *J. Control. Release* **2014**, *190*, 465–476.
(11) Sainz, V.; Conniot, J.; Matos, A. I.; Peres, C.; Zupančič, E.; Moura, L.; Silva, L. C.; Florindo, H. F.; Gaspar, R. S. *Biochem. Biophys. Res. Commun.* **2015**, *468* (3), 504–510.
(12) Shi, J.; Kantoff, P. W.; Wooster, R.; Farokhzad, O. C. *Nat. Rev. Cancer* **2016**, *17*, 20.
(13) Hua, S.; de Matos, M. B. C.; Metselaar, J. M.; Storm, G. *Front. Pharmacol.* **2018**, *9*, 1–14.
(14) Tinkov, S. Elsevier Inc., 2018.

(15) Shi, Y.; Van Steenbergen, M. J.; Teunissen, E. A.; Novo, L.; Gradmann, S.; Baldus, M.; Van Nostrum, C. F.; Hennink, W. E. *Biomacromolecules* **2013**, *14* (6), 1826–1837.
(16) Shi, Y.; Van Der Meel, R.; Theek, B.; Oude Blenke, E.; Pieters, E. H. E.; Fens, M. H. A. M.; Ehling, J.; Schiffelers, R. M.; Storm, G.; Van Nostrum, C. F.; Lammers, T.; Hennink, W. E. *ACS Nano* **2015**, *9* (4), 3740–3752.
(17) Naksuriya, O.; Shi, Y.; van Nostrum, C. F.; Anuchapreeda, S.; Hennink, W. E.; Okonogi, S. *Eur. J. Pharm. Biopharm.* **2015**, *94* (2015), 501–512.
(18) Gelderblom, H.; Verweij, J.; Nooter, K.; Sparreboom, A. *Eur. J. Cancer* **2001**, *37* (13), 1590–1598.
(19) Shi, Y.; Van Steenbergen, M. J.; Teunissen, E. A.; Novo, L.; Gradmann, S.; Baldus, M.; Van Nostrum, C. F.; Hennink, W. E. *Biomacromolecules* **2013**, *14* (6), 1826–1837.
(20) Kopeček, J.; Bažilová, H. *European Polymer Journal*. 1973, pp 7–14.
(21) Bagheri, Mahsa; Bresseleers, Jaleesa; Varela-Moreira, Aida; Meeuwissen, Silvie A.; Schiffelers, Raymond M.; Metselaar, Josbert M.; van Nostrum, Cornelus F.; van Hest Jan C.M.; Hennink, W. E. . *Langmuir* **2018**.
(22) De Vos, R.; Goethals, E. J. *Polym. Bull.* **1986**, *15*, 547–549.
(23) Talelli, M.; Rijcken, C. J. F.; Oliveira, S.; Van Der Meel, R.; Van Bergen En Henegouwen, P. M. P.; Lammers, T.; Van Nostrum, C. F.; Storm, G.; Hennink, W. E. *J. Control. Release* **2011**, *153* (1), 93–102.
(24) Dhimitruka, I.; SantaLucia, J. *Org. Lett.* **2006**, *8* (1), 47–50.

SUPPLEMENTARY FIGURES AND TABLES

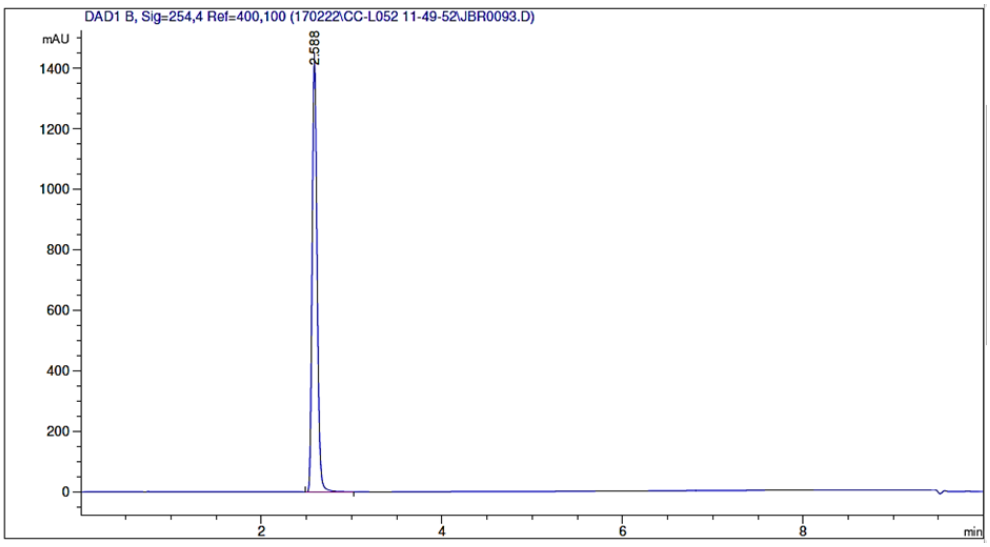

Figure S4.1. HPLC chromatogram of HPMA (2.6 min) giving a purity of 99.9 %.

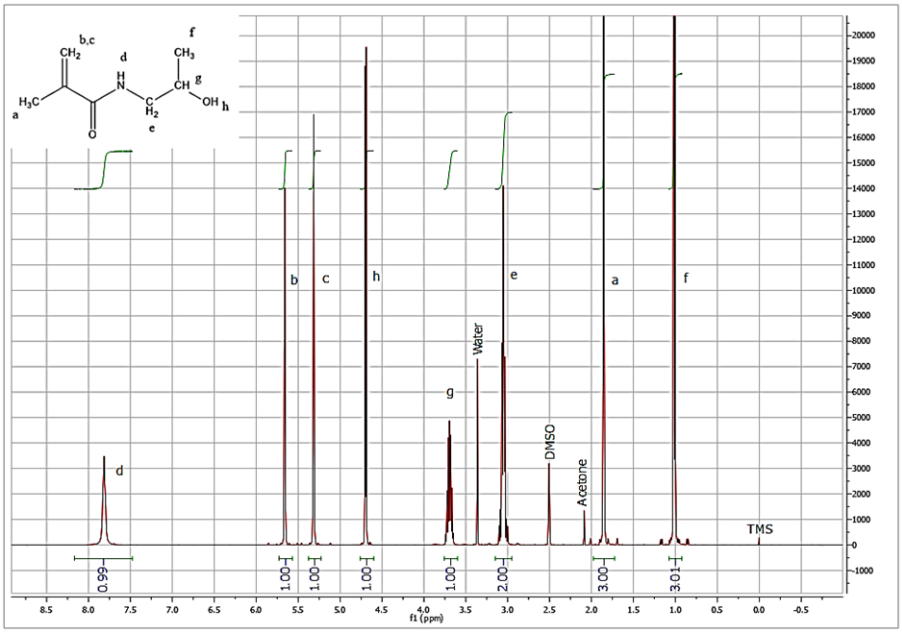

Figure S4.2. ^{1}H-NMR spectrum of HPMA.

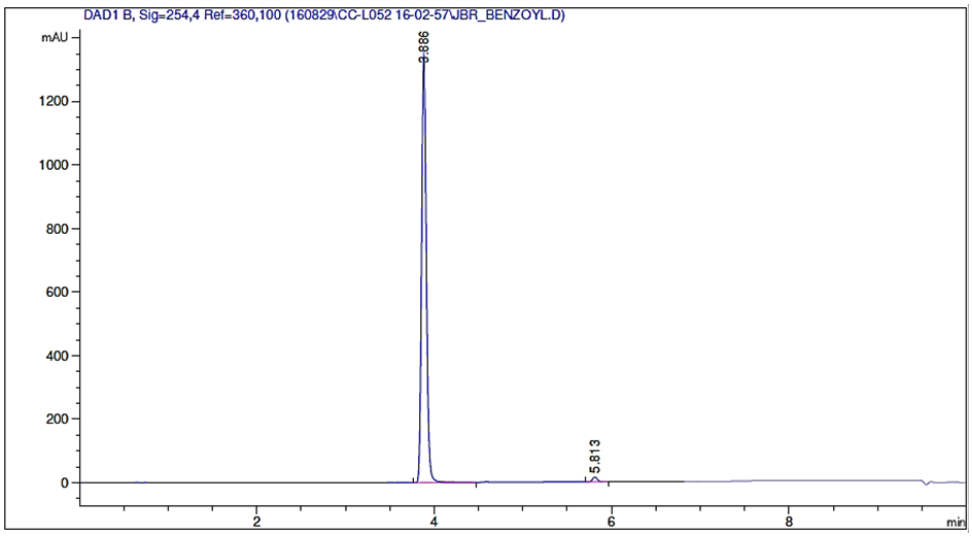

Figure S4.3. HPLC chromatogram of the benzoyl chloride starting material. The benzoyl chloride is visible as benzoic acid (3.9 min) due to fast reaction with water. At 5.8 min it can already be noticed that there is also some benzoic anhydride present in the benzoyl chloride or that it is formed during sample preparation.

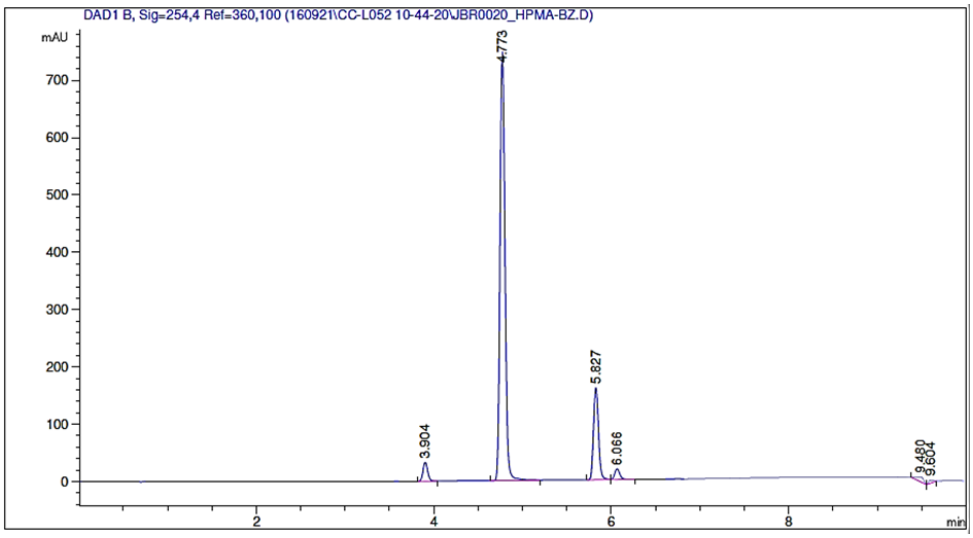

Figure S4.4. HPLC chromatogram of HPMA-Bz (4.8 min) prior to solid liquid extraction with heptane. The peak at 3.9 min is assigned to benzoic acid and the peak at 5.8 min is assigned to benzoic anhydride.

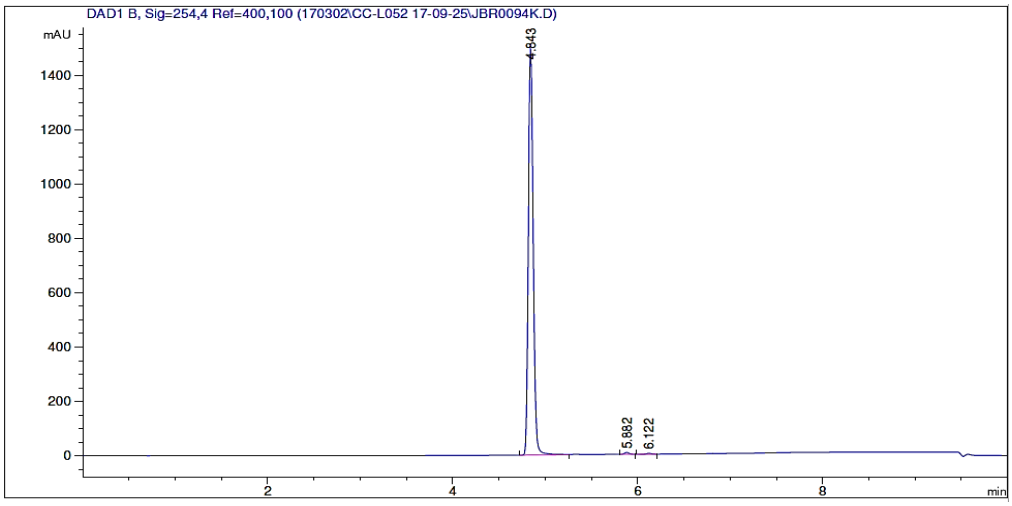

Figure S4.5. HPLC chromatogram of HPMA-Bz after the solid liquid extraction with heptane. Only trace amounts of benzoic anhydride remain, giving a purity of 99.3 %.

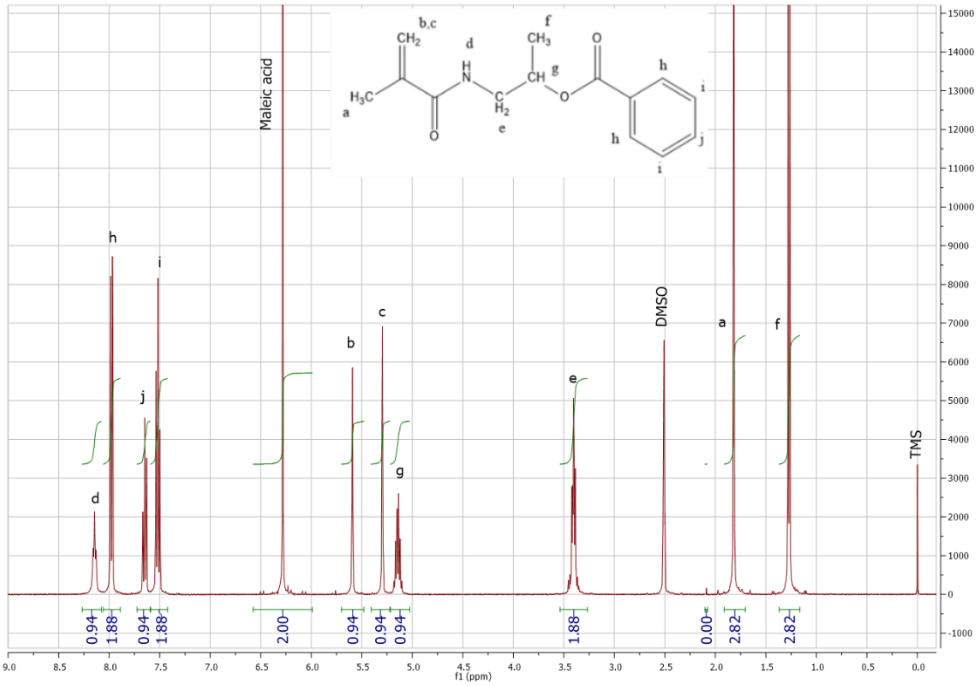

Figure S4.6. ^{1}H-NMR spectrum of HPMA-Bz of which the content was determined. Maleic acid was used as internal standard, resulting in a purity of 98.5 % using the equation below.

$$Px = \frac{I_x * N_{std} * M_x * W_{std}}{I_{std} * N_x * M_{std} * W_x} * P_{std}$$

$$= \frac{0.94 * 2 * 247.29\ g/mol * 9.62\ g}{2 * 1 * 116.072\ g/mol * 19.55\ g} * 99.94\% = 98.5\ \%$$

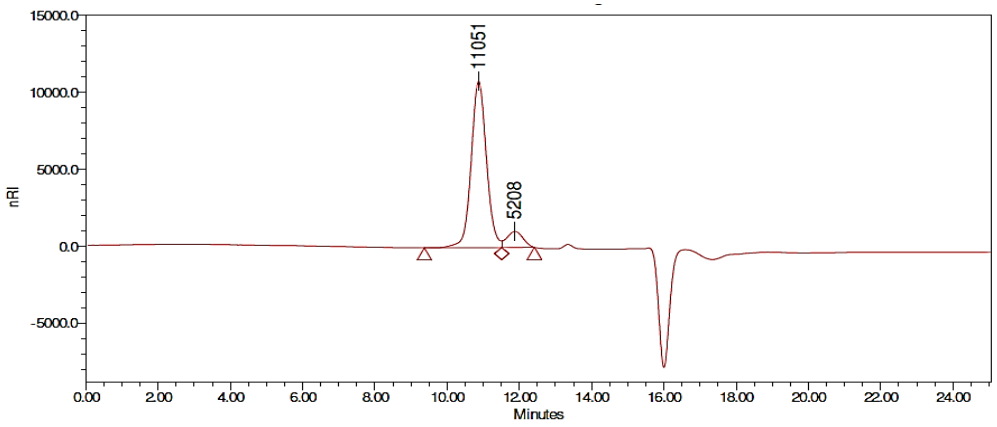

Figure S4.7. GPC chromatogram of mPEG$_{5K}$-ABCPA-mPEG$_{5K}$ macro-initiator (peak labelled 11051) with approximately 9 % of free mPEG$_{5K}$ (peak labelled 5208).

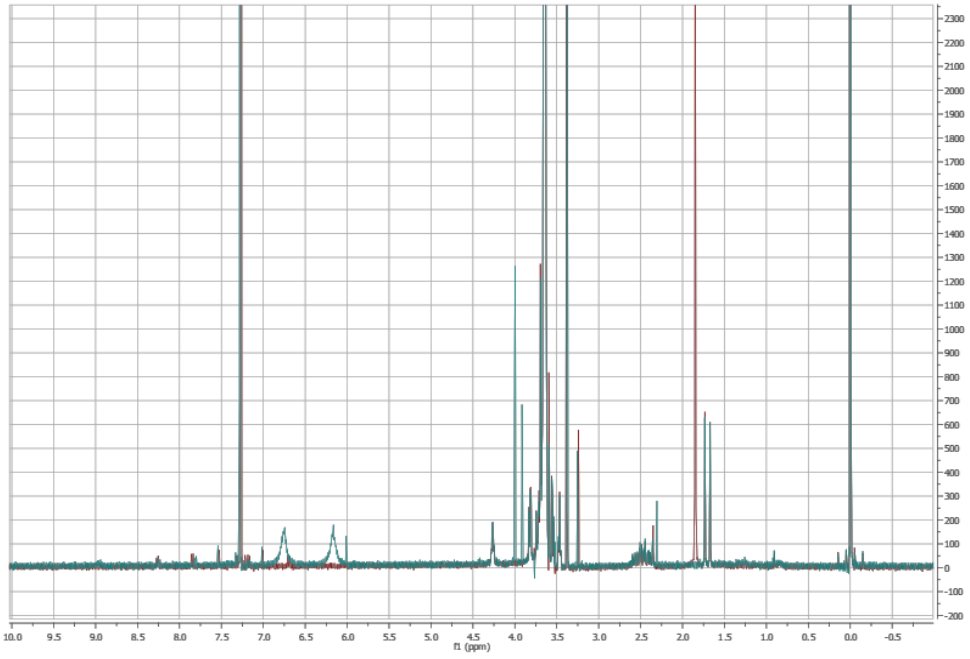

Figure S4.8. ^{1}H-NMR spectra of the mPEG$_{5K}$-ABCPA-mPEG$_{5K}$ macro-initiator. Red: the spectrum before and Blue: the spectrum after addition of TAIC. The spectra show that the synthesized macroinitiator contains 9 % unreacted mPEG according to the signal of the methylene group neighboring the terminal hydroxyl group, which shifts from 4.2 to 4.4 ppm.

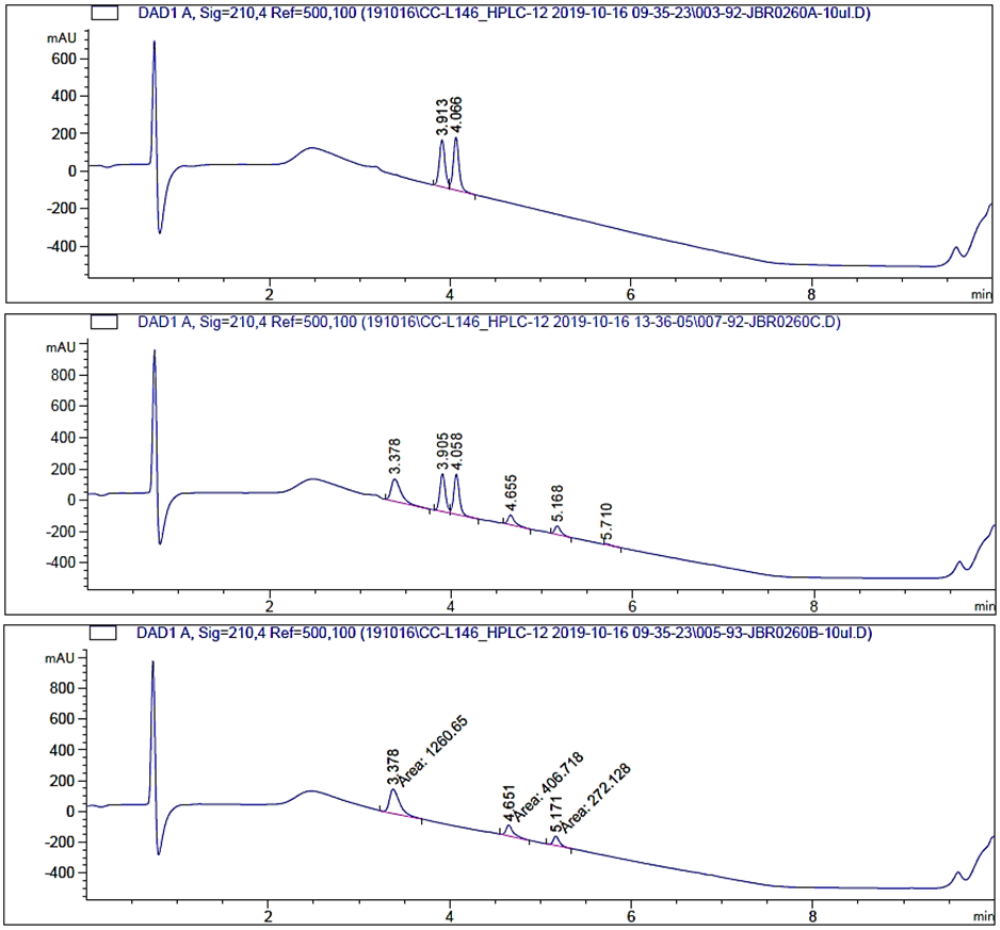

Figure S4.9. HPLC chromatograms. Top chromatogram is of ABCPA, middle chromatogram is of the MI spiked with ABCPA and the bottom chromatogram is of the MI. In the latter, no ABCPA could be detected.

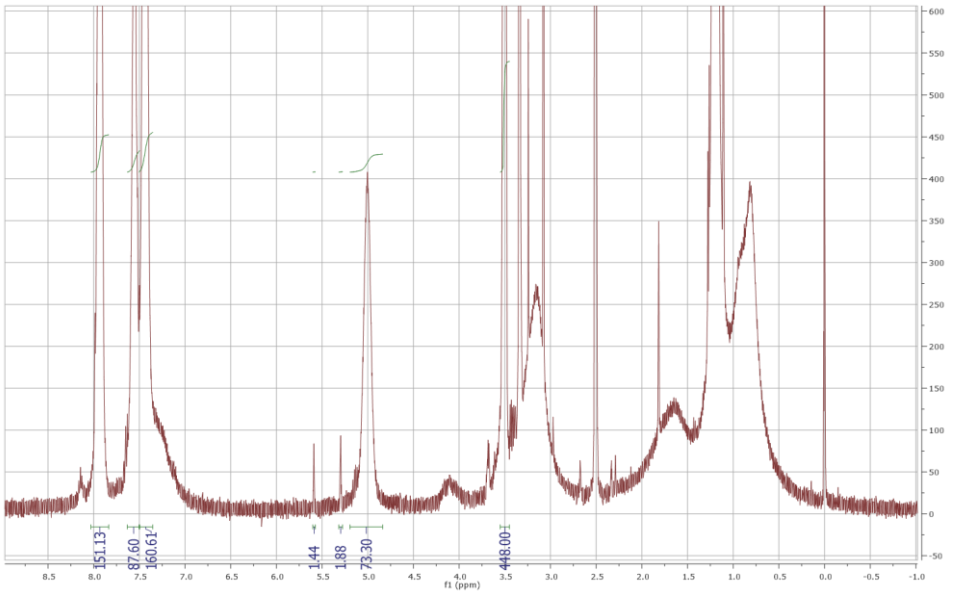

Figure S4.10. ^{1}H-NMR of mPEG-b-p(HPMA-Bz) prior to homopolymer removal. An M_n of 23.7 kDa was calculated and some trace amounts of monomer are still present (5.6 ppm and 5.3 ppm).

$$\boldsymbol{M_n = \left(integral\ at\ 8.0\ ppm/2\ * M_{w(HPMA-Bz)}\right) + 5000\ g/mol}$$
$$\boldsymbol{= (151/2 * 247.29\ g/mol) + 5000\ g/mol = 23.7\ kDa}$$

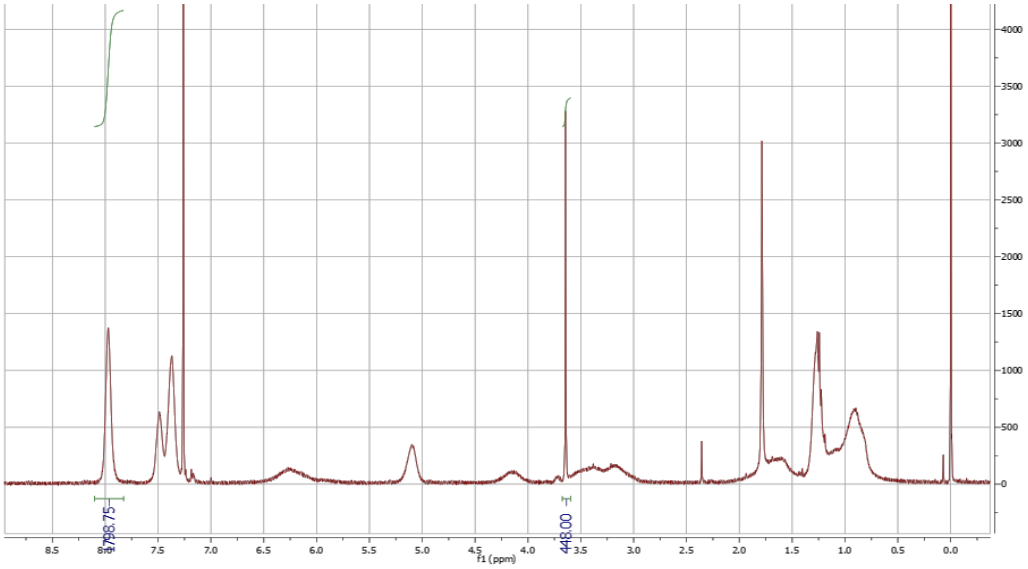

Figure S4.11. ^{1}H-NMR spectrum of precipitate obtained after centrifugation and drying in the vacuum oven. The NMR data provides insight in the composition of the isolated precipitate. It is clear that the peaks in the aromatic domain (between 7.25 and 8.25 ppm) are a lot bigger than the peak from mPEG (3.6 ppm). When the M_n is calculated, as if it were a normally synthesized block copolymer, a value of 222.3 kDa is obtained. This gives a weight fraction of PEG of only 2 %. This is 10 times smaller than envisioned for the block copolymer and therefore contributes to the suspicion that the precipitate mainly exists of p(HPMA-Bz) homopolymer.

$$\boldsymbol{M_n = \left(integral\ at\ 8.0\ ppm/2\ * M_{w(HPMA-Bz)}\right) + 5000\ g/mol}$$
$$\boldsymbol{= (1798/2 * 247.29\ g/mol) + 5000\ g/mol = 222.3\ kDa}$$

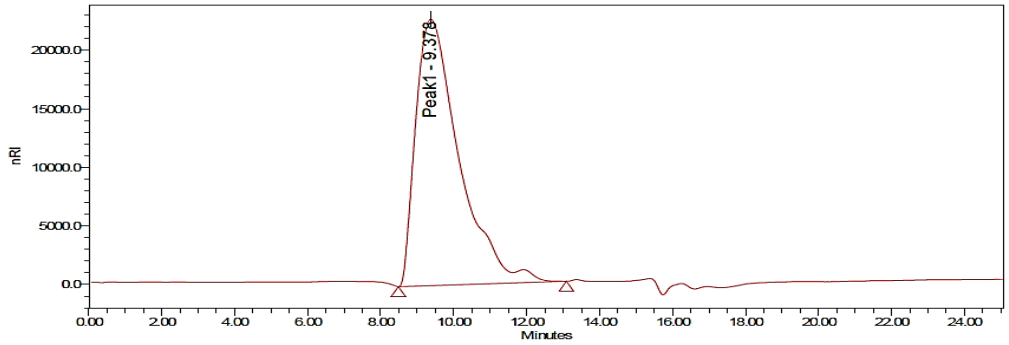

Figure S4.12. GPC chromatogram of the mPEG-*b*-p(HPMA-Bz) block copolymer after removal of homopolymer. (M_n: 19.3 kDa and M_w: 21.6 kDa). The shoulder at ~12 minutes is assigned to free $mPEG_{5K}$.

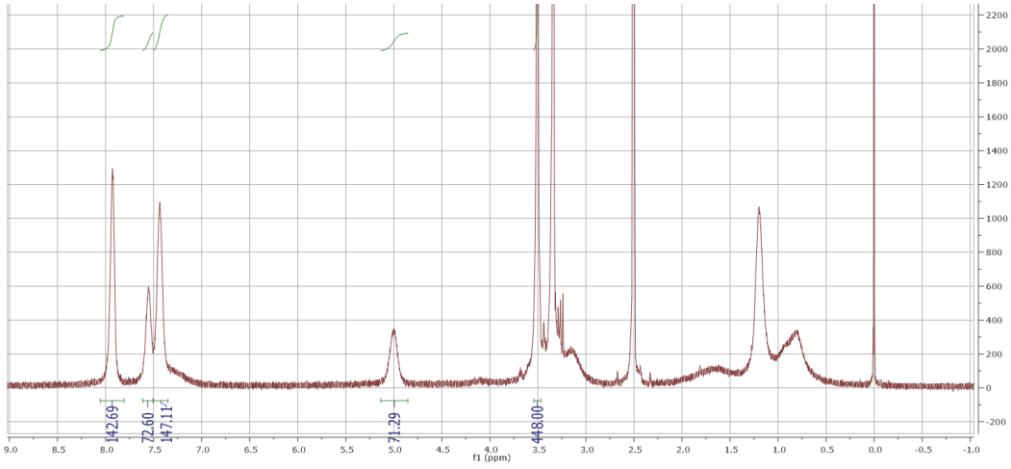

Figure S4.13. ^{1}H-NMR spectrum of the mPEG-*b*-p(HPMA-Bz) block copolymer after homopolymer removal. The calculated M_n: 22.5 kDa. The PEG integral at 3.4-3.6 is put at 448 for the average number of protons it contains. The M_n is calculated using the following formula:

$$\boldsymbol{M_n = \left(integral\ at\ 8.0\ ppm/2\ * M_{w(HPMA-Bz)}\right) + 5000\ g/mol}$$
$$\boldsymbol{= (142/2 * 247.29\ g/mol) + 5000\ g/mol = 22.5\ kDa}$$

Chapter 5

Development of the Manufacturing Process to Produce Dexamethasone-Loaded PEG-PDLLA Polymersomes

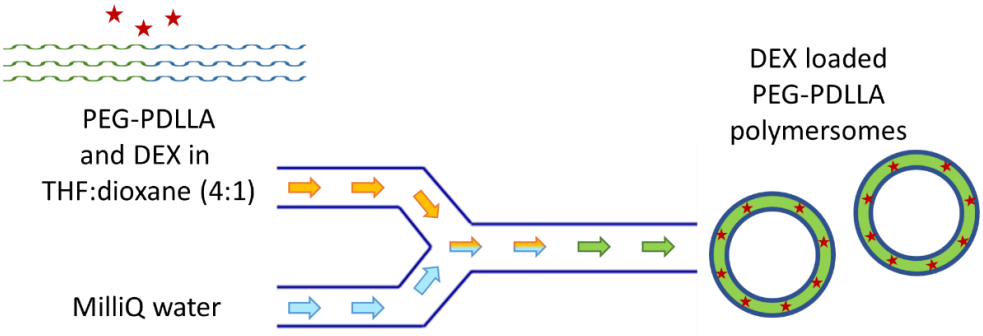

ABSTRACT

In this chapter, the efficient and scalable production of dexamethasone (DEX)-loaded PEG-PDLLA (PEG_{1K}-$PDLLA_{6.5K}$) polymersomes was explored. First, the use of a continuous flow setup for the production of PEG-PDLLA polymersomes was developed, for both DEX-loaded and unloaded particles, which would enable effective translation to larger scale production. To this end, PEG-PDLLA polymersomes of 300-500 nm were reproducibly prepared. Secondly, the purification in flow, using tangential flow filtration, of the resulting product was investigated and compared with regular dialysis methods. Via this procedure 40 mL of a DEX-loaded polymersome dispersion was produced with an encapsulation efficiency of ~ 4 %, which was comparable to batchwise production methods. These particles were shown to be stable for at least 6 weeks when stored at 4 ˚C in water, with good drug retention. Finally, possibilities of enhancing drug loading of the polymersomes were explored by using a less hydrophobic DEX-β-cyclodextrin complex, which could be captured in the aqueous lumen of the particles. Unfortunately, the use of the DEX-β-cyclodextrin complex did not improve the encapsulation efficiency when using the developed batch and flow processes. We can therefore conclude that polymersome formation can be translated effectively from a batch to a continuous flow process, with the opportunity to achieve an efficient and large-scale production method. To improve drug loading, however, clearly additional optimization is required.

INTRODUCTION

As mentioned in ***Chapter 1*** and ***Chapter 4***, a scalable and reproducible production process is one of the main challenges in nanomedicine development. [1–4] This is caused for a large part by the fact that nanomedicines are usually complex assemblies of multiple components, in the simplest form an excipient and an active pharmaceutical ingredient, complicating the manufacturing process and also the quality control. Subtle changes in the production process of nanomedicines can already dramatically affect the particle composition and therefore a thorough physicochemical understanding of the assemblies is essential to develop a reproducible manufacturing process. This is also the case for polymeric vesicles, or polymersomes, which have attracted increased attention from the nanomedicine community over the past years.

Polymersomes are spherical bi-layered structures that resemble liposomes. They are built up from amphiphilic block copolymers instead of phospholipids, making them chemically more versatile. Polymersomes can easily be tuned in size and membrane thickness by adjusting the molecular weight and composition of the used amphiphilic block copolymers.[5] Besides that, polymersomes have the capacity to accommodate both hydrophobic and hydrophilic drugs. The hydrophobic domain of the polymer membrane allows the solubilization of poorly water-soluble drugs, whereas in the lumen of the polymersomes, hydrophilic drugs can be encapsulated. Polymersomes have therefore been proposed and investigated as drug delivery systems. [6,7]

In our group, a highly promising polymersome formulation based on poly(ethylene glycol)-*block*-poly(D,L-lactide) (PEG-PDLLA) has been developed. [8–12] These vesicles are potentially suitable for medical and pharmaceutical applications as the PEG corona provides stealth properties to these assemblies and prevents undesired interactions with the immune system, whereas the hydrophobic PDDLA block has been demonstrated in many studies to be biocompatible and biodegradable. [13] Interestingly, these PEG-PDLLA polymersome formulations can be resized via extrusion[10] and possess the ability to be shape transformed into prolate [11] (tubes) and oblate [8] (discs or stomatocytes) morphologies under osmotic pressure. [8,11] The shape transformation into tubes has been studied in detail and is affected by surface charge [12] and solvent mixture interactions [9].

The goal of the research described in this chapter was to develop an efficient and scalable process for the manufacturing of PEG-PDLLA polymersomes, both unloaded and loaded with a therapeutic agent. This was achieved by a thorough evaluation of batch and continuous flow production processes. The corticosteroid dexamethasone (DEX) was chosen as model drug. DEX has already been extensively used as an anti-inflammatory agent for the treatment of ocular and pulmonary disorders, amongst others. Unfortunately, the free drug showed limited efficacy and multiple side-effects. To improve the efficacy and reduce side-effects of DEX it should therefore be combined with a suitable delivery system [14], which in the present study are the PEG-PDLLA polymersomes. Two different encapsulation procedures were investigated. First, the free drug was loaded into the hydrophobic membrane of the polymersomes. The applied process resulted in a low encapsulation efficiency and therefore it was also explored whether the drug content could be improved by loading a more hydrophilic moiety into the lumen of the polymersomes. For the latter, the host-guest complex of DEX with β-cyclodextrin (β-CD) (β-CD-DEX) was used as a more hydrophilic variant of DEX to be encapsulated into the lumen of the polymersomes.

RESULTS AND DISCUSSION

PEG-PDLLA polymer and polymersome preparation

The PEG-PDLLA block copolymer (PEG_{1K}-$PDLLA_{6.5K}$) was successfully synthesized in 74 % yield *via* a previously published protocol. [11] In short, the polymerization was performed using a ring-opening polymerization in DCM at room temperature of DL-Lactide with mPEG (1 kDa) as a macro-initiator and 1,8-diazabicyclo[5.4.0]undec-7-ene (DBU) as the catalyst. ^{1}H-NMR spectroscopy confirmed the completion of the polymerization of the block copolymer and the polydispersity (Đ) was determined using GPC against PEG calibration standards (**Table 5.1**, **Figure 5.6 and 5.7**).

Table 5.1. Characteristics of the synthesized PEG-PDLLA block copolymer as determined by ^{1}H-NMR and GPC. M_n = number average molar mass (kDa), N_{DLLA} = degree of polymerization, M_w = weight average molar mass (kDa), Đ = molar mass dispersity.

^{1}H-NMR		**GPC**		
M_n	N_{DLLA}	M_n	M_w	Đ
7.5	46	12.3	14.5	1.18

In previous studies, the self-assembly of the PEG-PDLLA block copolymer into polymersomes was performed using an established solvent switch method [8–12]. According to this protocol, PEG-PDLLA was first dissolved in a THF/dioxane mixture (4:1 v/v, 10 mg/mL) and 50 vol % Milli-Q water was added to this mixture over a period of 2 hours. In this research, the THF/dioxane mixture was chosen to dissolve the PEG-PDLLA block copolymer, anticipating shape transformation studies of these formulations in future work. [9] Subsequent removal of the organic solvent mixture, by dialysis against Milli-Q, resulted in spherical polymersomes. Using this protocol, polymersomes with a size 390 nm were produced with PDI values around 0.2 (**Figure 5.1**). This was comparable to previously reported results (300-500 nm). [8–12] The polymersome morphology was confirmed using cryo-TEM (**Figure 5.3 A**) and the size of the polymersomes measured by cryo-TEM was in agreement with DLS data.

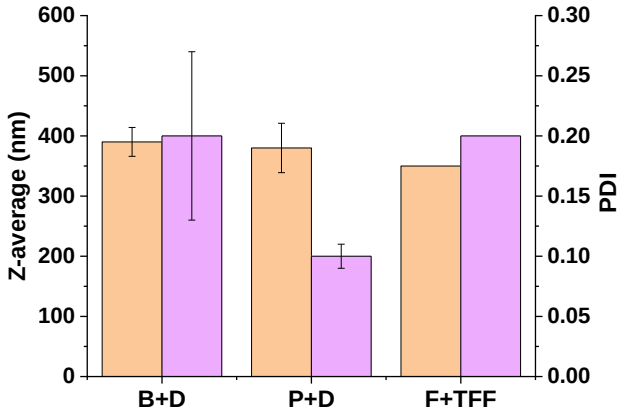

Figure 5.1. Characteristics of unloaded PEG-PDLLA polymersomes obtained using different preparation techniques. Average hydrodynamic diameters (orange) and PDI values (pink) as measured by DLS are depicted. Preparation techniques were (B+D): prepared in batch and purified by dialysis, (P+D): prepared by pipetting a polymer solution in THF/dioxane and water via two pipettes simultaneously in a vial and (F+TFF): prepared using continuous flow and purified by TFF. n = 2, except (F+TFF) where n = 1.

To prepare larger amounts of the polymersome dispersion, needed for anticipated extensive pharmaceutical development, the feasibility of a continuous flow setup, to replace batch production, was investigated. This was first tested by simply pipetting the PEG-PDLLA in THF/dioxane mixture (10 mg/mL) and Milli-Q simultaneously in a vial while stirring continuously. After overnight dialysis against Milli-Q at room temperature, this resulted in the formation of spherical polymersomes with a size of 380 nm (**Figure 5.1**). These results are comparable to the in batch prepared unloaded polymersomes and a first indication that using a continuous flow setup will also result in the formation of polymersomes.

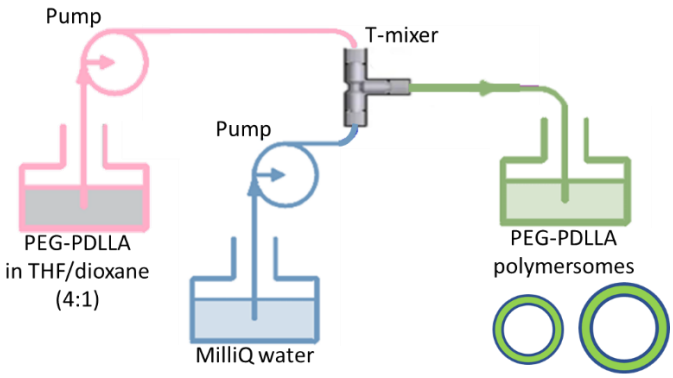

Figure 5.2. Schematic representation of the continuous flow setup.

Next, polymersomes were prepared using a home-made continuous flow set-up consisting of two piston pumps, which delivered the polymer/THF:dioxane mixture and Milli-Q water via different inlets through a T-junction (**Figure 5.2**). The ratio at which the polymer/THF:dioxane mixture was added to the Milli-Q water was kept at 1:1 and a total flow rate of 2 mL/min was applied. To ensure further mixing, the outlet flow was collected in a flask and continuously stirred. In order to replace the batch-wise dialysis process with a scalable procedure, continuous transient flow filtration (TFF) was explored. Using this setup, a total of 40 mL purified unloaded polymersome dispersion with a concentration of 10 mg/mL was collected. The polymersome dispersions displayed a size of 350 nm and a PDI value of 0.2 which were comparable to the batch-produced polymersome dispersions (**Figure 5.1**). Cryo-TEM measurements confirmed that the preparation method did not have an influence on the appearance of the unloaded polymersomes (**Figure 5.3 B**) and the size of the polymersomes was in agreement with DLS measurements.

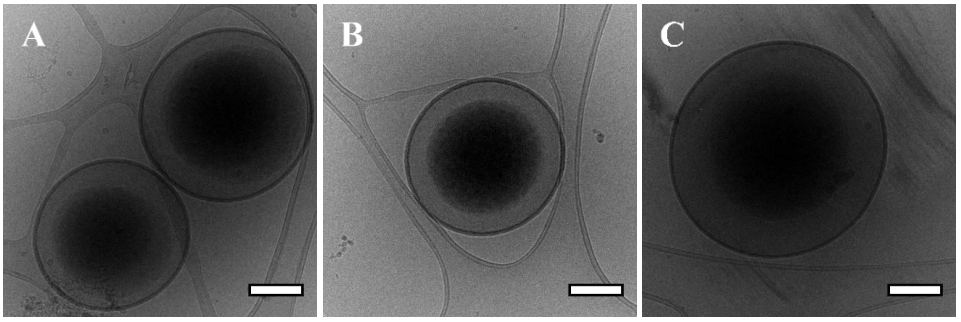

Figure 5.3. Cryo-TEM images of the PEG-PDLLA polymersomes. (A) unloaded and prepared in batch; (B) Unloaded and prepared using continuous flow; (C) DEX loaded and prepared using continuous flow. Scale bars correspond to 200 nm.

Preparation of DEX-loaded polymersomes

In previous work by our group, the loading of PEG-PDLLA polymersomes with DEX was investigated in a batch type process. [15] DEX and PEG-PDLLA block copolymer were both dissolved in a THF/dioxane mixture (4:1 v/v), after which the solution was added to water to induce polymer assembly. DEX was solubilized in the PDLLA membrane as a result of hydrophobic interactions between the guest molecule and the polymer. It was shown, however, that this process was rather challenging, since an encapsulation efficiency of only 5 % was achieved, corresponding to a loading capacity of 0.45 % and loading concentrations of DEX of only ~ 25 μg/mL.

The low encapsulation efficiency could be explained by the long dialysis process to remove the organic solvent from the polymersome dispersion, which resulted in removal of substantial amounts of DEX from the membrane. It was envisioned that by using a faster manner to remove the solvent, for example by using TFF, this would increase the loading of DEX due to less extraction of the drug from the membrane. The traditional batch type process and the developed continuous flow method for the preparation of polymersomes were therefore compared with regard to the encapsulation efficiency of DEX.

First, for the preparation of DEX-loaded PEG-PDLLA polymersomes in batch, PEG-PDLLA was dissolved in a THF/dioxane mixture (4:1 v/v, 10 mg/mL). DEX was subsequently dissolved in the polymer mixture (final concentration of DEX was 1 mg/mL). Next, 2 mL of Milli-Q water was added to 2 mL polymer/DEX solution while continuously stirring. Removal of the organic

solvent and unencapsulated DEX by dialysis against Milli-Q overnight resulted in the formation of DEX-loaded polymersomes with an average size of 480 nm and a PDI of 0.15 (**Figure 5.4 A**). This is slightly larger as compared to our unloaded polymersomes. The loading of the polymersomes with DEX was low, as expected and in agreement with previous findings[15], with only 19 µg/mL loaded into the bilayer membrane (**Figure 5.4 B**). This corresponds to an encapsulation efficiency of 3.8 % and a loading capacity of 0.35 %.

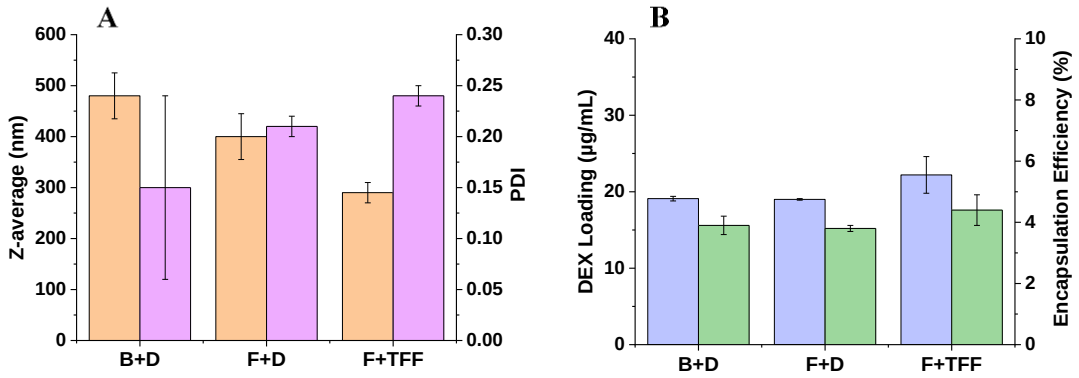

Figure 5.4. Characteristics of DEX-loaded PEG-PDLLA polymersomes obtained using different preparation techniques. (A) Average hydrodynamic diameters (orange) and PDI values (pink) as measured by DLS. (B) DEX loading (blue) and encapsulation efficiencies (green) as measured by HPLC. The different preparation techniques were (B+D): prepared in batch and purified by dialysis, (F+D): prepared using continuous flow and purified by dialysis and (F+TFF): prepared using continuous flow and purified by TFF. For all experiments n = 2.

Secondly, to investigate the effect of using the continuous flow setup instead of the batch wise process on the formation of DEX-loaded polymersomes, first this preparation technique was combined with purification via the standard dialysis method. A polymer/DEX solution in a THF/dioxane mixture (4:1 v/v, 10 mg/mL) was pumped through the T-piece simultaneously with Milli-Q water at a 1:1 ratio and a total flow rate of 2 mL/min, and collected in a flask while continuously stirring (**Figure 5.2**). 20 mL of the DEX-loaded polymersome dispersion was collected and purified by dialysis against Milli-Q water. This resulted in the production of DEX-loaded polymersomes with a size of approximately 400 nm and a PDI value of 0.21 (**Figure 5.4 A**). Although the size was slightly smaller compared to the in batch prepared DEX-

loaded polymersomes, it was comparable to the unloaded polymersomes. The loading of the polymersomes was equally low as the in batch prepared DEX-loaded polymersomes, with only 19 µg/mL loaded into the bilayer. This corresponds to an encapsulation efficiency of 3.8 % and a loading capacity of 0.35 % and indicated that the flow preparation process did not influence the loading (**Figure 5.4 B**).

Finally, the effect of the purification method on DEX loading was tested by utilizing TFF after polymersome preparation via the continuous flow setup. After collection of 40 mL of the DEX-loaded polymersome dispersion, purification by TFF was quickly accomplished in less than 1 hour. This resulted in the production of DEX-loaded polymersomes with a size of approximately 290 nm and a PDI value of 0.24 (**Figure 5.4 A**). The size of the particles was lower compared to all the other preparations. Furthermore, the loading with DEX did not increase, with only 22 µg/mL loaded into the bilayer membrane (**Figure 5.4 B**). Which corresponds to an encapsulation efficiency of 4.4 % and a loading capacity of 0.40 %. Cryo-TEM measurements confirmed that there was no difference in appearance between in-flow produced DEX-loaded polymersomes and unloaded polymersomes produced either in batch or in flow (**Figure 5.3 C**).

The stability of the produced DEX-loaded polymersomes was studied for a period of 6 weeks, by storing the dispersion at 4 ˚C. After 6 weeks, the polymersome size had not changed (**Table 5.2**). The loading concentration on the other hand decreased slightly, from 21 to 19 µg/mL.

Table 5.2. Stability of DEX-loaded PEG-PDLLA polymersomes. Average hydrodynamic diameters as measured by DLS, and DEX loading as measured by HPLC over time. Time points are starting point (D_0), after 2 weeks (W_2) and after 6 weeks (W_6).

Time point	Z-average (nm)	PDI	DEX loading (µg/mL)	Encapsulation efficiency (%)	Loading capacity (%)
D_0	420	0.25	21	4.2	0.38
W_2	350	0.20	21	4.2	0.38
W_6	410	0.19	19	3.7	0.35

In general, the results mentioned above are promising. The unloaded polymersomes that were prepared using the continuous flow setup were very much comparable to the in-batch produced unloaded polymersomes. This was also the case for the loading of the polymersomes with DEX. It can therefore be stated that using a continuous flow process for the production DEX-loaded polymersomes is feasible and can potentially be exploited for production on a larger scale in the future. Besides that, the produced polymersomes are very stable with low DEX release during storage. Nevertheless, there is still enough room for improvement regarding the overall loading of the particles.

For now, using the developed methods, it seems that the maximum of loading with DEX is around 20 µg/mL. The choice of a different hydrophobic block copolymer, like poly(ε-caprolactone) or poly(trimethylene carbonate), might increase solubilization of DEX into the polymersome membrane. This however could have an effect on the ease of shape transformation of the spherical vesicles, which has been optimized for PEG-PDLLA systems, but has turned out to be difficult for other biodegradable hydrophobic blocks.

Something else to consider is that the low loading of the DEX might be due to the solubility of the drug in the continuous phase during preparation. The 50/50 vol%/vol% mixture of THF/dioxane (4:1 v/v) and water, is likely a relatively reasonable solvent for DEX. If this is the case, then DEX is not driven to be solubilized into the hydrophobic membrane but will also remain in the continuous water/dioxane/THF phase and subsequently be removed from the polymersome dispersion by dialysis. An option to overcome this, might be to try and add a small volume of highly concentrated polymer/DEX in THF/dioxane to a larger volume of water. In this way the solubility of DEX in the final mixture is substantially reduced, favoring the solubilization of DEX into the polymer membrane of the polymersomes. However, the anticipation of shape transformation of the polymersomes might again be more challenging to achieve due to different solvent to water compositions.

Preparation of β-CD-DEX-loaded polymersomes

Another option that might increase the loading of the polymersomes, is the use of a more hydrophilic drug. As already mentioned, besides the capacity to accommodate drugs in their hydrophobic membrane, polymersomes also have the ability to load cargo in the aqueous lumen. In order for DEX to be encapsulated in the lumen it should be made water soluble, which can be

accomplished by forming a host-guest complex with a water-soluble host. An often-used host in this respect is β-cyclodextrin (β-CD). β-CD is a well-known water-soluble cyclic oligosaccharide that possesses a hydrophobic pocket. [16–18] Complexation of β-CD with a hydrophobic drug in this pocket can easily be achieved and enhances the solubility of the drug, in our case DEX. For our study, a commercially available β-CD-DEX complex comprising 6.7 wt% of DEX (19 mol%) was used. It was shown in previous studies, that adding the β-CD-DEX complex to the organic phase together with PEG-PDLLA and subsequent addition of Milli-Q water resulted in polymersome formation and loading. It resulted in a reasonable DEX encapsulation (~ 200 µg/mL, 24 % encapsulation efficiency and 1.1 % loading capacity) and was therefore selected to be further investigated.[15] For this experiment, in order to co-dissolve 1 mg of DEX, approximately 15 mg of β-CD-DEX was co-dissolved per 10 mg of block copolymer in 1 mL THF: dioxane (4:1 v/v).

First, drug-loaded polymersomes were prepared in batch using dialysis as purification with the same batch protocol as previously described. This resulted in the production of β-CD-DEX-loaded PEG-PDLLA polymersomes with a size of 500 nm and PDI values of 0.15 (**Figure 5.5 A**), which is slightly bigger compared to the unloaded polymersomes but still comparable to previously reported results. [8–12,15] Though the loading of the polymersomes was increased to 34 µg/mL DEX compared to our other DEX loading experiments, corresponding to an encapsulation efficiency of 6.8 % and a loading capacity of only 0.27 %, these values are still much lower as observed in the previous study [15] (**Figure 5.5 B**).

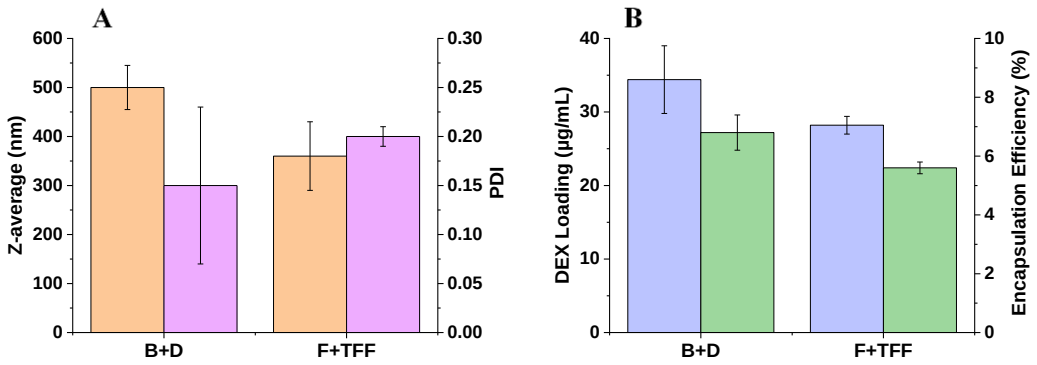

Figure 5.5. Characteristics of β-CD-DEX-loaded PEG-PDLLA polymersomes obtained using different preparation techniques. (A) Average hydrodynamic diameters (orange) and PDI values (pink) as measured by DLS. (B) DEX loading (blue) and encapsulation efficiencies (green) as measured by HPLC. The different preparation techniques were (B+D): prepared in batch and purified by dialysis, and (F+TFF): prepared using continuous flow and purified by TFF. For all experiments n = 2.

In order to assess if the preparation method had an effect on the encapsulation efficiency, the continuous flow method, followed by TFF was employed. This resulted in the production of β-CD-DEX -loaded polymersomes with a size of approximately 360 nm and a PDI value of 0.20 (**Figure 5.5 A**). The size of the obtained particles was slightly lower compared to the β-CD-DEX-loaded polymersomes prepared in batch. Furthermore, the loading with β-CD-DEX did not increase but was even slightly lower with 28 µg/mL DEX loaded into the lumen (**Figure 5.5 B**), corresponding to an encapsulation efficiency of 5.6% and a loading capacity of 0.22 %.

Although the continuous flows method worked as efficiently as the batch process in the formation of the polymersomes, it did not improve the encapsulation efficiency for the hydrophilic β-CD-DEX complex, in contrast to earlier batch-type experiments. Further analysis indicated that there was one difference between the in-batch β-CD-DEX-loaded PEG-PDLLA polymersome preparation protocols. In the previous experiment the dialysis was done at a low temperature of 4 ˚C and only for 6 hours instead of at room temperature and overnight, which were the conditions used in this chapter. It should therefore be further investigated if temperature during dialysis has a direct influence on encapsulation efficiencies. Another aspect to consider, is

that due to the high solubility of the β-CD-DEX it will be equally distributed inside and outside the lumen of the polymersomes. The encapsulation of this complex is therefore a passive process and is directly dependent on the entrapped volume in the polymersomes. By working in a more concentrated environment, higher encapsulation efficiencies might be accomplished.

CONCLUSION

The goal of this study was to develop an efficient and scalable process for the manufacturing of DEX-loaded polymersomes based on a PEG-PDLLA block copolymer. The unloaded and DEX-loaded polymersome production and purification was accomplished using continuous flow setups, which can be potentially scaled-up for future production. The loading of the polymersomes with DEX using the continuous flow setup was comparable with batch production, with encapsulation efficiencies between 3-5 % meaning that there is room for improvement regarding encapsulation. The use of a more hydrophilic DEX, β-CD-DEX complex, using the developed protocols did not result in a much higher loading as only 34 µg/mL DEX was encapsulated in batch production and 28 µg/mL DEX in flow production. Most importantly, the first steps were taken for the development of a production methodology for the efficient production of large amounts of loaded polymersomes.

ACKNOWLEDGEMENTS

Roxane Ridolfo is thanked for the introduction she gave to this project and the many useful discussions. Dr Alexander Mason and Imke Welzen-Pijpers are acknowledged for providing the cryo-TEM images.

We are also grateful for the financial support received from the European Union's Horizon 2020 research and innovation program Marie Sklodowska-Curie Innovative Training Networks (ITN) under grant No. 676137.

MATERIALS AND METHODS

Materials

DL-Lactic acid (DLL), 1,8-diazabicyclo[5.4.0]undec-7-ene (DBU) and bovine serum albumin (BSA), DEX and β-CD-DEX were obtained from Merck (Darmstadt, Germany and used without further purification. Poly(ethylene glycol) methyl ether (mPEG) 1 kDa, was obtained from JenKem technology (Plano, USA) and lyophilized prior to use. Spectra/Por® dialysis membranes of 12-14 kDa were used for dialysis. Easivial PEG standards for GPC analysis were obtained from Agilent (Santa Clara, USA). All solvents were purchased from commercial suppliers and used as received.

^{1}H-NMR

^{1}H-NMR measurements were performed on a Bruker 400 MHz NMR with a 5 mm PABBO BB probe using $CDCl_3$ as the solvent and TMS as an internal standard.

GPC

GPC measurements were performed on a Shimadzu Prominence-i GPC system with a PL gel 5 µm mixed D and mixed C column (Polymer Laboratories) equipped with a Shimadzu RID-20A. THF was used as eluent with a flow rate of 1 mL/min. Calibration was done with PEGs of narrow molecular weights.

HPLC

For determination of DEX loading, samples were prepared by freeze drying 1 mL of DEX-loaded polymersome dispersion and dissolving the dried product in 1 mL ACN. HPLC measurements were performed using an XBridge-C8 (50 x 4.6 mm, 5 µm) column. As eluent 0.1% formic acid versus 0.05% formic acid in ACN was used in a gradient flow of 1 mL/min. The gradient went from 95 % (0.1 % formic acid in water) and 5 % (0.05 % formic acid in ACN) to 95 % (0.05 % formic acid in ACN) and 5 % (0.1 % formic acid in water). Detection was performed at 254 nm. Samples of 10 µL were injected.

Dynamic light scattering (DLS)

DLS measurements were performed on a Malvern Zetasizer nano series ZS90 with a measurement angle of 173° and a temperature of 25 °C. Polymersome samples were diluted 100 times prior to measuring. Zetasizer software was used to process and analyze the data.

Cryogenic transmission electron microscopy (cryo-TEM) analysis

Cryo-TEM measurements were performed on selected polymersome samples using a CryoTitan (Thermo Fisher Scientific) equipped with a field emission gun and autoloader and operated at 300 kV acceleration voltage in low-dose bright-field TEM mode. Samples for cryo-TEM were prepared by glow-discharging the grids (Lacey carbon coated, R2/2, Cu, 200 mesh, EM sciences) in a Cressington 208 carbon coater for 40 seconds. Then, 4 µL of the polymersome dispersion was pipetted on the grid and blotted in a Vitrobot MARK III at room temperature and 100% humidity. The grid was blotted for 3 seconds (offset -3) and directly plunged and frozen in liquid ethane. Cryo-TEM images were acquired with zero loss energy filtering mode (Gatan GIF 2002, 20eV energy slit) on a CCD camera (Gatan model 794).

Polymer synthesis

The synthesis of PEG-PDLLA was performed using a previously published protocol. [11] In short, 0.194 g mPEG 1 kDa (0.2 mmol) and 1.30 g (9.03 mmol) DLLA were dried using azeotropic distillation with dry toluene as the solvent. The dried starting materials were then dissolved in 13 mL dry DCM and the reaction mixture was put under argon. Then 15 µL DBU (0.5 equivalents with respect to the initiator mPEG) was added and the solution was stirred at RT until ^{1}H-NMR spectroscopy confirmed that the reaction was completed, which was achieved after approximately 2 hours. The solution was washed twice with 1 M $KHSO_4$, once with brine and dried with Na_2SO_4. After filtering and evaporating most of the solvent, the formed PEG-PDLLA polymer was precipitated in ice cold diethyl ether. The remaining wax was dried under nitrogen, dissolved in dioxane and lyophilized yielding a white powder (75-85 %). The resulting polymer product was analyzed by ^{1}H-NMR (**Figure 5.6**) and GPC (**Figure 5.7**).

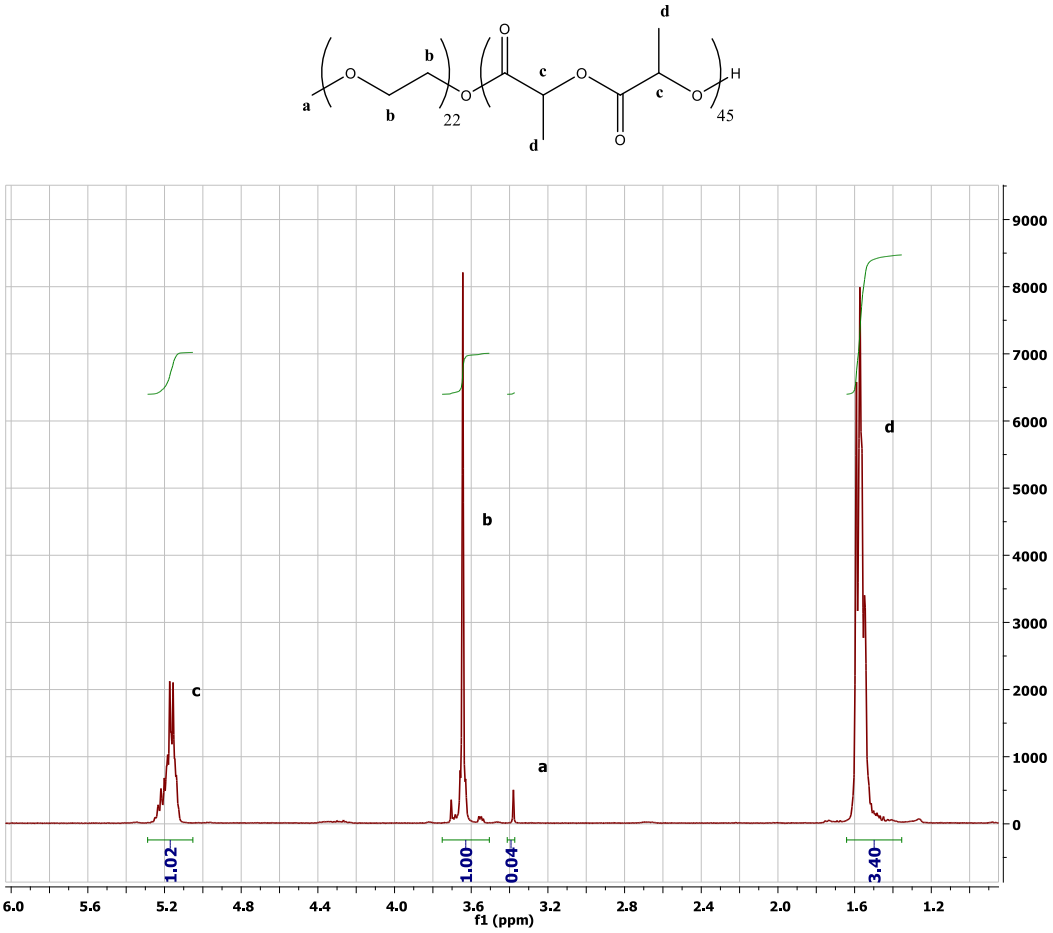

Figure 5.6. ^{1}H-NMR spectrum of PEG$_{22}$-PDLLA$_{45}$. A M_n of 7.5 kDa could be calculated which indicated a N_{DLLA} of 46.

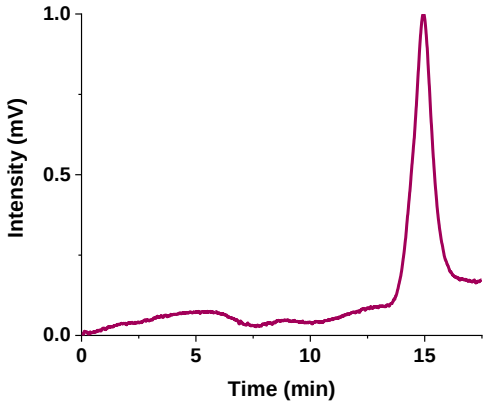

Figure 5.7. GPC trace of PEG_{22}-$PDLLA_{45}$ block copolymer. The y-axis shows the intensity of the dRI signal. M_n = 12.3 kDa, M_w = 14.5 kDa and Đ = 1.18.

Polymersome preparation in batch

PEG-PDLLA polymersomes were prepared in batch using previously published protocols. [11] In short, 20 mg PEG-PDLLA polymer was dissolved in 2 mL THF:dioxane (4:1 v/v), the vial was capped with a rubber septum and the mixture was stirred for 30 min. Using a syringe pump, 2 mL Milli-Q water was added at a 1 mL/hour rate. The obtained polymersome dispersion was dialyzed against Milli-Q water overnight.

Polymersome preparation in flow

PEG-PDLLA block copolymer was dissolved in THF:dioxane (4:1 v/v) at a concentration of 10 mg/mL. A home-made setup consisting of two Knauer HPLC piston pumps (K-501) was used, which were both set at 1 mL/min, to pump both the polymer/THF:dioxane mixture and Milli-Q water via different inlets through a simple PEEK™ Tee connection (inner diameter through hole was 0.5 mm and < 0.57 µL swept volume) to ensure rapid mixing (**Figure 5.2**). All tubings were classical 1/16" PTFE HPLC tubings from Merck with an inner diameter of 0.5 mm. From the vials to the pumps a length of 10 cm tubing was used, from the pump to the T-mixer again a length of 10 cm tubing was used and from the T-mixer to the collection flask a length of 20 cm tubing was used. The outlet stream was collected in a flask and continuously stirred until a total of 40 mL polymersome dispersion was collected. The THF:dioxane was either removed through dialysis or TFF against Milli-Q water.

For regular dialysis purification, Spectra/Por® dialysis membranes of 12-14 kDa were used. The polymer dispersions were dialyzed overnight at room temperature against Milli-Q water, with a water change after 1 hour.

For TFF, a Sius^{TM}-LS TFF Prostream, 100 kDa, 0.02 m^2 cassette was used with a flow rate of 100 mL/min. Due to the low compatibility of the TFF membrane (neutrally charged PES membrane) in the cassette with THF and dioxane, the polymersome dispersion was diluted 10 times using Milli-Q water prior to loading onto the TFF membrane. Next, using the TFF setup, the polymersome dispersion was concentrated back to the original 5 mg/ml and further purified with 4 dia-filtration volumes of water to ensure complete solvent depletion.

DEX-loaded polymersomes

DEX-loaded PEG-PDLLA polymersomes were prepared using the same procedures as for the unloaded polymersomes described above, both in batch and flow. DEX was co-dissolved with the block copolymer in THF:dioxane (4:1). For each 10 mg of block copolymer, 1 mg of DEX was co-dissolved. After dialysis or TFF, the DEX-loaded polymersome dispersion was passed through a 1 µm disk filter to remove any precipitated non-encapsulated DEX.

β-CD-DEX-loaded PEG-PDLLA polymersomes were also prepared using the same procedures as for DEX-loaded polymersomes. The commercially available β-CD-DEX complex used contained 6.7 % of DEX per mass, an equivalent of 19 mol%. β-CD-DEX complex was co-dissolved with the block copolymer in THF:dioxane (4:1). In order to co-dissolve 2 mg of DEX, approximately 30 mg of β-CD-DEX was co-dissolved per 20 mg of block copolymer.

Stability study

The stability of the in-flow prepared DEX-loaded polymersomes was determined by storing samples at 4 °C up to 6 weeks. At different time points, samples of the stored polymersome dispersions were filtered through a 1 μm disk filter to remove released/free DEX. The size of the DEX-loaded polymersomes was measured by DLS and the remaining DEX in the polymersomes was determined by HPLC.

REFERENCES

(1) Tinkov, S. *Chapter 15 - Contemporary Industrial Practice for Manufacturing of Nanomedicines*; Elsevier Inc., 2018.
(2) Shi, J.; Kantoff, P. W.; Wooster, R.; Farokhzad, O. C. *Nat. Rev. Cancer* **2016**, *17*, 20.
(3) Hua, S.; de Matos, M. B. C.; Metselaar, J. M.; Storm, G. *Front. Pharmacol.* **2018**, *9*, 1–14.
(4) Desai, N. *AAPS J.* **2012**, *14* (2), 282–295.
(5) Bermudez, H.; Brannan, A. K.; Hammer, D. A.; Bates, F. S.; Discher, D. E. *Macromolecules* **2002**, *35* (21), 8203–8208.
(6) Lee, J. S.; Feijen, J. *J. Control. Release* **2012**, *161* (2), 473–483.
(7) Zhang, X.; Zhang, P. *Curr. Nanosci.* **2016**, *13* (2), 124–129.
(8) Pijpers, I. A. B.; Abdelmohsen, L. K. E. A.; Williams, D. S.; Van Hest, J. C. M. *ACS Macro Lett.* **2017**, *6* (11), 1217–1222.
(9) Pijpers, I. A. B.; Meng, F.; van Hest, J. C. M.; Abdelmohsen, L. K. E. A. *Polym. Chem.* **2019**, 275–280.
(10) Wauters, A. C.; Pijpers, I. A. B.; Mason, A. F.; Williams, D. S.; Tel, J.; Abdelmohsen, L. K. E. A.; Van Hest, J. C. M. *Biomacromolecules* **2019**, *20* (1), 177–183.
(11) Abdelmohsen, L. K. E. A.; Williams, D. S.; Pille, J.; Ozel, S. G.; Rikken, R. S. M.; Wilson, D. A.; Van Hest, J. C. M. *J. Am. Chem. Soc.* **2016**, *138* (30), 9353–9356.
(12) Ridolfo, R.; Williams, D. S.; Van Hest, J. C. M. *Polym. Chem.* **2020**, *11* (16), 2775–2780.
(13) Meng, F.; Hiemstra, C.; Engbers, G. H. M.; Feijen, J. *Macromolecules* **2003**, *36* (9), 3004–3006.
(14) Metselaar, J. M.; Wauben, M. H. M.; Wagenaar-Hilbers, J. P. A.; Boerman, O. C.; Storm, G. *Arthritis Rheum.* **2003**, *48* (7), 2059–2066.
(15) Ridolfo, R. Polymeric Nanoparticle Shape Effects in a Drug Delivery Context (Doctoral Dissertation), TU Eindhoven, 2020.
(16) Sharma, N.; Baldi, A. *Drug Deliv.* **2014**, *23* (3), 739–757.
(17) Jacob, S.; Nair, A. B. *Drug Dev Res* **2018**, *79* (5), 201–217.
(18) Challa, R.; Ahuja, A.; Ali, J.; Khar, R. K. *AAPS PharmSciTech* **2005**, *6* (2), 329–357.

Chapter 6

Summary and Outlook

SUMMARY

Even though numerous promising nanomedicines are reported every year in literature, the translation into clinical products is still limited. One of the bottlenecks on the road towards clinical products regards the development of robust and scalable manufacturing processes of the nanomedicines and their building blocks. In this thesis, the various steps towards nanoparticle production processes that are efficient, scalable and comply with good manufacturing practices (GMP) have been investigated in detail.

In ***Chapter 1***, a number of important nanoparticle structures were highlighted, followed by an overview regarding typical challenges that limit translation into clinical products and in the end the aim of this thesis was described in more detail.

Understanding the correlation between varying formulation and process parameters and the resulting physicochemical characteristics of the nanoparticles is of utmost importance for the development of robust and scalable manufacturing processes. Therefore, in C***hapter 2*** we investigated the parameters influencing the self-assembly of poly(ethylene glycol)-*b*-poly(*N*-2-benzoyloxypropyl methacrylamide (mPEG-*b*-p(HPMA-Bz)) block copolymers into micelles. Among the tested parameters were the degree of polymerization of the hydrophobic block and thus the hydrophobic to hydrophilic ratio of the used block copolymers, homopolymer content, block copolymer concentrations, addition rates and solvent usage. It was shown that these parameters all had an influence on the resulting micelle size, which could be exploited to precisely tailor micelle sizes between 25 to 100 nm. The size control could be achieved via both the molecular weight of the block copolymers and the processing methods that had a direct influence on the saturation conditions during micelle preparation.

In ***Chapter 3***, the influence of the saturation conditions and nucleation rate of block copolymers to self-assemble into nanoparticles was further investigated with microfluidics. This technique allowed for control over minute fluidic volumes, which provided precise regulation of mixing rates and therewith directly influenced saturation conditions. It was shown in that chapter that the self-assembly of mPEG-*b*-p(HPMA-Bz) block copolymers could be easily tailored in size and even in morphology of the resulting nanoparticles. Together with the hydrophobic to hydrophilic ratio of the block copolymers

and the used concentration, the flow rate proved to be a determining factor regarding particle size. It was even possible to produce polymersomes, when using lower polymer concentrations and slower flow rates during preparation, from the same block copolymers whose self-assembly usually results in micelle formation when produced with a traditional nanoprecipitation method.

With the knowledge obtained from the research in ***Chapter 2*** and ***Chapter 3***, a scalable manufacturing process for the production of drug-loaded micelles was developed, which was described in ***Chapter 4***. In that chapter, the synthesis of the mPEG-*b*-p(HPMA-Bz) block copolymers was first optimized through a step-by-step investigation and optimization of the batch synthesis procedures. After the production of 1 kg of the block copolymer, its self-assembly into unloaded and docetaxel (DTX)-loaded micelles was investigated in both batch and flow processes to ensure product quality and consistency of the manufacturing processes. In the end, a continuous flow process was developed for the large-scale production of the DTX-loaded micelles. While developing these efficient, scalable and highly controlled manufacturing processes, the quality requirements of the European Medicines Agency (EMA) and U.S. food and drug administration (FDA) were constantly taken into account. The developed manufacturing processes can therefore be readily translated for GMP production of the corresponding clinical product.

In ***Chapter 5*** the production of dexamethasone (DEX)-loaded poly(ethylene glycol)-*block*-poly(D,L-lactide) (PEG-PDLLA) polymersomes in a reproducible, efficient and scalable manner was explored. To achieve this, the use of a continuous flow setup for the production of both DEX-loaded and unloaded polymersomes was developed and tangential flow filtration (TFF) was investigated as an in-flow purification method. The DEX-loaded polymersomes showed good colloidal stability for at least 6 weeks at 4 ˚C with good drug retention. An attempt was also made to enhance the overall drug loading by using a water-soluble variant of DEX, DEX-β-cyclodextrin complex, which was used for encapsulation in the aqueous lumen of the polymersomes. However, using the developed processes, DEX-β-cyclodextrin complex usage did not improve drug loading, indicating that clearly additional optimization is required regarding drug loading. Nevertheless, it can be concluded that the first steps towards a production methodology for efficient and potential large-scale manufacturing of DEX-loaded polymersomes was accomplished.

OUTLOOK

Control in size and morphology of NPs

Being able to control the size and morphology of polymer self-assemblies is extremely important, because differences in sizes and morphologies lead to different pharmacokinetics, tumor penetration and therapeutic efficacies[1–4] and a precise control during production should be well established for efficient and reproducible manufacturing.

In ***Chapter 2 and 3*** it was extensively investigated how formulation and process parameters had an effect on the self-assembly of mPEG-*b*-p(HPMA-Bz) block copolymers into differently sized nanoparticles. Interestingly, under specific conditions also the morphology could be adjusted to a certain extent, as was shown by the production of small amounts of polymersomes together with micelles, whereas normally the polymers employed would only lead to micelle formation. Further investigation and modification of the process parameters might even provide the opportunity to produce mPEG-*b*-p(HPMA-Bz) polymersomes only. This could be achieved by lowering the nucleation rate of polymer assembly, which for example could be achieved via microfluidics employing low polymer concentrations and applying low flow rates. Another option might be to use mPEG-*b*-p(HPMA-Bz) block copolymers with even lower hydrophilic weight fractions, such as the polymers that were produced with $mPEG_{2K}$ in ***Chapter 2***, as their thermodynamically favorable assemblies are polymersomes. In general, it was demonstrated in previous research and in ***Chapter 2 and 3***, that a direct control over saturation conditions of block copolymers during production showed to have the most impact on the resulting nanoparticle size and morphology, whereas block copolymer characteristics showed to be less important. [5–7] It is therefore envisioned that, to some extent, the application of different saturation conditions with other types of block copolymers is also applicable to gain control over size and morphology of the resulting nanoparticles. Further investigations, using other block copolymers, are required to demonstrate the general applicability of the effect of processing conditions on particle formation, which could show that ultimately not necessarily the characteristics of the block copolymer but rather the preparation conditions are most important for production of specific types of nanoparticles.

In ***Chapter 5***, the investigated PEG-PDDLA system possesses several interesting features. Upon formation, these polymersomes can be resized via extrusion [8] and be shape transformed into prolate [9] (tubes) and oblate [10] (discs or stomatocytes) morphologies under osmotic pressure. It would be very interesting to establish if these features can be reproduced on a larger scale for both the drug-loaded and unloaded polymersomes.

Production of drug-loaded NPs on a large scale for clinical translation

The ultimate goal of this dissertation, to produce drug-loaded NPs in a scalable and reproducible manner, was reached in the research described in ***Chapter 4*** and partly in ***Chapter 5***. In ***Chapter 4***, DTX-loaded mPEG-*b*-p(HPMA-Bz) micelles were produced using efficient, scalable and highly controlled manufacturing batch and flow processes. It was shown that by changing from microfluidic flow production to regular flow production using simple HPLC tubing and pumps the production scale could be effectively increased. These processes, together with the developed analytical methods, can be readily translated for GMP production of large amounts of the corresponding clinical product. The next step would be to take this formulation to clinical trials and hopefully get regulatory approval. Eventually, for commercialization, flow reactors can be effectively scaled up to allow increased production without the need for process optimization.

In order to achieve translation from preclinical to clinical development of nanoparticle formulations, three aspects are important: therapeutic profiling, biocompatibility and production robustness. Though the latter was studied and discussed in the research described in this dissertation, pharmacokinetic and toxicokinetic studies are still necessary to comply with the other two aspects in order to go to clinical trials. An indication regarding these preclinical efficacies was investigated by our colleagues who worked with similar mPEG-*b*-p(HPMA-Bz) micelle formulations loaded with a different chemotherapeutic drug, namely paclitaxel (PTX). It was shown that PTX-loaded mPEG-*b*-p(HPMA-Bz) micelles are very promising regarding pharmacokinetics, biodistribution, tumor accumulation and even complete tumor regression in mice. [11] This study already provides an idea regarding preclinical proof-of-concept for both the efficacy and safety for our DTX-loaded micelle formulation.

For the research on DTX-loaded mPEG-*b*-p(HPMA-Bz) micelles, only the block copolymer with a 5 kDa PEG block and a 17.5 kDa p(HPMA-Bz) block was used. It would be interesting to verify that the other mPEG-*b*-p(HPMA-Bz) block copolymers can also be used for the production of large batches of smaller DTX-loaded micelles following the developed processes. The research described in ***Chapter 3***, already gives insight into the applicability of the production method. As long as fast mixing and high concentrations are used for the other block copolymers, no problems in homogeneity of the nanoparticles is expected when produced on a large scale. The loading of these micelles with DTX can however be more troublesome, as was also shown by our colleagues for the PTX-loaded mPEG-*b*-p(HPMA-Bz) micelles. In their research it was shown that using mPEG-*b*-p(HPMA-Bz) with a shorter hydrophobic block led to lower drug loading and less drug retention. [12] Besides that, the encapsulation of other drugs, like curcumin, or basically any other drug that has a suitable hydrophobicity and aromatic properties to contribute to the π-π stacking inside the micelle core, should be considered for production. Even combinations of imaging moieties and drugs can be examined to produce theranostic micelle products on a large scale.

In ***Chapter 5*** it was demonstrated that, exploiting very similar flow processes as described in ***Chapter 4***, DEX-loaded PEG-PDLLA polymersomes could be produced with the potential to be scaled up further. For this nanoparticle formulation, however, drug loading was challenging and should definitely be improved. Reducing the solubility of DEX in the end mixture during polymersome formation might already favor solubilization into the polymer membrane. Although the use of a more hydrophilic variant of DEX did not result in higher drug loading of the drug into the lumen, working under more concentrated conditions might lead to higher loading as the process is a passive one and is directly dependent on the entrapped volume in the polymersomes. Another strategy to achieve improved drug loading, is using polymer-drug conjugates in which the drug is attached to the block copolymer through a (cleavable) linker. During the self-assembly process the drug will automatically end up in the polymersome, without relying on passive or chemically driven loading. Depending on where the drug is conjugated and on the physicochemical properties of the drug it can even be easily directed to a certain part of the polymersomes. When a hydrophobic drug is conjugated to the hydrophobic block it will end up in the hydrophobic membrane of the polymersomes, whereas when a more hydrophilic drug is conjugated to the

hydrophilic block it will end up both in the lumen and attached to the outside shell of the polymersomes.

Besides optimization in drug loading, a suitable sterilization method should also be well established. In this formulation sterilization can be rather challenging, as 'simple' filtration over a 0.2 µm filter is not possible since the overall polymersome size is already around 400 nm. Unless the polymersomes are resized *via* extrusion [8] during production, aseptic production should be considered as other sterilization methods are most likely not applicable.

For both the mPEG-*b*-p(HPMA-Bz) micelles and the PEG-PDLLA polymersomes, the introduction of targeting moieties such as antibodies might result in intriguing nanoparticles for targeted delivery. This could be achieved by surface modifications after self-assembly of the polymersomes, or in case of the mPEG-*b*-p(HPMA-Bz) micelles also by conjugating it to the hydrophilic block prior to polymer self-assembly. Being able to produce those nanoparticles on a large scale would then of course be the ultimate goal.

Stability and release studies

Both the DTX-loaded and the DEX-loaded PEG-PDLLA polymersomes showed to be stable for a prolonged period, as described in ***Chapter 4 and 5***. The results for the DTX-loaded micelles showed that, even up to 2 months and also at room temperature, the particles were stable with negligible drug release over time. Similar results were observed for the DEX-loaded polymersomes that showed to be stable up to 6 weeks at 4 ˚C with negligible drug release. Nevertheless, more extensive and accelerated aging-studies should be performed using varying conditions. Besides that, also *in vitro* release profiles should be well established.

For the mPEG-*b*-p(HPMA-Bz) micelles this was already investigated by our colleagues for the drug PTX with very promising results.[12] This gives an indication on how the DTX-loaded micelles will behave in accelerated stability and release studies. If the formulations have an insufficient pharmaceutical stability, freeze drying protocols should be developed.

General remarks

Despite tremendous efforts of the polymer-based nanomedicine community, leading to many formulations with interesting preclinical results, the actual output of clinically relevant products is still low. As already mentioned, therapeutic profiling, biocompatibility and production robustness are the three important aspects to consider for the translation from preclinical to clinical development. The first two aspects are usually extensively studied, but the latter aspect (scalability and synthesis robustness) is hardly ever a criterium in the design of the nanomedicines. It often happens that highly potential nanoparticle formulations are discarded during translation by the pharmaceutical industry as they cannot be produced cost-efficiently and on a large scale. For example, if a protocol states that 10 mL reaction mixture should be precipitated in 100 mL non-solvent to obtain a total of 1 gram of a certain building block, it should be apparent that this protocol is not feasible if one wants to produce a couple of hundred kilograms. Another aspect that is often not considered is end product sterilization. For nanomedicines, the most commonly used and 'simple' method for sterilization is filtration by extruding the formulation through 0.22 μm membrane filters. It should be apparent that for example nanoparticles with a larger size than the membrane pores cannot go through these filters and other (more troublesome) sterilization techniques need to be investigated. These aspects are not highlighted enough and raising awareness on these matters is important to improve the success rate in the field of nanomedicine.

Therefore as a final suggestion, at the early stages of nanoparticle design, protocols for both production of the building blocks and the eventual self-assembly of those building blocks into nanoparticles as well as end-product sterilization should be critically assessed, in order to create nanomedicines with impact that extend beyond the conceptual phase.

REFERENCES

(1) Cabral, H.; Matsumoto, Y.; Mizuno, K.; Chen, Q.; Murakami, M.; Kimura, M.; Terada, Y.; Kano, M. R.; Miyazono, K.; Uesaka, M.; Nishiyama, N.; Kataoka, K. *Nat. Nanotechnol.* **2011**, *6* (12), 815–823.

(2) Wang, J.; Mao, W.; Lock, L. L.; Tang, J.; Sui, M.; Sun, W.; Cui, H.; Xu, D.; Shen, Y. *ACS Nano* **2015**, *9* (7), 7195–7206.

(3) Sun, Q.; Ojha, T.; Kiessling, F.; Lammers, T.; Shi, Y. *Biomacromolecules* **2017**, *18* (5), 1449–1459.

(4) Williams, D. S.; Pijpers, I. A. B.; Ridolfo, R.; van Hest, J. C. M. *J. Control. Release* **2017**, *259*, 29–39.

(5) Lebleu, C.; Rodrigues, L.; Guigner, J. M.; Brûlet, A.; Garanger, E.; Lecommandoux, S. *Langmuir* **2019**, *35* (41), 13364–13374.

(6) Hamdallah, S. I.; Zoqlam, R.; Erfle, P.; Blyth, M.; Alkilany, A. M.; Dietzel, A.; Qi, S. *Int. J. Pharm.* **2020**, *584* (January).

(7) Keßler, S.; Drese, K.; Schmid, F. *Polymer* **2017**, *126*, 9–18.

(8) Wauters, A. C.; Pijpers, I. A. B.; Mason, A. F.; Williams, D. S.; Tel, J.; Abdelmohsen, L. K. E. A.; Van Hest, J. C. M. *Biomacromolecules* **2019**, *20* (1), 177–183.

(9) Abdelmohsen, L. K. E. A.; Williams, D. S.; Pille, J.; Ozel, S. G.; Rikken, R. S. M.; Wilson, D. A.; Van Hest, J. C. M. *J. Am. Chem. Soc.* **2016**, *138* (30), 9353–9356.

(10) Pijpers, I. A. B.; Abdelmohsen, L. K. E. A.; Williams, D. S.; Van Hest, J. C. M. *ACS Macro Lett.* **2017**, *6* (11), 1217–1222.

(11) Shi, Y.; Van Der Meel, R.; Theek, B.; Oude Blenke, E.; Pieters, E. H. E.; Fens, M. H. A. M.; Ehling, J.; Schiffelers, R. M.; Storm, G.; Van Nostrum, C. F.; Lammers, T.; Hennink, W. E. *ACS Nano* **2015**, *9* (4), 3740–3752.

(12) Sheybanifard, M.; Beztsinna, N.; Bagheri, M.; Buhl, E. M.; Bresseleers, J.; Varela-Moreira, A.; Shi, Y.; van Nostrum, C. F.; van der Pluijm, G.; Storm, G.; Hennink, W. E.; Lammers, T.; Metselaar, J. M. *Int. J. Pharm.* **2020**, *584*, 119409.

- Appendix -

About the author

Jaleesa Bresseleers was born on the 22nd of May 1989 in Merksem (Antwerp), Belgium. After finishing her secondary education ASO: Wetenschappen - Wiskunde in 2007 at the Koninklijk Atheneum Ekeren in Belgium, she studied Molecular Life Sciences at Radboud University Nijmegen. During her Master's degree, Jaleesa first completed an internship in the Bio-Organic Chemistry group of prof. Jan van Hest at Radboud University Nijmegen where she studied the possibilities in engineering self-assembly of capsid proteins and the creation of a nanoreactor. She then joined the Chemistry and Chemical Engineering group of prof. Dave Tirrell at California Institute of Technology, USA for an internship where she worked on the development of a FRET based stress sensor in protein hydrogels. After obtaining her Master's degree in 2013, she moved to Guadalajara, Mexico where she started working as a volunteer with underprivileged children for a short period and later on started a job as a quality control project leader in the veterinary pharmaceutical industry. In 2016 she came back to Europe and started her doctoral research as an external PhD student at ChemConnection BV – Ardena Oss and the Eindhoven University of Technology, in the Bio-Organic Chemistry group of prof. Jan van Hest. Her research focused on the development of robust and scalable manufacturing processes for nanocarriers and their polymeric building blocks. The most important results are described in this thesis.

List of publications

Sheybanifard, M. *; Beztsinna, N. *; Bagheri, M.; Buhl, E. M.; **Bresseleers, J.**; Varela-Moreira, A.; Shi, Y.; van Nostrum, C. F.; van der Pluijm, G.; Storm, G.; et al. Systematic Evaluation of Design Features Enables Efficient Selection of Π Electron-Stabilized Polymeric Micelles. *Int. J. Pharm.* 2020, *584*, 119409.

Bresseleers, J.; Bagheri, M.; Storm, G.; Metselaar, J. M.; Hennink, W. E.; Meeuwissen, S. A.; Van Hest, J. C. M. Scale-Up of the Manufacturing Process to Produce Docetaxel-Loaded mPEG- b-p(HPMA-Bz) Block Copolymer Micelles for Pharmaceutical Applications. *Org. Process Res. Dev.* 2019, 23, 2707–2715.

Bagheri, M *; **Bresseleers, J.** *; Varela-Moreira, A.; Sandre, O.; Meeuwissen, S. A.; Schiffelers, R. M.; Metselaar, J. M.; Van Nostrum, C. F.; Van Hest, J. C. M.; Hennink, W. E. Effect of Formulation and Processing Parameters on the Size of MPEG- b-p(HPMA-Bz) Polymeric Micelles. *Langmuir* 2018, 34 (50), 15495–15506.

Schoonen, L. *; Eising, S. *; van Eldijk, M. B.; **Bresseleers, J.**; van der Pijl, M.; Nolte, R. J. M.; Bonger, K. M.; van Hest, J. C. M. Modular, Bioorthogonal Strategy for the Controlled Loading of Cargo into a Protein Nanocage. *Bioconjug. Chem.* 2018, 29 (4), 1186–1193.

* Both contributed equally

Acknowledgements

Dan komen we aan bij het mooiste hoofdstuk van een proefschrift, het dankwoord. Het doorlopen van een promotietraject gaat namelijk niet zonder horten of stoten, een tegenslagje hier en een tegenslagje daar. Vaak zinkt de moed je simpelweg in de schoenen. Gelukkig zijn dat ook de momenten waarop je collega's, vrienden en familie je te hulp schieten, je opvrolijken en je weer een duwtje in de goede richting kunnen geven. Hiervoor ben ik immens dankbaar en daarom wil ik graag wat woorden wijden aan diegenen die al die tijd in mij hebben geloofd en mij hebben ondersteund.

Allereerst wil ik natuurlijk **Jan** bedanken. Gedurende mijn hele academische carriere was jij altijd een rode draad. Wij kennen elkaar inmiddels al een decenia lang, al vanaf de stage die ik tijdens mijn bachelor in jouw groep liep. Ik weet nog goed hoe alles alles begon met een zinnetje dat vaker de revu zou passeren, een "Hallo, Jan!" terwijl ik mijn hoofd door de deuropening van jouw kantoor in Nijmegen liet piepen. De stage die daarop volgde was mij zo goed bevallen dat ik ook ontzettend blij was dat ik ook mijn eerste masterstage in jouw groep mocht volbrengen en uiteindelijk was ook jij degene die mij in contact bracht met Dave Tirrell bij wie ik in de groep mijn master heb afgerond. Je hebt altijd veel vertrouwen in mij gehad en oorspronkelijk was dan ook het plan dat ik na mijn master, na een kleine tussenstop in Mexico, meteen als PhD student in jouw groep aan de slag zou gaan. Die kleine tussenstop in Mexico bleek uiteindelijk toch een ietsiepietsie langere tussenstop te worden. Je was dan ook verrast toen ik na bijna 3 jaar aan mariachi's, tacos en tequila wederom met een "Hallo, Jan!" mijn hoofd om het hoekje van jouw kantoor liet zien. Ik ben je ontzettend dankbaar voor de kans die jij mij wederom gaf en die ervoor zorgde dat ik al snel mocht beginnen binnen jouw groep als externe PhD student. Ook tijdens het af en toe hobbelige traject was jij altijd daar met je kennis, wijsheid, kritische blik en steun die er voor gezorgd hebben dat dit proefschrift hier nu ligt. Dankjewel!

Wim, met jou heb ik vanaf het begin van mijn gehele promotietraject nauw samengewerkt. Wat begon als een secondment in jouw groep, is uiteindelijk veel verder gegroeid en resulteert er in dat jij nu mijn 2^{e} promoter bent. In het begin werd ik een beetje nerveus van de emails met feedback op bijvoorbeeld manuscripten, ik wíst immers gewoon dat ze altijd volledig rood zouden terugkomen. Ook de eerste paar meetings met jou vond ik spannend. Met de

immense kennis en kritische blik die jij hebt, wist je namelijk altijd heel precies de zwakke plekjes in mijn onderzoek te porren en vragen te formuleren die überhaupt nog niet in me waren opgekomen. Hierdoor wist je wel elke keer weer het onderste bij mij uit de kan te halen en mij telkens weer te pushen om het beter te doen. Uiteindelijk ben ik het dan ook heel erg gaan waarderen en heeft het mij ontzettend geholpen om tot dit punt te komen. Ik was dan ook enorm vereerd toen je toestemde om mijn 2e promotor te zijn en wil je bedanken voor je continue support.

Ook mijn copromoter, **Silvie**, wil ik graag bedanken. In het begin dacht ik dat het werken aan dit project binnen een bedrijf een eenzaam traject zou zijn, omdat ik toch als enige bezig zou zijn aan dit bepaalde onderwerp. Gelukkig viel dit dankzij jou heel erg mee. Tijdens onze wekelijkse meetings was er genoeg ruimte om te sparren over problemen, inzichten en nieuwe ideeën. Je wist altijd een positieve draai te geven aan resultaten en stond altijd voor me klaar. Dankzij jouw expertise en kennisoverdracht in het schaalbaar produceren van nanomedicijnen, heb ik heb onwijs veel geleerd en ik wil je dan ook heel graag bedanken voor al je input en ondersteuning en af en toe dat duwtje in de goede richting.

Ferry en **Gerjan**, jullie wil ik graag bedanken om mij de kans te geven om dit hele traject bij (wat in het begin nog) ChemConnection (heette) te mogen voltrekken. Al tijdens het sollicitatiegesprek had ik een goede klik met jullie en dit reflecteerde zich ook in de intresse die jullie altijd hadden in mijn onderzoek. Het was fijn om voor jullie te mogen werken en af en toe bij het koffieapparaat bij te kletsen over de vooruitgang van mijn project. Ik heb daarnaast ook altijd vol bewondering gekeken naar hoe jullie Chemconnection hebben doen groeien, wat uiteindelijk resulteerde in de overname door Ardena. Jullie zijn toppers!

Ik wil daarnaast ook graag mijn manuscript commissie: **Koen Raemdonck, Rint Sijbesma, Ilja Voets, Timothy Noël** en **Loai Abdelmohsen** bedanken voor hun kritische oordeel op mijn proefschrift en voor hun tijd en deelname tijdens de verdediging.

Mijn paranimfen, **Kelly** en **Sjoerd**, zonder jullie had ik dit nooit vol kunnen houden. **Kelly**, bedankt voor elke keer weer je luisterende oor op momenten dat ik er helemaal doorheen zat. De rondjes frustratie eruit skaten, biertjes drinken en gekke shit samen doen, hebben de afgelopen periode een stuk

kleurrijker gemaakt. En **Sjoerd**, als de frustraties hoog opliepen door een mislukt experiment oid wist jij me met je flauwe grapjes altijd weer op te vrolijken. Wetende dat er weer een dag van synchroon, maar afschuwelijke en uit de toon gefluit met jou aan zat te komen, maakte het toch makkelijker om ook weer met een positieve blik door te pakken.

I consider myself unbelievably lucky to have had the opportunity to work within the horizon 2020 NANOMED Marie Curie ITN. The unique interdisciplinary exchange of knowledge and skills definitely helped me become a better scientist. It was an amazing experience to be able to work together with such an international team of so many recognized scientists. I would like to take this opportunity to thank all of my NANOMED fellows: **Shoupeng**, **Mona**, **Roxane**, **Esra**, **Vangelis**, **Jerry**, **Mahsa**, **Roberta**, **Molood**, **Jelle**, **Conor**, **Shirin**, **Vijay** and **Mike**. I was always amazed by the progress you all made during the entire project and really enjoyed our moments together. One of the people from NANOMED I would especially like to thank is **Mahsa**. We worked together a lot on the mPEG-*b*-p(HPMA-Bz) micelles from the beginning of our PhDs and thanks to you quite some of the chapters in this thesis look like they do now. It wasn't always easy and we encountered several bumps along the road, but we eventually made it. I really enjoyed working together with you and hope that our paths will cross again someday. Of course, **Roxane**, thank you for taking me under your wings regarding the PEG-PDLLA polymersomes. I especially enjoyed your enthusiasm and sparkling personality and definitely learned a lot from you. Good luck in France, I hope you find your dream job and who knows where in the world we'll meet again. And **Esra**, thank you for making me feel so at home during my secondment in Bordeaux, I enjoyed every minute working there.

Mijn collega's bij wat ooit begon als ChemConnection maar nu Ardena Oss; Alle kantoorgenootjes die de revu zijn gepasseerd dankjulliewel voor alle valse meezing momenten en ook om er voor te zorgen dat mijn "schrijf-dagen" wat dragelijker waren. Alle nano-team collega's dankjulliewel voor alle hulp die jullie mij elke keer boden als ik er weer eens niet uit kwam met bepaalde opstellingen of reacties, zonder jullie had ik het niet gekund. Ook de gezelligheid op het lab en de vrijdagmiddagdansmuziekjes zullen me altijd bijblijven. De lunch was ook altijd een moment om naar uit te kijken, na zo'n maal met een flinke dosis humor kon ik altijd weer met herwonnen energie de rest van de dag aan. Ik wil graag iedereen bedanken voor hun hulp, steun en gezelligheid.

Mark, ook jij bent net als Jan altijd een rode draad geweest. Mede dankzij jou, heb ik de kennis die ik nu heb. Ooit begonnen als naïef bachelor studentje met jou als mijn directe begeleider, liet jij mij de wondere wereld van het wetenschappelijk onderzoek ontdekken. Het beviel ons beiden goed, want ook mijn eerste masterstage heb ik onder jouw begeleiding doorlopen. Ik vond het heel prettig dat je me mijn eigen gang liet gaan, maar nog steeds wel nauw betrokken was met de dingen die ik deed en de zaken waar ik mee worstelde. Hierdoor kreeg ik vertrouwen in mijn eigen kennis en kunnen. Op jouw aanraden ben ik uiteindelijk ook richting Pasadena vertrokken voor mijn tweede stage. Ongeveer 2 jaar later ben ik je daar vervolgens ook nog een keer komen opzoeken, toen ik al in Mexico woonde en jij bij Dave in de groep bezig was met je postdoc. Toeval, daar geloof ik niet in, maar op z'n minst grappig dat we vervolgens anderhalf jaar later op precies dezelfde dag zijn begonnen bij Ardena. Dankjewel voor al je hulp, advies en vetrouwen.

Even though I wasn't around a lot at TU-Eindhoven, everyone from the van Hest group made me feel at home during my sporadic visits. Thank you for all the input everyone gave me during group meetings and for all the fun we had together during groups outings, conferences and borrels. Special shout-outs to **Lise**, zo leuk dat we uiteindelijk toch nog heel eventjes collega's waren en dat ik zelfs nog als co-autheur op 1 van je papers sta. Ik heb altijd een beetje naar je op gekeken, hoe je zo gestructureerd en gefocused kunt werken en ook nog tijd weet te vinden voor gezelligheid. Als er iemand is die alles kan bereiken wat ze zich in het hoofd haalt dan ben jij dat, powervrouw! **Bastiaan**, wie stalkt nu wie inderdaad?! Ik ben heel blij dat ik toch nog samen met jou in de van Hest groep heb mogen werken, jij maakte mijn bezoekjes aan de TU altijd tot een feestje. Ik ben benieuwd waar we elkaar de volgende keer tegenkomen; Nederland, Frankrijk of misschien wel de andere kant van de wereld.. Ik kijk er in ieder geval naar uit! **Imke**, GODMILJAAR wat heb ik het toch altijd leuk met jou gehad. Samen zeuren over wat nou het praktische nut was van het doen van een PhD heeft mij echt vanaf het begin en ook door die laatste loodjes heen geholpen. Samen gedemotiveerd toch nog ergens motivatie vandaan weten toveren is een kunst die we inmiddels allebei kennen. Je had altijd tijd voor een helpende hand of een bakkie koffie/thee, ondanks je af en toe mega drukke planning, en ik heb me altijd goed geamusseerd tijdens onze gesprekken om alles en niets. Ik hoop je nog veel tegen te komen op feestjes/festivals/...! **Pascal**, ik kan me niet voorstellen wat ik zonder al jouw flauwe, grove, vuile en vieze grapjes had moeten doen. Dankjewel voor al deze awesome momenten. Natuurlijk ook **Marjo**; Als echte mama van de groep stond je altijd

voor mij klaar en wist je me telkens weer door de wirwar aan regelwerk binnen de TU te loodsen. Als er ergens iets niet klopte, loste je het in 1-2-3 op. Je bent altijd in voor een praatje en het was dan ook altijd kei gezellig met jou tijdens de verschillende groeps-activiteiten en uitjes. Dankjewel voor alle goede zorgen.

Mijn lieve vriendjes en vriendinnetjes wil ik ook graag extra in het zonnetje zetten. Dankzij jullie heb ik, ondanks de af en toe zware perioden, heel veel mooie momenten meegemaakt en ben ik blijven genieten van de kleine dingetjes in het leven.

De lollies, als ik jullie niet had gehad, was het me waarschijnlijk überhaupt nooit gelukt om me door mijn bachelor en master heen te worstelen laat staan mijn PhD. **Kelly**, je ben niet voor niets mijn paranimf. Samen huilen, samen boos zijn, samen zuipen, samen dansen en samen lachen. Slechts een greep van het hele assortiment aan dingen die wij samen keer op keer deden om de wereld weer aan te kunnen. **Sanne**, het opperschaap van de groep en nu ook mama in real life, het voelt altijd als een warm dekentje elke keer dat ik je zie. Behalve alle gezelligheid, hecht ik altijd heel veel waarde aan jouw mening en ik vind het zo fijn om te weten dat ondanks dat we elkaar niet altijd even vaak zien, ik wel altijd bij je terecht kan. **Lise**, ik heb het al eerder gezegd in dit verhaal, hoe jij het allemaal voor elkaar krijgt is me een raadsel. De ontzettende drive die jij altijd hebt om beter te worden en het beste uit jezelf te halen, heeft me zeker geholpen om ook zelf vaak net dat beetje meer te doen. **Anne**, met jou heb ik altijd een hele speciale connectie gehad. Ondanks dat wij twee totaal verschillende mensen zijn, denken we op heel veel vlakken toch hetzelfde en lopen we ook regelmatig tegen dezelfde dingen des levens aan. Het is fijn om op die manier toch iemand te hebben als steun en toeverlaat. **Karen**, jij bent altijd zo lekker down-to-earth en ik vind het heerlijk om met jou te kletsen. Jouw nuchtere kijk op het leven, zorgt er vaak voor dat ik zelf met mijn beiden benen op de grond blijf. **Elunde**, jij bent altijd de rustige en misschien wel meest belangrijke factor geweest in de groep. Waar ikzelf altijd als een wervelwind doorheen stuiter, zorg jij er vaak voor dat ik af en toe toch gas terug neem en even op adem kom.

Mijn **halla-back-girls** aka **boobdiedoo** aka **vrouwelijke hondjes** aka **spill-the-T** chicas, het meest gezellige en grootste zooitje ongeregeld. Dankzij jullie zullen casual Fridays nooit meer zijn wat ze geweest waren en is het leven in den Bosch toch écht velen malen leuker. Niet alleen lang-leve-de-lol, want ik

weet ook dat ik op jullie kan rekenen wanneer het even wat minder goed met me gaat en daar ben ik jullie ontzettend dankbaar voor. **Nina**, lieve schat, samen zijn wij telkens weer degenen die tot in de laatste uurtjes overblijven op de dansvloer terwijl de "broekies" alweer een hele tijd op bed liggen. Jij bent er altijd zo goed in om dingen in perspectief te brengen en hebt me enorm geholpen door me te leren vooral naar mijn eigen lichaam te luisteren. De vele uitwaai-momentjes die wij elke keer hadden, als we weer eens een flink eind gingen wandelen, zorgden altijd voor weer wat meer rust in dat chaos hoofd van mij. **Sanne**, ik heb er bewondering voor hoe jij zo lekker recht voor zijn raap kunt zijn en je er altijd meteen uitflapt wat er ook maar in je opkomt. Je weet bij jou altijd meteen wat je aan je hebt en dat vind ik echt geweldig. Daarbovenop vind ik het ook geniaal dat welke conversatie dan ook meteen escaleert wanneer jij inhaakt. **Levina**, jij laat niet snel aan mensen de echte jij zien en ik voel me dan ook heel erg vereerd dat ik af en toe wél een kijkje in jouw hoofd mag nemen. Je quirky persoonlijkheid en je toewijding naar je vriendinnen zijn echt goud, blijf alsjeblieft altijd zo'n mooi mens! **Veerle**, jij bent ook al zo'n geweldig persoon, zo lekker jezelf. Jij bent er niet vies van om jouw ongezouten mening te geven en dat is ook precies wat vriendinnen horen te doen. Ik waardeer je mening en hulp dan ook enorm. Kom maar snel weer wat dichter bij den Bosch wonen!

Al mijn andere lieve vrienden en vriendinnen die er elke keer weer voor mij waren. **Arturo**, si no fuera por tí, no sé si algún día hubiera hecho mi doctorado. Siempre me empujabas para sacar lo mejor de mí mismo y por eso te estoy enteramente agradecida. Sé que las cosas no iban como nos imaginábamos, pero siempre vas a tener un pedazito de mi corazón. Muchísimas gracias por siempre creer en mí. **Sarah**, van al mijn vrienden ben jij toch wel een hele speciale. Zoveel samen meegemaakt en al vanaf het eerste kleuterklasje friends for life. Ik vind het jammer dat we elkaar niet supervaak zien, maar ik weet dat ik op je kan rekenen en de keren dat we elkaar wel treffen, lijkt het alsof het sinds gisteren was. **Ron**, ik ben zo blij dat ik jou heb leren kennen. Ik vind het fijn dat ik bij jou gewoon compleet mijn stuiterige ik kan zijn, want laten we heel eerlijk zijn, jij bent even gek. Ohja, dankjewel voor je "input" tijdens het schrijven van dit proefschrift. **Harry**, ik word er vrolijk van te weten dat ik jouw blije hoofd ooit tegen het lijf ben gelopen. Superbedankt allereerst voor het ontwerpen van de kaft van dit proefschrift, ik ben er mega blij mee. Met jou is er altijd leven in de brouwerij en ik hoop dan ook dat we nog vaak pintjes zullen gaan pakken. **Gerlof**, waar ik er vroeger altijd een godsgruwelijke hekel aan had om met jou te praten, ben ik blij dat je

het nooit hebt opgegeven om het te proberen. Ik heb heel veel van jou geleerd en ik kijk altijd uit naar weer een keertje bijkletsen met jou. **Glenn**, voor jou heb ik één woord: WERELDOVERHEERSING. **Antje**, mijn skate-mama, mede dankzij jou heb ik mijn liefde voor rolschaatsen ontdekt en daarvoor kan ik je niet genoeg bedanken. Jouw onuitputtelijke bron van energie werkt aanstekelijk en het is elke keer weer een fijn vooruitzicht om met je naar de sauna te gaan, een rondje te skaten of gewoon samen een hapje te eten. **Thomas**, ik ben heel blij dat je die ene keer toch weer je Facebook pagina geopend had, om er achter te komen dat ik stiekem toch alweer een tijdje in Nederland woonde. Vanaf dat moment leek het alsof ik helemaal niet weg was geweest en ben je een geweldige vriend voor mij. Hopelijk lukt het ons om binnenkort toch door te breken als cabe.., nee cabaet..., nee cabara,... grappenmakkersduo. **Joey**, ondanks dat je al lang een kop groter bent dan ik, zul je altijd mijn kleine broertje zijn. Dankjewel voor al je geduld, het moet heel lastig geweest zijn met mij als oudere zus.

Dan is het tijd om de belangrijkste mensen in mijn leven bedanken. Lieve **papa** en **mama**, aan jullie heb ik het allemaal te danken. Jullie onvoorwaardelijke liefde, steun en vertrouwen hebben mij gevormd tot de persoon die ik nu ben en ik ben heel blij met die persoon. Als ik terugblik, kan ik niet anders dan ontzettend dankbaar zijn voor de vrijheid die jullie mij telkens weer gaven om te doen en laten wat er ook maar in mij op kwam. Zelfs bij de meest idiote en wilde ideeën stonden jullie toch achter mij. Ook als ik er vervolgens achter kwam dat dat idee misschien toch niet het beste idee was, waren jullie altijd daar. Dankjewel voor alle mooie levenslessen, ik hou van jullie.

Last but not least, **Azula**, mijn kleine muppet, de enige kale poes die terug likt, hyperactief draakje. Het is fijn om te weten dat er altijd iemand blij is wanneer ik weer naar huis terugkeer. Dankjewel voor je knuffels, je liefde en de onuitputtelijke reeks aan mogelijkheden voor flauwe grappen. Oftewel in jouw taal: miw miw miew miauw miw.

Liefs,

Jaleesa